Universidade de Évora - Escola de Ciências e Tecnologia Universidade Nova de Lisboa - Faculdade de Ciências e Tecnologias

Mestrado em Tecnologias em Agricultura de Precisão

Dissertação

Spatio-temporal modeling of Halyomorpha halys (Hemiptera: Pentatomidae) populations on Emilia Romagna (Italy)

Luís Miguel Moleiro Grilo

Orientador(es) | José Rafael Silva

José António de Almeida

Évora 2024

Universidade de Évora - Escola de Ciências e Tecnologia Universidade Nova de Lisboa - Faculdade de Ciências e Tecnologias

Mestrado em Tecnologias em Agricultura de Precisão

Dissertação

Spatio-temporal modeling of Halyomorpha halys (Hemiptera: Pentatomidae) populations on Emilia Romagna (Italy)

Luís Miguel Moleiro Grilo

Orientador(es) | José Rafael Silva

José António de Almeida

Évora 2024

A dissertação foi objeto de apreciação e discussão pública pelo seguinte júri nomeado pelo Diretor da Escola de Ciências e Tecnologia:

Presidente	|	Adélia Sousa (Universidade de Évora)
Vogais	|	José António de Almeida (Universidade Nova de Lisboa - Faculdade de Ciências e Tecnologias) (Orientador) josé Manuel Herrera (Universidad de Cadiz) (Arguente)

Évora 2024

Acknowledgements

The successful conclusion of this project would not have been possible without the help of a lot of people and entities, so I express my gratitude to:

Cimice.net, for the Brown marmorated stink bug trap and capture data.

CER, for the soil use data.

ARPAE, for the meteorological data.

HALY.ID network, for taking me in and supporting the development of this project.

Thanks to Seequent company for providing academic licenses of Leapfrog Geo to NOVA-FCT.

Os meus orientadores, Professor José Almeida, UNL-FCT e Professor José Rafael, UÉ, por me guiarem durante a realização deste projeto, pela paciência e pela dedicação que demostraram do início ao fim.

Alla maestra Maria Pinotti, UNIPG, per tutto il suo supporto e fiducia nelle miei ideie.

Alla maestra Lara Maistrello, UNIMORE, per tutto l'aiuto riguardo lo studio del cimice asiatica, i dati messi a disposizione, ed i momenti di confronto in merito.

Ai tre colleghi e amici di lavoro sul campo Daniele Giannetti, Niccolò Patelli e Francesco Sorbelli, per il supporto , insegnamenti ed preziosi scambi culturali.

To those I have crossed paths with in Haly.ID network, who inspired me and shared experiences with.

Aos meus clientes/amigos que direta e indiretamente apoiaram o meu crescimento pessoal e profissional ao preferirem os produtos da minha pequena produção agrícola.

Aos meus amigos e professores do mestrado em Tecnologias em Agricultura de Precisão da UÉ e da NOVA-FCT pelo apoio e pelas conversas, em especial ao Alexandre Amaral e ao Manuel Verdasca.

Aos meus amigos e professores da licenciatura em Agronomia, ESAS, em especial ao João Marcelino, ao Gonçalo Neves e ao Leonardo Santos, (*Três Beirões e uma Amarga*), pela amizade e pelos momentos de descontração e divertimento que partilhámos!

Aos meus amigos, que sempre me inspiraram com as suas experiências de vida e me apoiaram, em especial á Diana Santos e ao Fernando Silva.

Á Eduarda Silva, por todo o amor, carinho e por me lembrar sempre do meu “potencial”!

Aos meus pais e ao meu irmão pelo suporte e apoio incondicional. Em especial aos meus avós, Cremilde e Manuel, por serem um exemplo para mim, pelo apoio constante e por me ensinarem desde tenra idade o que sabem sobre trabalho de campo e a vida.

Sumário

Modelagem espaço temporal de populações de *Halyomorpha halys* (Hemiptera: Pentatomidae) em Emília Romanha (Itália)"

Halyomorpha halys (Stål, 1855), (Hemiptera: Pentatomidae), vulgarmente referido como o percevejo asiático, é um inseto altamente polífago, originário da Ásia e que se estabeleceu como espécie invasora com distribuição global. Este tem causado prejuízos em todo o mundo, em Itália atingiu o seu apogeu em danos em 2019, com prejuízos estimados em 600 milhões de euros. Os métodos comuns para controlar esta praga utilizam abordagens químicas e biológicas que têm de ser aplicadas numa fase específica do desenvolvimento deste inseto bem como na localização e momento específico. Para resolver este problema, desenvolvemos um modelo espaço-tempo e um modelo preditivo para a região da Emília Romanha. A interpretação deste modelo permite uma decisão mais informada sobre as áreas e os prazos ideais para a aplicação de medidas de controlo.

Palavras-chave: BMSB; Geoestatística; Pragas agrícolas; Monitorização; Variograma

Abstract

Halyomorpha halys (Stål, 1855), (Hemiptera: Pentatomidae) commonly referred to as the Brown Marmorated Stink Bug, is an extensively polyphagous insect, indigenous to eastern Asia which established itself as a pervasive invasive species with a global distribution. Causing damage worldwide, in Italy, it reached its zenith in 2019, with 600 million euros of estimated costs. The common methods to control this pest use chemical and biological approaches which need to be applied at specific BMSB life stage and on a defined location. To address this problem, we developed a spatial-temporal model and a predictive model for the Emilia Romagna region. The interpretation of this model allows for a more informed decision on the areas and the ideal timepoints for the application of control measures.

Keywords: BMSB; Geostatistics; Agriculture pests; Monitoring; Variogram

General Index

Index of Charts and Tables

Index of Figures

List of Abbreviations and Acronyms

3D – Three dimensional

AF – Anisotropy Factor

ANOVA – Analysis of Variance

ARPAE – *L'Agenzia regionale per la prevenzione, l'ambiente e l'energia dell Emilia-Romagna*

BMSB – Brown Marmorated Stink Bug

CSO – Central Statistical Office

DD – Degree days

DSD – Degree of Spatial Dependence

DSS – Direct Sequential Simulation

EPPO – European and Mediterranean Plant Protection Organisation

ER – Emilia-Romagna

Ex – Exponential model

L:D – Light/Dark regime

Li – Linear model

LSD – Level of Spatial Dependence

MATTM – Italian Ministry of Environment and of Land and Sea Protection

MV – Missing Values

Nu – Nugget model

ODA – Oregon Department of Agriculture

RGB – Red Green Blue

RH – Relative Humidity

RMSE – Root Mean Square Error

RSS – Residual Sum of Squares

RSSE – Residual Sum of Squared Errors

SADIE – Spatial Analysis by Distance Indices

SINAB – *Sistema d'informazione Nazionale sull'Agricoltura Biologica*

Sp – Spherical model

TPL – Taylor's power law

UAV – Unmanned Aerial Vehicles

WOTY – Weeks of the Year

1. Introduction

Halyomorpha halys (Stål, 1855), (Hemiptera: Pentatomidae) commonly referred to as the Brown Marmorated Stink Bug (BMSB), is an extensively polyphagous insect, indigenous to eastern Asia which established itself globally as a pervasive invasive species. (Maistrello et al., 2018). The first instances of BMSB appearing in Italy were documented in Emilia Romagna, a key fruit cultivation region in Europe. This region yields an annual fruit production of 1,335,607 tons, as noted by Fanfani and Pieri (2016). The impact of BMSB on fruit production in northern Italy reached its zenith in 2019, with estimated damages approaching 600 million euros, according to data from the Italian Central Statistical Office (CSO).

In Emilia-Romagna, the threat posed by BMSB is particularly pronounced for pear cultivation. Italy stands out as the foremost pear producer in Europe, and nearly 65% of Italian pears are originated from Emilia-Romagna, as reported by the *Sistema d'informazione Nazionale sull'Agricoltura Biologica* (SINAB). On average, approximately 150,000 tons of pears are exported to international markets, equivalent to a market value of approximately 160 million euros. All this economic activity is in jeopardy due to the presence of this invasive pest. To address this issue, among the various available approaches, such as chemical treatments and cultural interventions, the most promising solution is biological control. Specifically, the introduction of parasites wasps, at the eggs stage to manage the BMSB population is a promising proposal.

However, there are challenges associated with implementing this strategy to combat the BMSB, such as the relatively brief lifespan of these wasps and their restricted distribution within the area of interest.

In this context, the primary objective of this research is to create a spatial-temporal model for the BMSB in the Emilia Romagna region, for years 2020 to 2022. This spatial-temporal model allows a better understanding of the BMSB's yearly generations and life cycle and supports the determination of the optimal time and location for releasing the parasitoid wasps.

2. Literature Review

2.1. *Halyomorpha halys*

2.1.1. Origin, invaded countries, or regions.

The *Halyomorpha halys* (Stål, 1855) (Hemiptera: Pentatomidae), also known as BMSB, is native to eastern Asia, primarily from China, Japan, Korea, and Taiwan (Hoebeke & Carter, 2003; Lee et al., 2013; Zhu et al., 2012), and has become an invasive species in many countries.

Currently, BMSB has invaded various locations worldwide. It was first recorded as an invasive species in 1996, near Allentown, Pennsylvania, United States of America (Hoebeke & Carter, 2003). Table 2.1 lists some of the countries where the BMSB is invasive and the year it was first detected. On the European and Mediterranean Plant Protection Organisation (EPPO) website, it is possible to consult the current countries invaded by this pest https://gd.eppo.int/taxon/HALYHA/distribution.

Global trade is pointed out as the most probable cause of the entrance of BMSB into other countries (Fogain & Graff, 2011). Suitable locations for the occurrence of this pest across the world are the regions between 30º and 50º latitude in both the northern and southern hemispheres (Kriticos et al., 2017; Leskey et al., 2012; Zhu et al., 2012). However, with the ongoing climatic change, BMSB may begin to appear in greater latitudes and not only in regions already suitable for its development. It is possible that BMSB will have more generations per year. On the other hand, some regions might reach very high temperatures and consequently leading to a reductions in the population of this insect (Kistner, 2017).

Table 2. 1 - List of countries / regions and the year of first detection of BMSB

Country / region	First detection	Author/year
United States near Allentown, PA	1996	(Hoebeke & Carter, 2003)
Switzerland	2004	(Haye et al., 2014)
Canada	2011	(Fogain & Graff, 2011)
Greece	2011	(Damos et al., 2020)
France	2012	(Callot et al., 2013)
Germany	2012	(Heckmann, 2012)
Italy	2007	(Cianferoni et al., 2018)
Hungary	2013	(Vétek & Korányi, 2017)
Abkhazia and Krasnodar	2013	(Gapon, 2016; Musolin et al., 2019)
Romania	2014	(Macavei, 2015)
Austria	2015	(Kment, & Vilmová, E. 2015)
Luxembourg	2015	(Döring, et al., 2017)
Bulgaria	2016	(Simov, 2016)
Slovakia	2016	(Hemala & Kment, 2017)
Spain	2016	(Dioli et al., 2016)
Chile	2017	(Faúndez, & Rider, 2017)
Croatia	2017	(Šapina & Jelaska, 2018)
Kazakhstan	2017	(Esenbekova, 2017)
Malta	2017	(Tassini & Mifsud, 2019)
Slovenia	2017	(Rot et al., 2018)
Georgia	2018	(Murvanidze et al., 2018)
Portugal	2018	(Grosso-Silva et al., 2020)
Turkey	2019	(Güncan & Gümüş, 2019)

2.1.2. Economic Importance of Crops

The BMSB is a highly invasive and mobile pest that feeds and reproduces on a broad spectrum of plants, including more than 300 ornamental and agricultural plants (Leskey et al., 2012; Leskey & Nielsen, 2018; Rice et al., 2014). In its native habitat, the BMSB is considered as a pest of cypress trees and other timber sources, yet it will opportunistically feed on cultivated fruit crops as a secondary food source (Funayama, 2012; Tsutsumi T, 2003). Although it has been documented to cause injury to cultivated fruit crops in Japan, the economic impact of its feeding damage is not widely detectable (Haye et al., 2015; Tsutsumi, T, 2003). Generally, the BMSB persists as an occasional outbreak pest in its native range, with damage levels varying among different fruit crops (Haye et al., 2015).

The BMSB feeds by piercing and sucking on plant tissues, mainly fruits and seeds, and can cause deformities, scars, and discolorations. These damage to fruits make them unmarketable and can increase secondary and post-harvest infections (Maistrello et al., 2017). Furthermore, plants where BMSB has fed can become infected with pathogens, increasing the risk posed by this pest (Maslen, 2016).

This pest can inflict economic damage to a wide variety of crops, including apple (Malus domestica Borkh.), peach (Prunus persica (L.) Batsch), pear (Pyrus communis L.), grape (Vitis vinifera L.), soybean (Glycine max (L.) Merr.), sweet corn (Zea mays L. var. saccharata), and tomato (Solanum lycopersicum L.), among others (Lee et al., 2013; Rice et al., 2014). On stone fruits, mainly peaches and nectarines, BMSB feeding activity causes depressions or sunken areas, while on pome fruit, including apples and pears, feeding results in indented depressions on the surface and suberification spots in the flesh of the fruit. Furthermore, feeding may also lead to premature abortion of fruiting structures (Nielsen & Hamilton, 2009). According to (Koch & Rich, 2015; Rice et al., 2014; Venugopal et al., 2015), it is also a serious pest of vegetables.

The BMSB can also produce defensive secretions that contaminate and persist in wines. Undesirable flavours are detected in wine in which insects are unintentionally incorporated into fermentations, leaving a taint that is detectable and undesired by consumers (Wiman et al., 2015). Results are ambiguous, some preliminary data indicate that the taint does not survive fermentation, while others authors suggest the opposite (Mohekar et al., 2017).

In the United States , mid-Atlantic region, 15 years passed from BMSB first detection until it became a key pest in fruit orchards, such as apples, peaches, and pears (Leskey et al., 2012). In 2010, this region of the USA suffered severe pest pressure, resulting in $37 million loss in apples alone, and the loss of more than 90% of stone fruit crops (Leskey et al., 2012). The Oregon Department of Agriculture (ODA, 2013), in the United States alone, more than $21 billion worth of crops are estimated to be threatened by BMSB feeding activity.

In Georgia, 2016, BMSB caused around $60 million in damage to hazelnuts (Corylus avellana L.) alone (Murvanidze et al., 2018).

In Emilia Romagna, two years since its first official detection, fruit injuries were reported in the area, especially in privately-owned untreated orchards (Maistrello et al., 2014). Several years after its first discovery, BMSB became the main key pest of fruit orchards in northern Italy (Maistrello et al., 2017), causing the greatest damage in pears (Bariselli et al., 2016). It also caused severe damage to hazelnut production in 2017 (Bosco et al., 2018).Losses in fruit production in northern Italy peaked in 2019 when the estimated damage was nearly EUR 600 million (CSO, Italy).

2.1.3. Biology

The BMSB possesses numerous biological traits that contribute to its success as an invasive species. These traits include a predominantly r-selected life history and a strong connection to ecosystems modified by human activities. Once it establishes a foothold, its remarkable ability to disperse over long distances, its broad diet, and its competitive prowess enable it to rapidly expand its range across continents (Sakai et al., 2003).

2.1.3.1. Life cycle

The BMSB emerges in the spring as an immature adult or in a reproductive diapause state (Watanabe 1979; Cira et al. 2016, Nielsen et al. 2017b) from the shelters where it stayed during overwinter; these shelters can be the bark of trees, dead upright trees, or man-made structures (Watanabe 1979).

The emergence of BMSB is related to biotic as well as abiotic factors. Depletion of fat reserves is a biotic factor that, according to Funayama (2012), can trigger the exit from

the overwintering state. The abiotic factors that can be a cue for the termination of overwinter state are photoperiod (Tauber & Tauber, 2003) or temperature (Bergh et al., 2017; Lee et al., 2013).

After the exit from the shelters, the BMSB will start to feed, when the photoperiod reaches a certain threshold, the reproductive diapause will terminate (Leskey & Nielsen, 2018; McDougall et al., 2021; Nielsen et al., 2017), from this point forward the overwinter generation will reproduce until the end of their lifespan. According to the temperature, it will take a few days to complete the following stages after mating (Figure 2.1-A), egg laying (Figure 2.1-B), egg hatching, first instar (Figure 2.1-C), second instar (Figure 2.1-D), third instar (Figure 2.1-E), fourth instar (Figure 2.1-F), and fifth instar (Figure 2.1-G) emergences, and finally, adults instar (Figure 2.1-H) moulting instar (Damos & Savopoulou-Soultani, 2012).

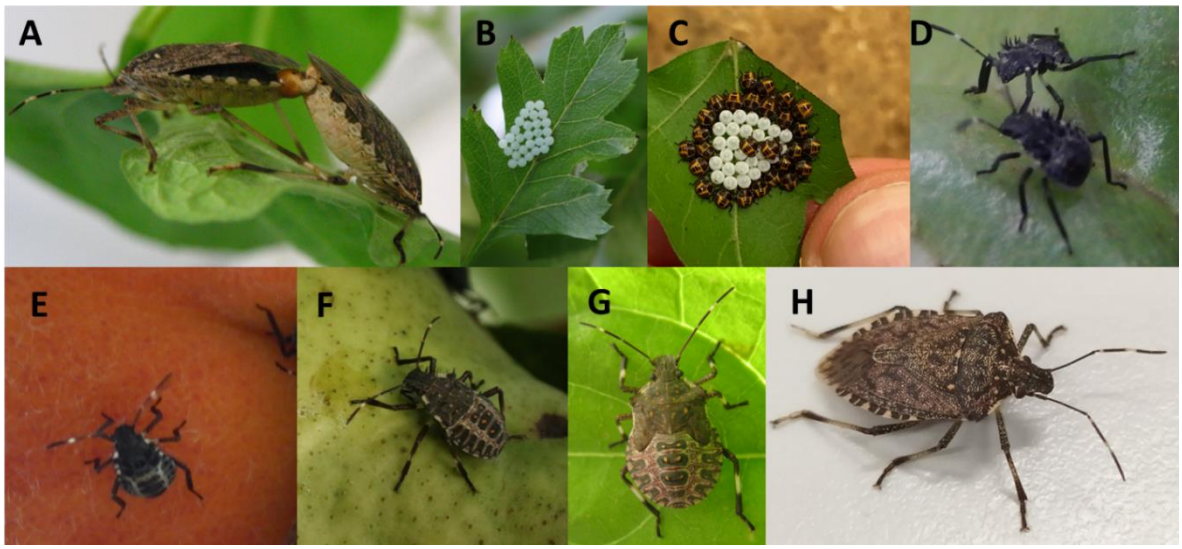

Figure 2. 1- Different stages in the Brown marmorated stink bug life cycle. A – mating; B – egg mass; C – egg hatching/first instar; D – second instar; E – third instar; F – fourth instar; G – fifth instar; H – adult. Source: Pictures from Laboratory of entomology, University of Modena and Reggio Emilia (UNIMORE)

2.1.3.2. Longevity

There exists some disagreement in the scientific community regarding the lifespan of the BMSB. According to Wang and Wang (1988), the lifespan is 365 days, while Zhang et al. (1993) reported it to be 301 days, and Kawada & Kitamura (1983) stated an average of

111 days. More recently, Medal et al. (2013) found that at 25° C, females lived an average of 84 days, while males lived for 119 days.

In a study conducted by Govindan & Hutchison (2020), it was observed that the longevity of BMSB was highest at the lowest temperature tested and started to decline at higher temperatures. These results align with a study conducted by Baek (2017).

Concerning the USA, Mermer et al. (2023) reported that in Oregon, it took 1615 degree days for full mortality since the egg stage, while in New Jersey, it took 1717 degree days.

2.1.3.3. Reproduction

The reproductive development of the BMSB is influenced by various factors, including photoperiod, temperature, and nutrition. Exposure to specific photoperiods affects both the adult and nymphal stages, influencing their reproductive processes (Niva & Takeda, 2003) Photoperiod cues impact physiology, melanin formation, feeding behaviour, body size, and reproductive activity in BMSB (Hahn & Denlinger, 2007). However, photoperiod variations during the egg stage do not appear to have a significant effect (Watanabe 1979).

While the photoperiod initiates reproductive development, temperature plays a primarily role in driving the reproductive processes of BMSB after diapause termination. Warmer temperatures are conducive to reproductive development, and higher temperatures promote increased egg production and oviposition (Acebes-Doria et al., 2017).

BMSB mating behaviour involves multiple copulations, with mating occurring throughout the day (Kawada et al., 1983). Overwintered female BMSB start laying eggs from mid to late May in some regions, with the highest proportion of females having mature eggs observed from mid-July through August (Wang and Wang 1988; Zhang et al. 1993). Eggs are typically laid in clusters, with an average of 28 eggs per mass, and are deposited on the undersides of leaves and in the upper tree canopy (Nielsen et al., 2008).

Female BMSB can continue to oviposit throughout their lifespan, with egg production influenced by factors such as multiple mattings and age (Kawada et al., 1983). The optimal temperature for oviposition appears to be around 25°C, with oviposition periods ranging from 6 to 113 days, depending on temperature conditions (Kawada et al., 1983;

Nielsen et al., 2008). The pre-oviposition period ranges from 7 to 23 days, with variations based on temperature (Nielsen et al., 2008).

Understanding the complex interactions among photoperiod, temperature, nutrition, and reproductive behaviour is essential to manage BMSB populations, especially considering the impact of this invasive species on agriculture. Temperature ranges between 18°C and 32°C have been identified as favourable for the oviposition and survival of BMSB (Haye et al., 2014).

2.1.3.3.1. Reproductive diapause

Stink bugs, particularly those in the Hemiptera: The Pentatomidae family showcase a remarkable adaptation known as facultative diapause, a state of prolonged suspended development. This sophisticated adaptation allows BMSB to suspend their development in response to changing environmental conditions, primarily triggered by reduced photoperiod and temperature regimes (Saulich & Musolin, 2012).

When daylight hours fall below a certain threshold, pentatomids undergo significant physiology changes. These changes include processes such as melanin formation (Niva and Takeda, 2003), alterations in feeding behaviour and body size (Hahn & Denlinger, 2007), cessation of reproduction, and a tendency to abandon their host plants in search of suitable overwintering sites (Niva and Takeda, 2003).

This adaptation serves as a vital survival strategy in regions with harsh winter climates, enabling them to endure and thrive under challenging conditions.

2.1.3.4. Voltinism

Voltinism refers to the number of generations of an organism within a year (Kistner, 2017; Stoeckli et al., 2020). For invasive species, multivoltinism is considered an adaptive advantage over univoltinism, because it allows for faster spread and exploitation of new habitats (Stoeckli et al., 2020). In fact, the more rapid build-up of BMSB populations and greater severity as a pest in Italy versus Switzerland were attributed to its bivoltine and univoltine phenology in these locations, respectively (Costi et al., 2017). Table 2.2 provides information on the voltinism capability of the BMSB in different countries or regions.

Table 2. 2 - Voltinism accordingly to countries/regions and latitude

Country/Region	Generations/year	Author/year	Latitude
China / Southern	Bivoltine	(Zhang et al. 1993)	18° to 35°
United States/Southern	Bivoltine	(Bakken et al., 2015; Leskey et al., 2012)	26° to 35°
United States	Capacity for bivoltinism	(Nielsen et al., 2016)	26° to 48°
Japan	Capacity for bivoltinism	(Funayama, 2008)	31° to 45°
Japan/ eastern region	Bivoltine	(Watanabe, 1980)	34°
Greece/ Southern	Capacity to up to 3	(P. G. Milonas & Partsinevelos, 2014)	35°
Japan/Western	Univoltine	(Watanabe, 1980)	35°
United States/mid-Atlantic	Capacity for bivoltinism	Nielsen et al. 2008a	35°
United States/Northern	Capacity for bivoltinism	(Ogburn et al., 2023)	40° to 48°
United States/Northern	Univoltine	(Nielsen & Hamilton, 2009)	40° to 48°
Georgia/Western	Bivoltine	(Murvanidze et al., 2018)	42°
Russia/Sochi	Capacity for bivoltinism	(Dmitry L. Musolin et al., 2018	43°
Italy/Northern	Bivoltine	(E. Costi et al., 2017)	45°
Switzerland/Northern	Univoltine	(Haye et al., 2014; Rot et al., 2022)	46°

2.1.3.5. Overwintering

During overwintering, the BMSB adopts a nonfeeding and nonreproductive diapause state (Lee et al., 2014). BMSB adults begin migrating to overwintering sites as early as September (Kawada et al., 1983), with a significant intensification of this activity by mid-October (Zhang et al., 1993). This migration extends into November (Funayama, 2012). During this period, adults tend to form clusters in dark and sheltered areas within their chosen overwintering sites. Once settled, these individuals exhibit minimal mobility unless their stored nutrient reserves in the fat body are depleted (Funayama, 2012).

Overwintering BMSB adults have been found in various natural landscapes, often in dark dry locations (Inkley, 2012), and under the bark of cedar trees (Lee et al., 2014). Remarkably, BMSB frequently selects human-made structures, such as buildings, as their

preferred overwintering sites. This predilection for man-made structures has led to the BMSB becoming a significant household nuisance due to the large numbers of invading adults searching for overwintering sites (Inkley, 2012; Nielsen & Hamilton, 2009).

2.1.4. Abiotic parameters

The BMSB, as an ectothermic organism, relies heavily on environmental conditions, particularly temperature and humidity (Harrison, 2012).

2.1.4.1. Temperature

The impact of temperature on insects is a crucial factor (Govindan & Hutchison, 2020). In the case of the BMSB, temperature plays a significant role at various stages of its life cycle. Overwintering adults, for instance, are subject to a distinct temperature range as they endure winter in a state of dormancy.

The impact of temperature on insects is a crucial factor (Govindan & Hutchison, 2020). In the case of the Brown Marmorated Stink Bug (BMSB), temperature plays a significant role at various stages of its life cycle. Overwintering adults, for instance, are subject to a distinct temperature range as they endure winter in a state of dormancy.

For overwintering adults, survival rates start to decline when the temperature drops to -5°C (Scaccini et al., 2020). This author also found that exposure to an episodic cold temperature shock of two hours at -10.4ºC or six hours at -7.6°C resulted in the death of half of the population. Furthermore, when temperatures dropped below -13.5°C and persisted for at least six hours, a high mortality rate was recorded.

The ability to acclimate to colder temperatures can also enhance cold tolerance and promote increased survival after diapause (Chen and Walker, 1994).

The BMSB, like all species in the Heteropteran suborder, is chill intolerant and will die before freezing (Bale, 1991; Saulich & Musolin, 2012). The range of winter supercooling points for BMSB is between -17.1ºC and −13.9° C, with an average of -16.11ºC (Cira et al., 2016). Another study by Lowenstein and Walton (2018) reported that an episodic shock at -6°C caused more than 75% mortality in adults with diapause.

For active BMSB individuals that are not in dormancy, there is a range of temperatures within which they can survive. Within this range, there is also a specific temperature range for their development. Scaccini et al. (2020) found that exposure to an episodic cold temperature shock of six hours at -3.3°C or two hours at -5.7ºC resulted in the death of half the population.

Most BMSB become inactive below 9°C (Ogburn et al., 2023; Li et al., 2007), and according to this study, feeding begins only above 17°C. However, Leskey and Nielsen (Leskey & Nielsen, 2018) stated that BMSB adults stop feeding below 3°C to 6°C and considered 16°C and 17°C the optimal temperatures for adult feeding.

For oviposition (egg laying), the minimum temperature required is 18°C (Mermer et al., 2023), and according to Rot et al. (2022), oviposition begins when average daily temperatures reach 17°C.

Maximum temperatures for adult feeding range from 26°C to 29°C (Leskey & Nielsen, 2018), while oviposition ceases at 32°C (Maslen, 2016).

The first instar nymphs of BMSB must ingest the egg chorions containing intestinal symbionts that were deposited during oviposition. However, above a certain temperature, these gut symbionts die before being ingested, which affects the overall fitness of BMSB (Ingels & Daane, 2018).

According to Aigner and Kuhar (2016), an episodic high temperature shock of four hours at 35°C, 38°C, 40°C and 42°C resulted in the death of 5%, 12%, 38% and 91% to 100% of the population, respectively. Furthermore, exposure to an hour at 45°C can kill 91% to 100% of the population. Additionally, Scaccini et al. (2019) found that at temperatures of 50ºC and 47.5ºC, exposures of 10 minutes and 20 minutes, respectively, can result in the death of 100% of the population.

The optimal temperature range for BMSB survival is reported to be between 20°C and 30°C (Govindan & Hutchison, 2020). The most favourable temperature for oviposition is 25°C (Maslen, 2016), while the best temperature for egg survival is 30°C (Haye et al., 2014). Development temperatures below 15°C or above 36°C do not support development (Nielsen et al., 2008), with the optimal temperature for development being 27.8ºC (Mermer et al., 2023).

Nielsen et al. (2008) reported that optimal temperatures for the stages of the BMSB lifecycle are between 30ºC and 33ºC for eggs, first instar, and second instar, while the optimal temperature for the remaining stages is 27ºC. The same study also revealed that BMSB populations from Switzerland developed faster than populations from the United States at the same temperatures.

There is a temperature threshold for the development of BMSB based on the location and stage of the insect, which can be found in Table 2.3.

The temperature also impacts the lifespan of BMSB, showing an inverse relationship with development. Govindan and Hutchison (2020) reported optimal survival rates between 20°C and 30°C, with faster development occurring closer to 30°C and a longer lifespan at temperatures closer to 20°C. Maslen (2016) found that the median survival times of female adults at 15°C, 18°C, 22°C, 25°C, 27°C, 30°C and 32°C were 89, 71, 60, 40, 41, 28, and 35 days, respectively. The increase in temperature resulted in a decrease in the mean survival periods of both female and male adults.

Several authors have also reported that temperature is related with the emergence of BMSB adults from overwintering sites. These temperature values were reported as 10°C by Qin (1990), starting at a daily maximum of 14°C and peaking at a daily average of 21°C according to Costi et al. (2017), and starting at a daily average of 12°C and peaking at a daily average of 15°C as stated by Rot et al. (2022).

Table 2. 3 - Development temperature thresholds for the Brown marmorated stink bug based on the location and stage of the insect (ºC).

Stage	*Lower*	*Upper*	*Location*	*Author/year*
Ovarian Development	16.3	-	Japan	*(Watanabe 1980)*
Egg	9.9 - 15.1	-	Japan	*(Kiritani 1997)*
Egg	10	33.6	Korea	
First instar	15	41.2	Korea	
Second instar	13	34.8	Korea	
Third instar	13.3	34.3	Korea	*(Baek et al., 2017)*
Fourth instar	12.2	33.6	Korea	
Fifth instar	10.9	33.5	Korea	
Adult	13.1	33.5	Korea	
Total Development	14.17 - 14.4	35.76	USA (PA)	*(Nielsen et al., 2008)*
Total Development	15	32	USA	*(Maslen, 2016)*
Total Development	14.26	35.9	USA	*(Mermer et al., 2023)*
Total Development	11.1 - 12.9	-	Japan	*(Kiritani 1997)*
Total Development	12.24 - 12.97	36.5	Switzerland	*(Haye et al., 2014)*

2.1.4.2. Humidity

In a study conducted by Khadka et al. (2020), eggs, nymphs, and BMSB adults were exposed to different levels of relative humidity (RH). The study observed that while egg hatching and nymphal survival occurred at all humidity concentrations, the highest rates at 55% to 90% RH. Additionally, females laid the highest number of egg clutches at 55% RH. This suggests that BMSB could thrive within the range of 55% to 90% RH, with the highest reproductive activity at 55% RH (Khadka et al., 2020).

However, a contrasting study by Fisher et al. (2021) found that at an ambient temperature of 27°C, humidity did not have a significant impact on BMSB survival. This disparity with the findings of Khadka et al. (2020) might be attributed to the shorter duration of low-humidity exposure in Fisher's experiment. Furthermore, Khadka et al. (2020) discovered that at a higher temperature of 40°C, exposure to low humidity (17% RH) significantly decreased survival compared to higher humidity levels.

Surprisingly, at the highest temperature evaluated (42°C), higher humidity did not increase survival. Instead, exposure to a moderate 39% RH significantly increased survival compared to both higher and lower humidity levels. This unexpected result could be due attributed to the reduction in evaporative cooling under high humidity conditions, leading to higher insect body temperatures (Fisher et al., 2021).

2.1.4.3. Macroclimatic Conditions versus Microclimatic Conditions in an Orchard

Standardised meteorological stations typically record weather conditions at a height of approximately 2 metres in open areas. This practise is designed to minimise the influence of microclimatic factors (Jarraud, 2008). As a result, the data collected at these stations are considered representative of long-term, free-air factors, indicative of macroclimatic conditions. However, it is important to note that many organisms encounter values of these factors during their life that differ significantly from those reflected in macroclimatic data (Bramer et al., 2018; De Frenne et al., 2021).

These distinct values are often referred to as microclimatic data and play a central role in the governance of biological and ecological processes. These processes include those related to vegetation, carbon and nutrient dynamics, and species distributions (Lembrechts et al., 2019).

To optimize their conditions, insects can manipulate their position in the tree canopy to take advantage of the cooling effects of leaf transpiration (Havko et al., 2020) or to obtain solar radiation and increases their warmth according to their needs.

2.1.5. Phenology

2.1.5.1. Degree days

Temperature-based phenology models, such as degree days (DD), find widespread application across various fields, notably in agricultural pest management and epidemiology (Rebaudo et al., 2018). Degree days, characterized by the accumulation of heat units over time, serve as a common metric for assessing the rate of insect development within specific temperature limits (Murray, 2008; Sridhar & Reddy, 2013).

These models play a crucial role in predicting key events in the life cycle of organisms, such as the emergence of specific life stages. They offer a standardised approach to articulate temperature-dependent processes in an organism's life cycle (Kamiyama et al., 2021). Additionally, these models facilitate the modelling of insect development, determination of the number of generations in different locations, and the prediction of temperature impacts on biological processes. The underlying principles of DD simulate the phenology of poikilothermic organisms, where a specific accumulation of heat units above a temperature threshold is requisite for a particular developmental event to unfold (Damos & Savopoulou-Soultani, 2012).

The calculation of DD in natural settings requires detailed methodologies due to daily cyclical temperature fluctuations. A range of techniques, from straightforward to intricate, exists for calculating DD based on daily maximum and minimum temperatures. These methodologies encompass averaging, single triangulation, double triangulation, single sine, and double sine methods (Zalom, et al., 1983).

Table 2.4 specifically details the cumulative DD required for the BMSB to complete various development stages. “Complete development” is the DD required from egg hatching until imaginal ecdysis. “Ovarian development” is the DD required from diapause termination until ovary development, while “egg incubation” represents the DD required from egg laying until eggs hatch.

Table 2.4 - Cumulative degree days the value in subscript after "DD" refers to the minimal development threshold considered by the author.

Complete development	*Ovarian Development*	*Egg incubation*	*Location*	*Authors*
	119 DD $_{16.3}$		Japan	*(Watanabe, 1980)*
537.63 DD $_{14.14}$	147.65 DD $_{14.14}$	53.30 DD $_{13.94}$	USA	*(Nielsen et al., 2008)*
588.24 DD $_{12.24}$	117.65 DD $_{12.24}$		Switzerland	*(Haye et al., 2014)*
546.4 DD $_{12.8}$			Korea	*(Baek et al., 2017)*
530 to 590 DD $_{13.3}$			Sochi, Russia	*(Musolin et al., 2019)*
530 to 545 DD $_{12.2}$	118.77 DD $_{12.2}$		Slovenia	*(Rot et al., 2022)*
590 DD $_{13.3}$	156 DD $_{13.3}$		Sochi, Russia	*(Reznik et al., 2022)*
520 DD $_{14.26}$		54 DD $_{14.26}$	USA (NJ)	*(Mermer et al., 2023)*

2.1.5.2. Photoperiod

The term "photoperiod" refers the period of time between sunrise and sunset, commonly recognized as day length. In species, especially those that experience adult overwintering, the initiation and conclusion of diapause are impacted by external elements such as temperature and photoperiod (Tauber & Tauber, 2003).

Previous studies with BMSB have suggested that a decrease in the photoperiod, regardless of the temperature, can suppress reproduction. Females were found to possess underdeveloped oocytes below a certain threshold of the photoperiod, while males exhibit a lack of discernible ectodermal sacs (Watanabe, 1980; Yanagi and Hagihara, 1980; Niva and Takeda, 2003). On the contrary, instances of females with developed ovaries, replete with sperm, and males with filled ectodermal sacs were noted when daylight duration was correlated with a seasonal pattern of reproductive activity. Reznik (2022) reported that as the natural photoperiod decreased below the critical day length (determined through experiments as 15.0-15.5 hours), the percentage of females with fully developed ovaries sharply diminished to zero.

According to Ogburn (2023), temperature is considered a secondary cue for the termination of diapause, since the photoperiod was the same in two studied locations. Musolini (2019) also demonstrated the importance of temperature by showing that under very long day conditions (L:D 18:6) at 20 °C, 50% of the individuals entered diapause.

While a reduction in photoperiod typically triggers diapause initiation, rapid temperature decreases can have a more significant impact on diapause success. Prolonged diapause induced by cold temperatures can lead to physiological trade-offs, such as a decrease in egg production following diapause and an increase in the lifespan of adult organisms (Denlinger, 1991; Ishihara and Shimada, 1995).

The diapause exhibited by the BMSB is classified as facultative, as noted by Nielsen et al. (2017), which helps the specie adapt to different regions. In regions where shorter days are borderline for the reproduction and establishment of BMSB, the facultative diapause serves a significant purpose. Interestingly, the discovery of a small population of reproductive BMSB females in central Florida during late winter, as reported by Penca and Hodges (2018), suggests that factors such as temperature or host plant quality can override signals for the onset of diapause (McDougall et al., 2021).

The photoperiod can function as a reference point (biofix) for calculating DD accumulations, with the termination of diapause marking the beginning of the accumulation (Leskey & Nielsen, 2018; McDougall et al., 2021; Nielsen et al., 2017).

Several authors have provided photoperiod thresholds for diapause induction and termination in BMSB populations from different locations, as presented in Table 2.5.

Using a biofix of 13.5 hours of photoperiod, Nielsen et al. (2016) predicted an above-average BMSB population in New Jersey in 2010, which aligns with the significant increase in crop damage observed in the mid-Atlantic region during those years by Leskey et al. (2012).

In a separate analysis by McDougall (2021), it was estimated that a critical photoperiod of 12.7 hours would be sufficient for approximately 10% of individuals to emerge from diapause. Furthermore, within the population, reproductive development in 50% of the individuals fell within the range of 13 to 13.5 hours of photoperiod. This observed variation aligns with the findings of Nielsen et al. (2016, 2017).

Table 2. 5 - Thresholds of photoperiod for diapause induction and termination in BMSB populations across different locations

Diapause Induction	*Diapause termination*	*Location*	*Authors*
13.5h to 14 h	13.5h to 14.75h	Japan, Toyama	*(Watanabe, 1979)*
15 h	13.5h to 14.75h	Asia	*(Yanagi and Hagihara, 1980)*
14 to 15 hours		Japan, Chiba	*(Fujiie, 1985)*
14.5h		Japan, Hyogo	*(Niva, 2003)*
13.5 h	13.5 h	USA, New Jersey	(Nielsen et al., 2016)
	12.7h	USA	*(Nielsen et al., 2017)*
15.5 h		Russia, Sochi,	*(Musolin et al., 2019)*
14.5h to 15 h		Korea	*(Musolin et al., 2022)*
15 to 15.5h		Italy, Torino	*(Musolin et al., 2022)*
15 to 15.5h		Switzerland, Basel	*(Musolin et al., 2022)*
15 to 15.5h		Russia, Sochi,	*(Musolin et al., 2022)*
13 h		Slovenia	*(Rot et al., 2022)*
14 to 14.5h		USA, NC	*(Ogburn et al., 2023)*

2.1.6. Ecology: Predators and Parasitoids

Natural enemies have become crucial allies in the ongoing battle against BMSB. These natural enemies primarily include egg parasitoids and generalist predators, playing a pivotal role in suppressing BMSB populations.

The egg parasitoids *Trissolcus japonicus* (Ashmead) and *Trissolcus mitsukurii* (Ashmead) (Hymenoptera: Scelionidae) are identified the most effective biocontrol agents of BMSB in its native range (Costi et al., 2022).

Predators from the families Acrididae, Anthocoridae, Coccinellidae, Forficulidae, Gryllidae, Miridae, and Tettigoniidae have been observed attacking BMSB eggs in previous field and laboratory studies (Abram et al., 2017; Morrison et al., 2016).

Poley et al (2018) found that the *Acheta domesticus* (L.), common known as house cricket could, could be classified as a beneficial arthropod predator on BMSB eggs.

The existing diversity of parasitoids and predators offers a potential solution for integrated pest management approaches.

2.1.7. Management strategies

2.1.7.1. Chemical control

The BMSB poses a significant threat to agriculture, leading to an increase in pesticide applications, notably pyrethroids and neonicotinoids, during outbreak years. However, this reliance on broad-spectrum insecticides has unintended consequences, triggering secondary pest outbreaks of aphids, scales, and mites that were traditionally controlled by natural enemies (Leskey et al., 2012; Rice et al., 2014).

To enhance efficiency and sustainability, there is a need for a more integrated approach to chemical control that considers the biology and behaviour of the BMSB. Neonicotinoids applied through drip chemigation offer extended control (up to 14 days) and minimise the use of foliar insecticides. Similar strategies have been explored in soybeans to reduce overall insecticide use (Rice et al., 2014).

It is crucial to develop selective insecticides with minimal impact on beneficial insects. Frequent rotation of insecticide classes can help prevent resistance (Leskey et al. 2012a). An "attract and kill" strategy, using lures to aggregate BMSB in specific areas, could reduce overall insecticide use, providing a more sustainable approach (Rice et al., 2014).

2.1.7.2. Cultural Control

Cultural control methods offer an alternative approach to managing BMSB populations, aiming to decrease dependence on chemical interventions. These approaches involve modifying agricultural practises to mitigate BMSB damage.

One promising strategy involves the implementation of attract-and-kill sites at the borders of orchards. In season-long trials, baited attract-and-kill sites in apple orchards proved effective in reducing BMSB populations and fruit injury. The number of BMSB adults with BMSB killed and the level of fruit injury were significantly lower in adjacent unbaited trees, indicating the potential for border-based attract and kill sites to protect orchard fruit (Morrison et al., 2016). This approach not only offers a targeted method of control but also minimises the use of broad-spectrum insecticides.

In Asia, where BMSB has long been a pest, cultural control methods have also been explored. Recommendations include mechanically removing eggs and nymphs from crops, destroying nearby alternate hosts, and constructing overwintering traps (Qin, 1990).

Another cultural control strategy involves trap cropping, redirecting BMSB away from valuable crops. Studies have investigated the use of early maturing soybeans and sour jujube trees as trap crops. Early maturing soybeans attracted more BMSB, but populations did not increase in later varieties upon the harvest of the early crop (Lee et al., 2013).

2.1.7.3. Biological control

Like cultural control, biological control methods offer promising strategies for managing BMSB populations without the environmental and ecological drawbacks associated with chemical interventions. Several natural enemies have been studied for their potential in controlling BMSB populations, providing valuable insight into their effectiveness.

One noteworthy discovery is the microsporidian *Nosema maddoxi*, identified as a systemic pathogen of BMSB in North America (Hajek et al., 2018). Research indicates that *N. maddoxi* infection has detrimental effects on BMSB, shortening the lifespan of females, reducing fecundity, and lowering egg viability. Furthermore, *N. maddoxi*, infection significantly increases nymphal mortality, reaching a mortality rate of 73.6% before reaching adulthood when infected as second instars. This native entomopathogen has the potential to negatively impact the BMSB survival and fitness in the field, offering a viable biological control (Hajek et al., 2018).

Another approach to biological control involves the use of predators and parasitoids, as discussed in a previous chapter. In this way there are several agents that could be used to biocontrol the BMSB, this solution despite being considered more sustainable, by reducing the reliance on chemical insecticides and mitigating the associated risks to the environment. This solution can also be a treat since some of the solutions consider the introduction of exotic biocontrol agents.

In European countries, the use of exotic biocontrol agents is restricted by the 'Habitats directive' (Council Directive 92/43/EEC, 21/05/1992, on the conservation of natural habitats and of wild fauna and flora) (Costi et al., 2022). However, due to significant economic losses in 2019 caused by BMSB on fruit production in Italy, the Italian Ministry of Environment and of Land and Sea Protection (MATTM, 2020) authorized the release of Trissolcus japonicus for the biological control of BMSB. This led to one of the largest biocontrol projects ever attempted in Italy (Costi et al., 2022).

Whether choosing chemical or biological control, the application of insecticides or release of biological control agents must be timed to coincide with specific life stages of the pest (Haye et al., 2014). To determine the precise timing that coincides with a specific life stage of a pest is essential to do a monitorization of the pest.

2.2 Monitorization Methods

In the agricultural context, crop adversaries have consistently proven to be the most challenging factor to manage (Donatelli et al., 2017). These adversaries include adventitious flora, diseases, and pests. Pests are animal organisms that pose a threat to agricultural crops, and key pests are specific types that appear regularly in each crop, causing substantial damage if not adequately controlled.

The monitoring of pests is of utmost importance, with a focus on early detection, as well as pinpointing their location and density. In the long term, monitoring makes it possible to identify growth trends and thus implement control measures in a timely manner. (Calvini et al., 2021; Headrick, 2021).

To achieve desired outcomes, two essential steps must be taken. The first involves sampling, and in the second stage, data modelling is conducted. In this context, it is more significant to conduct data modelling within a well-defined geographical context, considering various variables. Geostatistics provides the means to analyse variables distributed in space and/or time, assuming that the values of these variables are correlated in space and/or time (Belchior, 2022).

Geostatistical models operate on probabilistic models that account for the spatial structure of the phenomenon under study, utilizing georeferenced data. These models also serve the purpose of predicting the value of a variable in locations where no samples have been taken.

2.2.1 Sampling

Pest sampling methods are chosen based on the type of pest and its life stage. Table 2.6 categorizes samples according to the method of data counting, which can include direct visual observation, capture, capture with trap, estimation, or remote sensing, as exemplified in Figure 2.2.

Table 2.6 provides a summary of articles published between 1961-2022, detailing various counting methods, techniques, and the pests target for monitoring. Additionally, a comparative evaluation of acquisition costs and the time required for each execution method was included.

The choice of the most suitable counting method is influenced by factors as economic cost, the time required for execution/implementation, and the validity of the acquired data. Visual counting methods are typically used for pests of small dimensions, such as mites or thrips, where the pests are observed directly in their location.

The catch-and-count method involves actively collecting pests, commonly using sweeping nets for flying pests. With mango-shaped nets, organisms on or flying over the crops are collected. The beating technique, employed in medium to large crops like vineyards or orchards, involves a net covering the soil. Pests dislodged by beating the crop fall into the net for later collection. The aspiration technique employs a vacuum cleaner to collect pests in the crops.

Soil or plant portion collections are conducted for later recording in the laboratory, typically utilizing binocular magnifying glasses or microscopes. The soil flooding technique, although uncommon and often impractical in many places, involves saturating the soil with water to force soil pests to emerge for counting.

All the techniques in this capture method are non-selective, capturing both pests and beneficial organisms in the crops.

The method of estimation counting involves assessing the presence of predators or selective parasitoids of the targeted pest. To conduct this study, one estimates the number of individuals of the pest intended for sampling. Estimation can be accomplished through various means, including counting the number of exuviae or analysing herbivory traces.

For pests that can be sampled through trap catches, this is the most preferred counting method due to its simplicity of implementation.

Trap capture employs passive mechanisms to collect organisms, and for optimal results, attractants such as baits, artificial lights, or pheromones are used. However, a drawback of this method is the time needed for subsequent data collection and systematization. To automate data collection, traps can be equipped with sensors for pest detection, reducing the need for frequent trips to sampling sites. Despite their higher initial cost, in the long run, using these traps may prove advantageous.

Soon, there is a growing trend towards expanding sampling methods by incorporating traps with automatic detection sensors, as well as using remote sensing technologies, including unmanned aerial vehicles (UAVs).

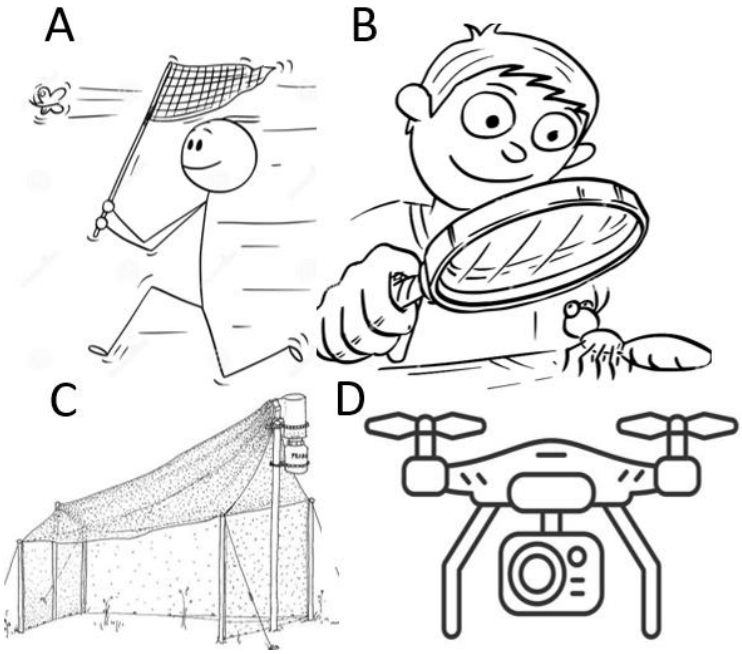

Figure 2. 2 - Counting methods Legend: A – Capture; B – Direct observation; C – Trap capture; D – Remote sensing.

Table 2. 6 - Sampling methods.

The last two columns are a comparison between the cost and the time required to sample with these methods.

Authors/Year	Counting method	Methods	Pests	Cost	Time
(McCravy, 2018)	Observation	Direct observation	Pests of reduced mobility	+	+ + +
(Pinto et al. (2017)	Observation	Magnifying Glass	*Frankliniella schultzei* (Thrips)	+	+ + +
(Shrestha et al., 2021)	Captures	Sweeping nets	*Hypera postica* (alfalfa weevil) and *Nabis* spp.	+	+ + +
(Seethalam et al., 2021)	Captures	Sweeping nets	*Helicoverpa armigera* (Moth)	+	+ + +
(Seethalam et al., 2021)	Captures	Shake method	*Helicoverpa armigera* (Caterpillar)	+	+ + +
(Dietrick, E.J., 1961)	Captures	Suction sampler	Small Insects	+ + +	++
(Weyman et al., 1995)	Captures	Suction sampler	Hemiptera and Hymenoptera orders	+ + +	++
(Gireesh et al., 2021)	Captures	Soil parcel collection	*Sphenophorus venatus vestitus* (Larvae)	+ +	+ +
(Panthi et al., 2021)	Captures	Collection of part of the plant	*Scirtothrips dorsalis* (Thrips)	+	+ +
(McCravy, 2018)	Captures	Soil Flood	Carabidae Staphylinidae families	++	+ + +
(López et al., 2012)	Trap Capture	Wireless sensor	Fruit insects	+ + +	+
(Woodcock, B.A.,2005	Trap Capture	Pitfall	Spiders, ants, Staphylinidae and Carabidae families	++	++
(Scaccini D.,2020)	Trap Capture	Pitfall	Carabidae family	++	++
(Gireesh et al., 2021)	Trap Capture	Pitfall	*Sphenophorus venatus vestitus* (Hunting billbug)	++	++
(McCravy, 2018)	Trap Capture	Vane traps	Flying insects	++	++
(McCravy, 2018)	Trap Capture	*Townes-style Malaise trap*	Flying insects	++	++
(McCravy, 2018)	Trap Capture	Sticky trap	Flying insects	++	++
(McCravy, 2018)	Trap Capture	Delta trap	Moths	++	++
(Couto et al., 2012)	Trap Capture	Chromotropic traps	*Bactrocera oleae* (Olive fruit fly)	++	++

(Noce et al., 2009)	Trap Capture	Pheromone trap	*Euschistus servus* and *Euschistus tristigmus*	++	++
(Cottrell et al. 2000)	Capture	Handpicking with Pheromones	*Murgantia histrionica* (harlequin cabbage bug)	++	+ + +
(Weber, D. C., 2014)	Trap Capture	Artificial light	Insects with nocturnal activity	+ + +	++
(Kim et al., 2019)	Estimation	Herbivory Estimation	Herbivore pests	++	++
(Kozlov et al., 2020)	Estimation	Estimation by Parasites	*Rhyacionia frustrana* (Moth)	++	++
(Silva et al., 2018)	Estimation	Herbivory Estimation	*Helicoverpaspp. and Spodoptera frugiperda* (caterpillar)	+	+++
(McCravity & Berisford, 2001)	Estimation	Predator Estimation	*Galleria mellonella* (Larva)	++	++
(Rijal et al., 2014)	Estimation	Exuviae count	*Vitacea polistiformis* (grape root borer)	+	+ + +
(Trufelea et al., 2021)	Remote Detection	UAV – RGB Sensor	Pentatomidae famaly	+++	+
(Vanegas et al., 2018)	Remote Detection	UAV - Hyper Spectral Sensor	*Phylloxera vastatrix* (Grape phylloxera)	+++	+
(Sorbelli et al., 2022)	Remote Detection	UAV – RGB Sensor	*Halyomorpha halys* (Brown marmoreted stink bug)	+++	+

2.2.2. Data Modelling and Geostatistics

The data collected during sampling must undergo modelled to identify patterns and correlations with meaningful implications for the user. Data modelling is also crucial for constructing predictive models, which play a vital role in supporting future decisions (Silva, 2008).

Methodologies employed for data modelling include the evaluation of frequency distributions, dispersion analysis, analysis of variance and covariance, and regression analysis, among others (Lawal, 2014). Table 2.9 summarises articles published between 2014-2022 that discuss the statistical and geostatistical approaches used for pest monitoring, specifying the sampling technique, location, and associated crop.

Based on the identified articles, the approach typically initiates with a descriptive analysis of the data, as exemplified in Table 2.7. This is followed by spatial modelling, involving the creation of an interpolation map and subsequent validation. The overall goal is to generate risk maps, serving as predictive models for monitoring key pest.

In the prevalent spatial modelling approaches, georeferenced data is modelled using a variogram function. Table 2.8 provides examples of variogram models and associated

parameters, as used by Rijal et al., (2014) for modelling the counts of *Vitaceae polistiformis* exuviae in vineyard plots in the Virginia state, USA.

Following this, maps are constructed, such as those depicted in Figures 2.3 and 2.4. These maps are created through Kriging, a geostatistical estimator enabling the prediction of a random variable in an unsampled location based on the known neighbouring values.

Subsequently, a validation test is performed to estimate the estimation error and evaluate the quality of the produced map. Figure 2.4 shows the cross-validation test, involving the estimation without the value of a known location, and subsequently comparing the estimated value with the known value to access the quality of the estimation (Hohn, 1991).

Table 2. 7 - Descriptive statistics of the count of *Anastrepha ludens*, in Tamaulipas, Mexico.

Year	Average	Median	Variance	Standard deviation	Coef. Skewness
2008	0.1944	0.0606	0.2024	0.4101	4.6021
2009	0.3689	0.1569	0.8009	0.66	3.5637
2010	0.1132	0.0084	0.1651	0.3248	5.3228
2011	0.1295	0.0252	0.1161	0.2719	3.905

Adapted from (Vanoye-Eligio et al., 2015)

Table 2. 8 - Variogram models and parameters of the distribution of exuviae of *Vitacea polistiformis* in vineyard plots.

Legend: **RSS** - residual sum of squares; **C0** - nugget; **C0+C** - threshold; **C0/C0+C** - threshold nugget ratio; **AF** - anisotropy factor; **Nu** - nugget model; **Ex** - exponential model; **Sp** - spherical model; **Li** - linear model. *Adapted from (Rijal et al., 2014).*

Plot	Average exuvia per vine ± error	Range (m)	Model	r^2	RSS	Active lag (m)	C_0	C_0+C	C_0/C_0+C	F
A	2.34±0.26	7.5	Ex.	0.56	0.149	37.65	0.37	3.38	0.109	.99
B	1.94±0.36	13.58	Sp	0.96	0.0017	34.21	0.045	0.632	0.071	.99
C	6.40±0.55	7.44	Sp	0.73	0.0003	35.81	0.038	0.43	0.088	.94
D	1.10±0.16	8.21	Sp	0.74	0.0013	43.42	0.05	0.382	0.131	.99
E	0.88±0.14	-	Li	0.02	0.027	43.42	0.965	0.997	0.968	
F	0.41±0.99	-	Nu	0.8	0.002	35.81	0.198	0.198	1	
G	0.43±0.09	-	Nu	0.64	0.0028	43.42	0.172	0.172	1	
H	0.49±0.09	7.24	Sp	0.35	0.0024	44.74	0.038	0.203	0.188	
I	0.73±0.11	-	Nu	0.47	0.0006	35.81	0.272	0.272	1	

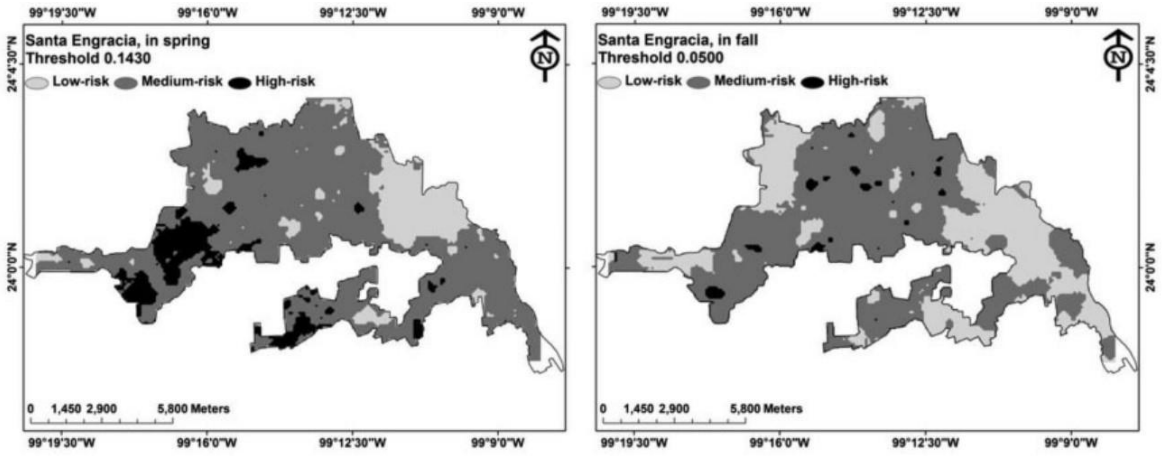

Figure 2. 3 - Maps depicting the risk of Anastrepha ludens occurrence in Tamaulipas, Mexico. Adapted from (Vanoye-Eligio et al., 2015)

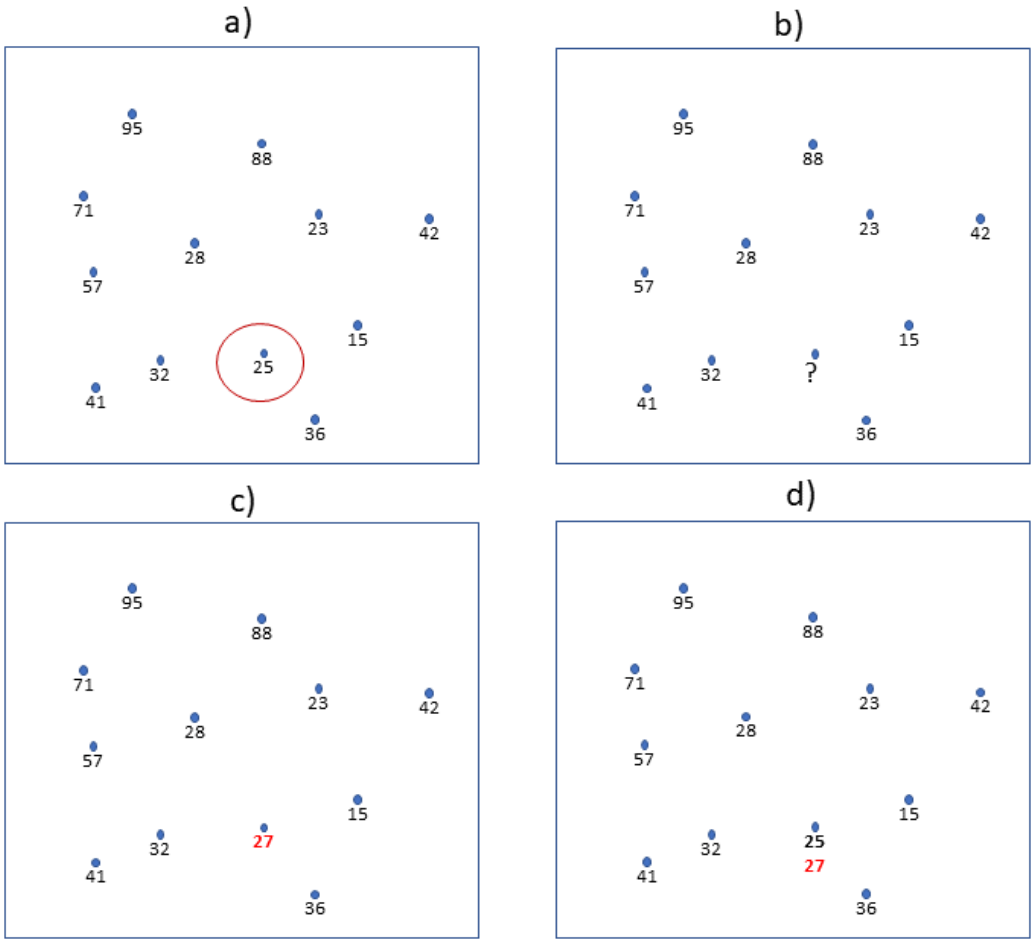

Figure 2. 4 - Schematic exemplification of the cross-validation test. Adapted from (Hohn, 1991)

Table 2. 9 - Studies using geostatistical models

Authors/Year	Location	Pests	Crop	Methods	Statistical approach
(Seethalam et al., 2021)	Hanamkonda, India	*Helicoverpa armigera* (caterpillar)	*Cajanus cajan* (Pigeon pea)	Direct observation	•Analysis of variance (ANOVA); •Variogram; •Kriging interpolation; •Interpolation by Voronoi diagrams; •Cross-validation with (RMSE);
(Shrestha et al., 2021)	Montana, USA	*Hypera postica (alfalfa weevil)*	*Medicago sativa* (Alfalfa)	Sweeping nets	•Variogram; •Estimation by the index root mean square error spatial analysis by distance indices (SADIE);
(Gireesh et al., 2021)	Geórgia, USA	*Sphenophorus venatus vestitus (Larvae)*	Grass	Soil extraction for larvae Pitfall for adults	•Variogram; •Estimation by SADIE; •Kriging interpolation;
(Pereira et al., 2020)	Tocantins, Brasil	*Frankliniella schultzei* (Thrips)	*Citrullus lanatus* (Watermelon)	Direct observation	•Variogram; •Cross-validation; •Level of spatial dependence (LSD);
(Panthi et al., 2021)	Florida, USA	*Scirtothrips dorsalis (Thrips)*	*Vaccinium myrtillus* (Blueberry)	Shoots colection	•Taylor's power law (TPL); •Poisson distribution; •Negative binomial distribution; •Estimation by SADIE; •Lloyd's patchiness;
(Grabarczyk et al., 2022)	Geórgia e Flórida, USA	*Euschistus servus e Euschistus tristigmus*	Variuos crops	Pheromone baited trap	•Analyse of generalised linear mixed-effect models; •Estimation by SADIE; •Interpolations;
(Pereira et al., 2020)	Tocantins, Brasil	*Bemisia tabaci* (whitefly)	*Citrullus lanatus* (Watermelon)	Direct observation	•Variogram; •Kriging interpolation; •Cross-validation test
(Sciarretta et al., 2018)	Roma, Itália	*Ceratitis capitata* (Mediterranean fruit fly)	*Prunus persica* (Peach)	Pheromone baited trap	•Pearson correlation; •Analysis of variance (ANOVA); •Games-Howell post-hoc test; •Omnidirectional variogram; •Kriging interpolation;

(Vanoye-Eligio et al., 2015)	Tamaulipas, México	*Anastrepha ludens* (Mexican fruit fly)	*Citrus sinensis* (orange) Citrus *paradisi* (grapefruit) Citrus *reticulata* (tangerine)	Baited trap	•Variogram; •Kriging indicator interpolation; •Production of regional risk map;
(A. V. Ribeiro et al., 2021)	Minas Gerais, Brazil	*Bemisia tabaci* (whitefly)	*Solanum lycopersicum* (tomato)	Adults - Shake method Nymphs - Direct observation	•Evaluation of LSD; •Variogram; •Ordinary Kriging interpolation; •cross-validation test;
(Rijal et al., 2014)	Virgnia, USA	*Vitacea polistiformis* (grape root borer)	*Vitis spp* (Vineyard)	Exuviae count	•*Taylor's power law*; •Variogram; •Estimation by SADIE; •Kriging interpolation;
(Silva et al., 2018)	Cajuri, Brasil	*Helicoverpasp p. and Spodoptera frugiperda* (Caterpillar)	*Zea mays* (Maize)	Herbivory Estimation	•Evaluation of the degree of spatial dependence (DSD); •Variogram; •Kriging interpolation; •Cross-validation test with residual sum of squared errors (RSSE);

3. Materials and methods

3.1. Location

This study was carried out in the Emilia-Romagna (ER) area, the northern region of Italy, as shown in Figure 3.1.

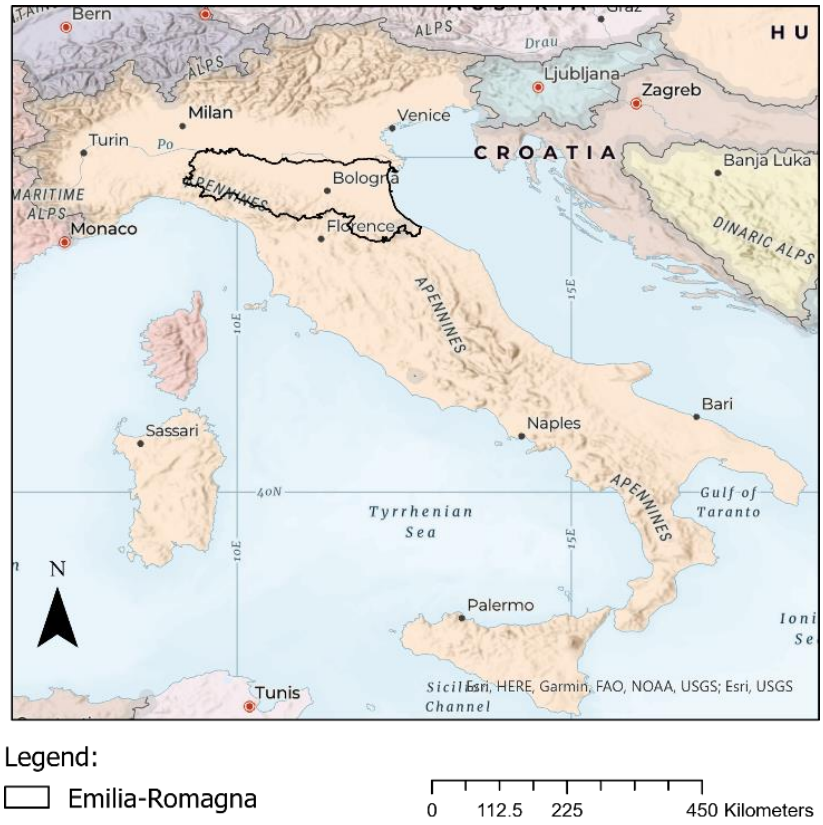

Figure 3. 1 - Emilia-Romagna location

The northern portion of this region consists of a vast plain that stretches from the Po River to the Apennine Mountains, as depicted in Figure 3.2. This plain is characterised by intensive farming, with primary crops including pears (*Pyrus communis*), wine grapes (*Vitis vinifera)*, cherry (*Prunus avium)*, apple (*Malus domestica)*, apricot (*Prunus armeniaca)*, and peach (*Prunus persica)*. Additionally, row crops such as alfalfa (*Medicago sativa*), soybean (*Glycine max*), sorghum (*Sorghum bicolor*), sunflower (*Helianthus annuus*), maize (*Zea mays*), and wheat (*Triticum aestivum*).

The orchard borders are typically surrounded by hedges containing a mix of shrubs and trees, including wild species such as *Prunus spp., Acer spp., Fraxinus spp., Cornus spp., Rhamnus frangula, Corylus avellana, Ligustrum spp., Morus spp., Ailanthus altissima,*

Elaeagnus rhamnoides, Viburnum spp., Carpinus spp. and Ulmus spp. (Maistrello et al., 2017).

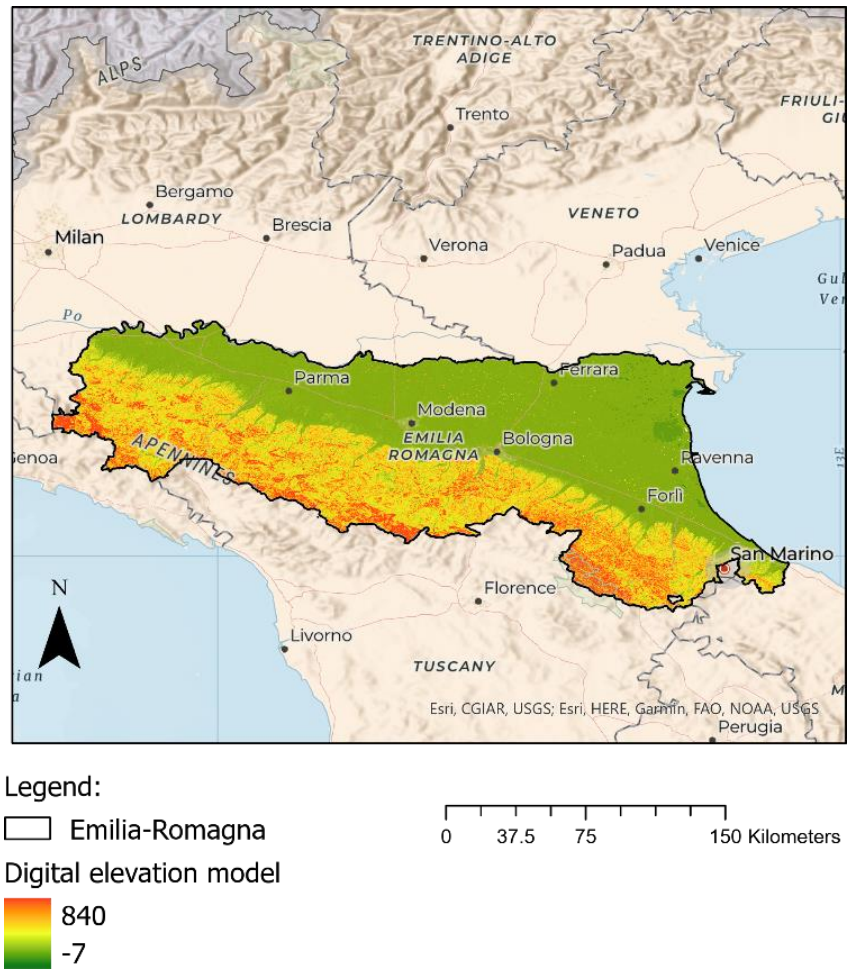

Figure 3. 2 - Digital elevation model of Emilia-Romagna

3.2. Data Collection

3.2.1. BMSB data

Between the years of 2020 and 2022 in the ER region, BMSB were collected every week from March to October using pheromone-baited traps scattered throughout the region, as shown in Figure 3.3. The number of traps changed every year, and the timepoints varied, as indicated in Table 3.1.

The collected data was subsequently divided into three classes: Small for the second and third instars, Large for the fourth and fifth instars, and Adults for adults.

Tabler 3. 1 Number of traps and timepoints (weeks) per year

Year	*Traps*	*Timepoints*
2020	139	24
2021	165	32
2022	101	29

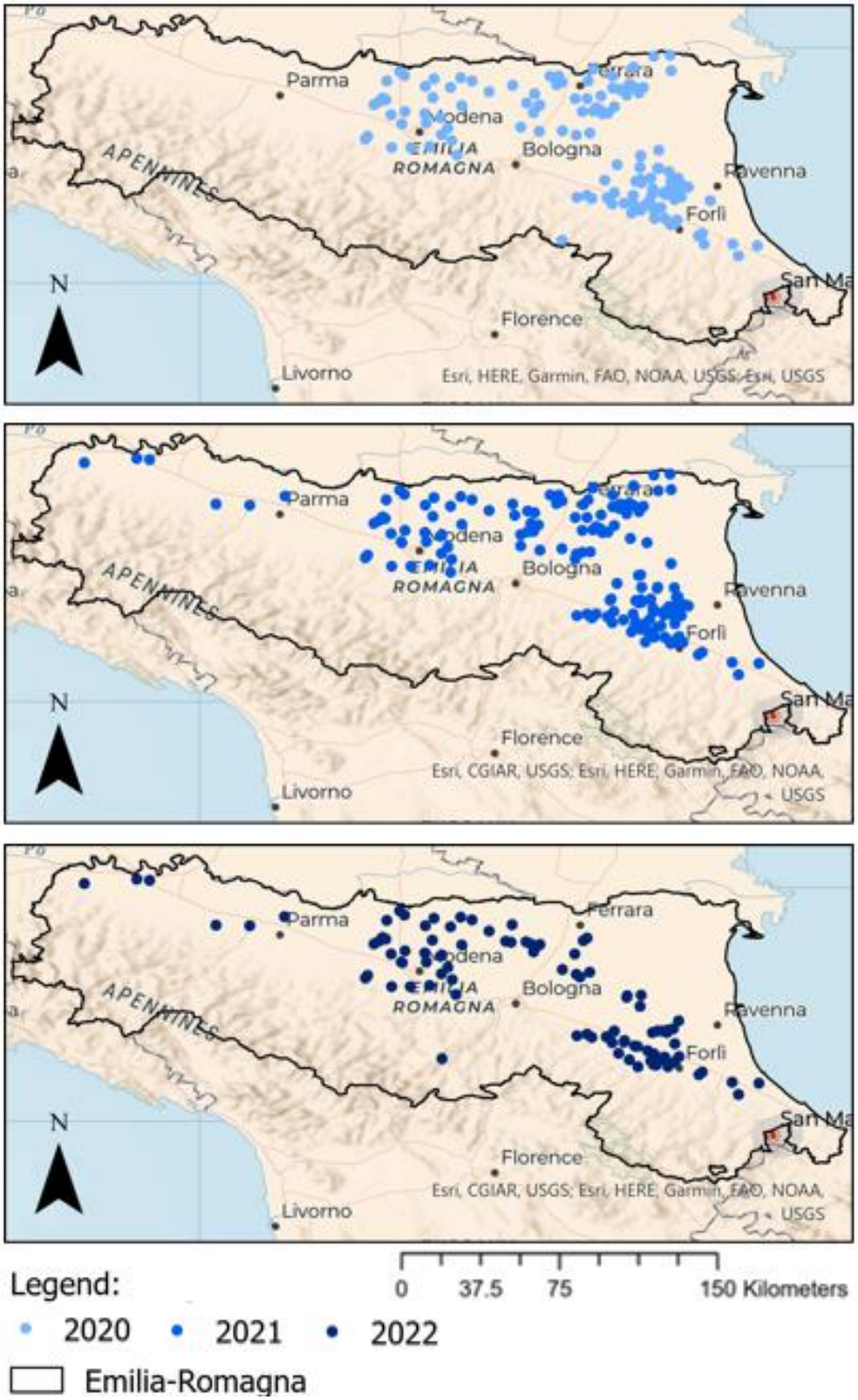

Figure 3. 3 - Location of pheromone baited traps in 2020, 2021 and 2022.

3.2.2. Meteorological data

Figure 3.4 illustrates the ER region, where several meteorological stations are situated, operated by the L'Agenzia regionale per la prevenzione, l'ambiente e l'energia dell'Emilia-Romagna (ARPAE).

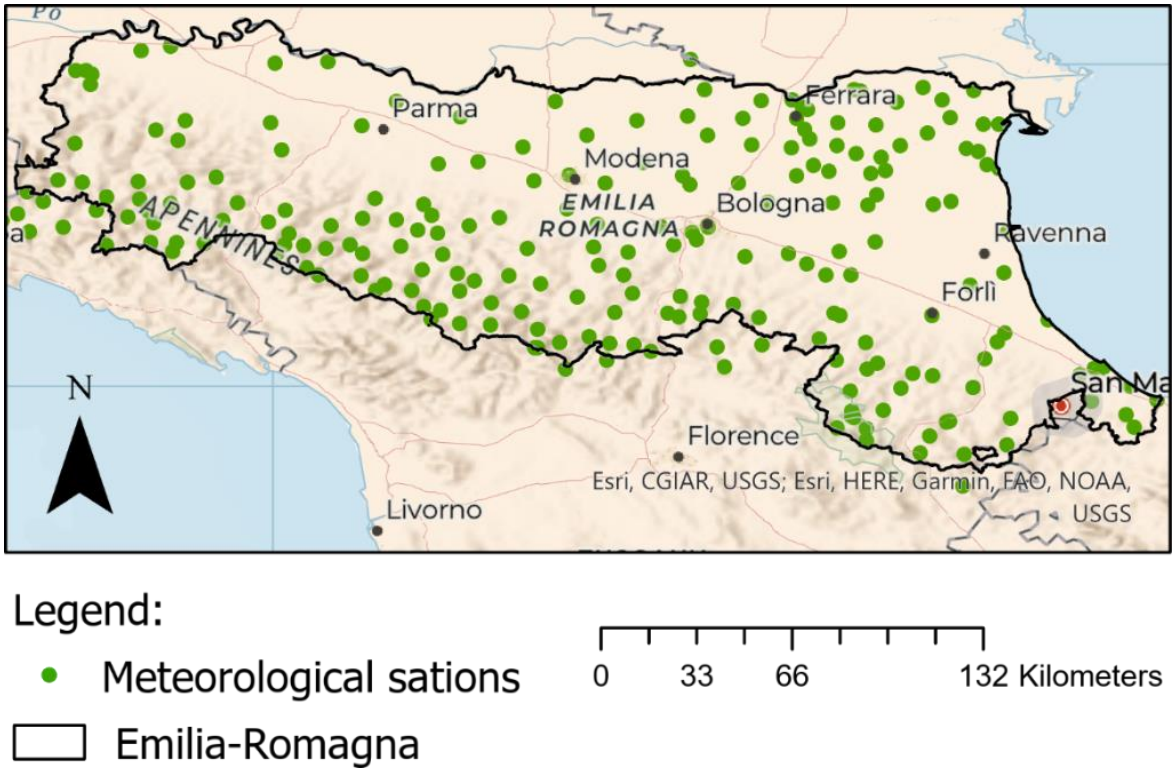

Figure 3. 4 - Location of the ARPAE meteorological stations.

3.2.3. Haly.ID sensors data

In the ER region near Carpi, Modena is located the Haly.ID experimental orchard. Within this pear orchard, several sensors collect data on different parameters, including temperature, humidity, light intensity, pressure, wind speed, and leaf wetness.

These sensors are housed in 3D printed Stevenson screen, powered by batteries with a lifespan of two years. The data is transmitted via a ZigBee network from the sensors to a central node box connected to the main power and the internet. Lastly this data reaches the *InfluxDB* website. The assembly and deployment of these devices are part of the Haly.ID project and are being developed by the partner *Technische Universität Braunschweig*,

Germany. These sensors are positioned at various heights on the trees, as illustrated in Figure 3.6.

From the data collected by the Haly.ID sensors, the temperature and humidity parameters were selected due to their potential impact on the BMSB life cycle.

These two parameters were recorded with the sensor sht3x for every four bridges of the Raspberry Pi *Fritz*, *Halyid-pi-01*, and *Heinz* and one bridge of the Raspberry Pi *Igor*. The positions of the mentioned Raspberry Pi devices are displayed in Figure 3.5 below.

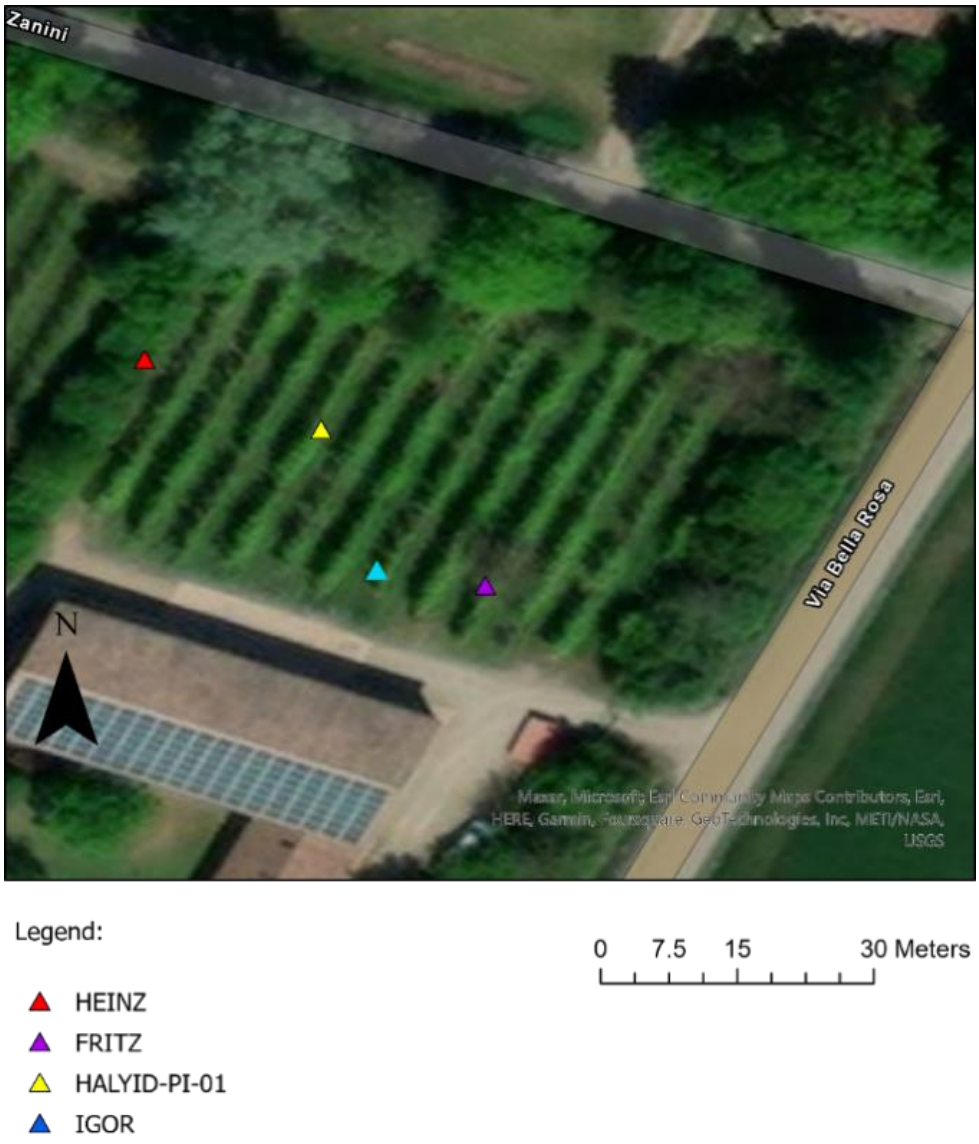

Figure 3. 5 - Raspberry Pi Positions in the Haly.ID experimental orchard

Figure 3. 6 - Different sensor heights on trees in the Haly.Id experimental orchard in the red circles in the pear tree

3.3. Data Analysis

3.3.1. BMSB Exploratory Data Analysis

To understand the type of data collected, an exploratory data analysis was conducted, involving the following steps:

1. Univariate Analysis: Examination of individual variables to provide insights into their distributions and characteristics.

2. Bivariate Analysis: The Pearson correlation was calculated between consecutive weeks' data to assess if there was a correlation between them.
3. Declustering by Moving Averages for Variogram Calculation and Simulation: As data locations mix close samples and sparse samples, the data were subjected to declustering using moving averages. This process aimed to enhance variogram calculation prior geostatistical simulations.
4. Adjustment to Exponential and Gompertz Functions: Attempts were made to fit exponential and Gompertz functions to the data. However, a unique function or model to explain all data was not employed due to the spatial irregularity nature of the data.
5. Variograms for Small, Large, and Adults Data: Variograms were constructed for the Small, Large, and Adults data sets. Variograms provide insights of the spatial variability and patterns within the data.
6. Build of a Space-Time Model: Geostatistical simulation was utilized to build a model of counts for the Small, Large, and Adults data sets over both space and time. This approach allows for the creation of a predictive model considering both spatial and temporal aspects of the data.

3.3.2. BMSB data

The data collected in the field underwent several preprocessing steps. Initially, the data was transformed and organized chronologically. The dates for each week were converted from the reference of the last day of that week to the number of weeks of the year (WOTY).

Subsequently, the data was segregated based on their class (Small, Large, and Adults) and the trap identification number, along with their associated geographic coordinates. The BMSB data were evaluated to understand the efficiency of the traps and identify weeks with missing values.

Then, the coordinates of the traps were transformed from geographic coordinates to projected coordinates, and the *Monte Mario TM Emilia-Romagna* projected coordinates system was chosen. Within the boundaries of ER, a polygon with an area of 663,746 hectares was defined as the study area, as illustrated in Figure 3.7. This step aimed to reduce the

extrapolation area, and the defined area was chosen by selecting the region where the majority of traps were located.

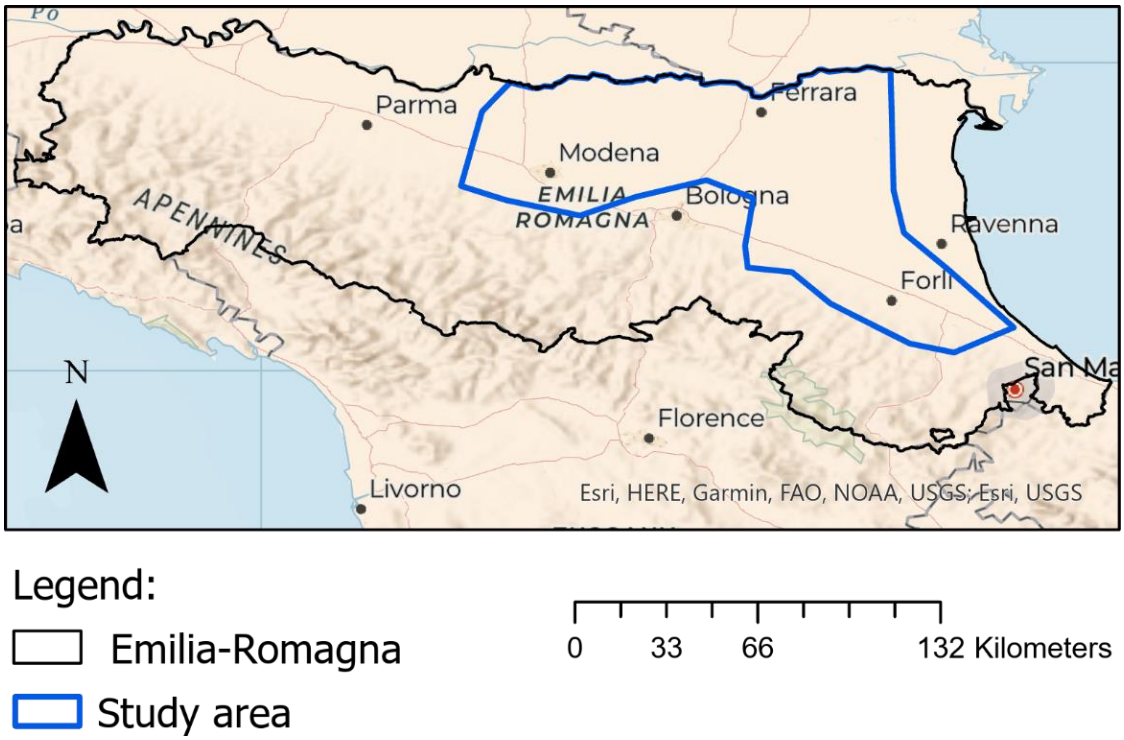

Figure 3.7 - Defined study area in Emilia-Romagna

3.3.2.1. Theoretical Foundations of Geostatistics

3.3.2.1.1. Variography

Variography is a fundamental tool in geostatistics, playing a crucial role in quantifying the spatial continuity of a variable for estimation and simulation purposes (Isaaks & Srivastava, 1989; Goovaerts, 1997; Smith, 2006). To prevent the propagation of errors in subsequent phases, a thorough understanding of the data and the influence distance of each data location is essential. Therefore, a meticulous analysis of basic statistics is necessary, with a particular focus on extreme or erratic values, as each value carries significant weight and has the potential to influence experimental variograms.

In geostatistical practice, the spatial continuity of a variable is assessed across various distances and vector directions (or steps) using the semivariogram:

$$\gamma(h) \approx \frac{1}{2N(h)} \sum_{\alpha=1}^{N(h)} [Z(x_\alpha) - Z(x_\alpha + h)]^2$$

Where N(h) represents the number of point pairs for each step value. To analyse spatial continuity in different spatial directions using this tool, it is essential to test the results with multiple values of N(h) and for several directions.

Variography considers the following fundamental parameters (Goovaerts, 1997; Soares, 2006):

Range (a): This corresponds to the distance at which the variogram reaches a plateau (C). The plateau indicates the distance beyond which the samples are no longer correlated with each other. A higher range implies a more continuous behaviour, indicating a strong correlation for the variable.

Plateau (C): Reflects the intrinsic variance of the variable being studied, representing its spatial dispersion.

Nugget Effect (C0): This parameter corresponds to the variogram value at distances like the minimum sample spacing. Characterise small-scale variability and provide insight into erratic values resulting from external factors, such as insufficient sampling or high variability at a small scale. Ideally, for step (h) values close to zero, the variogram value should be zero as well.

Modelling a variogram involves using positive functions that account for different situations of spatial phenomenon dispersion (Soares, 2006). For instance, the spherical model, one of the most employed models, consists of two parameters: the plateau and the range (Ca).

$$\gamma(h) = \begin{cases} C\left[1{,}5\frac{h}{a} - 0{,}5\left(\frac{h}{a}\right)^3\right], & para\ h \leq a \\ C, & para\ h > a \end{cases}$$

And for the exponential model.

$$\gamma(h) = C_0 \left[1 - exp\left(-\frac{h}{a}\right)\right]$$

3.3.2.1.2. The Kriging Geostatistical Estimator

The geostatistical estimator, known as kriging, is a technique employed for predicting values at unsampled locations (Goovaerts, 1997; Soares, 2006). This method relies on known values from neighboring locations to make accurate predictions. Kriging involves calculating weights for the known samples to achieve an unbiased estimation and minimize the variance of the estimation error, commonly referred to as the BLUE (Best Linear Unbiased Estimator) estimator. The kriging process can be represented as follows (ordinary kriging):

$$[Z(x_0)]^* = \sum_{\alpha=1}^{n} \lambda_\alpha . Z(x_\alpha)$$

3.3.2.1.3. Geostatistical simulation and direct sequential simulation

Geostatistical simulation, including direct sequential simulation, aims to generate virtual representations of reality that capture the characteristics of the variable or phenomenon studied, along with the variability observed in the sample data, the distribution law of the variable under study, and its spatial continuity. These models produce a set of equiprobable images, each exhibiting the same spatial variability as the experimental data evaluated through the variogram. Therefore, all images reproduce the same statistics of spatial variability, such as the histogram and variogram or spatial covariance, as quantified by the samples (Soares, 2006).

Unlike kriging estimation, geostatistical simulation does not aim to obtain a single most probable image of the characteristics of a specific resource. Instead, it generates a collection of equiprobable images that exhibit the same spatial variability as the experimental values. Local uncertainty is assessed on the basis of the local variability observed in the simulation results. This set of images also allows for the visualisation of extreme behaviours in the internal or morphological characteristics of a natural resource and

simultaneously quantifies the uncertainty associated with the spatial distribution of these characteristics.

It is noteworthy that in this study, simulation was chosen over kriging due to its superior capability to handle strings of data, particularly sparse spatial data and regularly recorded time intervals. Additionally, simulation allows for the effective imposition of counts for each time slice within the space-time model. Among geostatistical simulation methods, Direct Sequential Simulation (Soares, 2001) stands out for its straightforward and efficient integration of week averages for counts.

3.3.2.2. Spatial-temporal model

For every year a spatial-temporal model was built, with the counts from the Small, since this class was the one with more spatial continuity.

Stochastic simulation of images for the variables studied was performed using the Direct Sequential Simulation (DSS) method, considering the experimental data, variograms, and distribution laws obtained by ordinary kriging (ungrouped distribution laws).

In a generic representation, the DSS method can be summarised in the following steps (Soares, 2001):

a) Choose a random sequence of nodes from a regular mesh that allows all nodes to be visited.

b) For each node: x_u

c) Simulation of the value of: $z^s(x_u)$

   i) Perform a simple ordinary kriging estimation to determine the mean $z^*_{sk}(x_u)$ and variance $z^*_{sk}(x_u)$ of the variable $z(x)$ at that location x_u. Resample the histogram of the variable locally, $z(x_u)$, using techniques such as the Gaussian transformation applied to the working variable.

   ii) Calculate the auxiliary variable, z(x), which represents the transformed variable (for *example, applying the equation* $y^*(x_u) = \varphi(z^*(x_u))$.

   iii) Generate a random number p from a uniform distribution, denoted *U (0,1).*

   iv) Generate a value, denoted as y^s, from $G(y^*(x_u),\ \sigma^2_{sk}(x_u))$:

$$y^s = G^{-1}(y^*(x_u), \sigma_{sk}^2(x_u), p)$$

v) Compute the simulated value of the primary variable, $z^s(x_u)$ by applying the inverse of the function, denoted as. $\varphi^{-1}(y^s)$.

By following these steps, the DSS method enables the stochastic simulation of images for the primary variable, considering the conditioning of the experimental data, variograms, and distribution laws obtained through ordinary kriging.

3.3.3 Meteorological data

The data collected were from the following parameters: precipitation, irradiance, temperature, relative humidity, wind direction, and wind speed. These parameters were analysed to understand whether they have any correlation with the BMSB numbers across the region of the ER and in time. These data were downloaded by hourly average from selected meteorological stations (Figure 3.8), located inside or in the vicinity of the study area and have readings of these parameters.

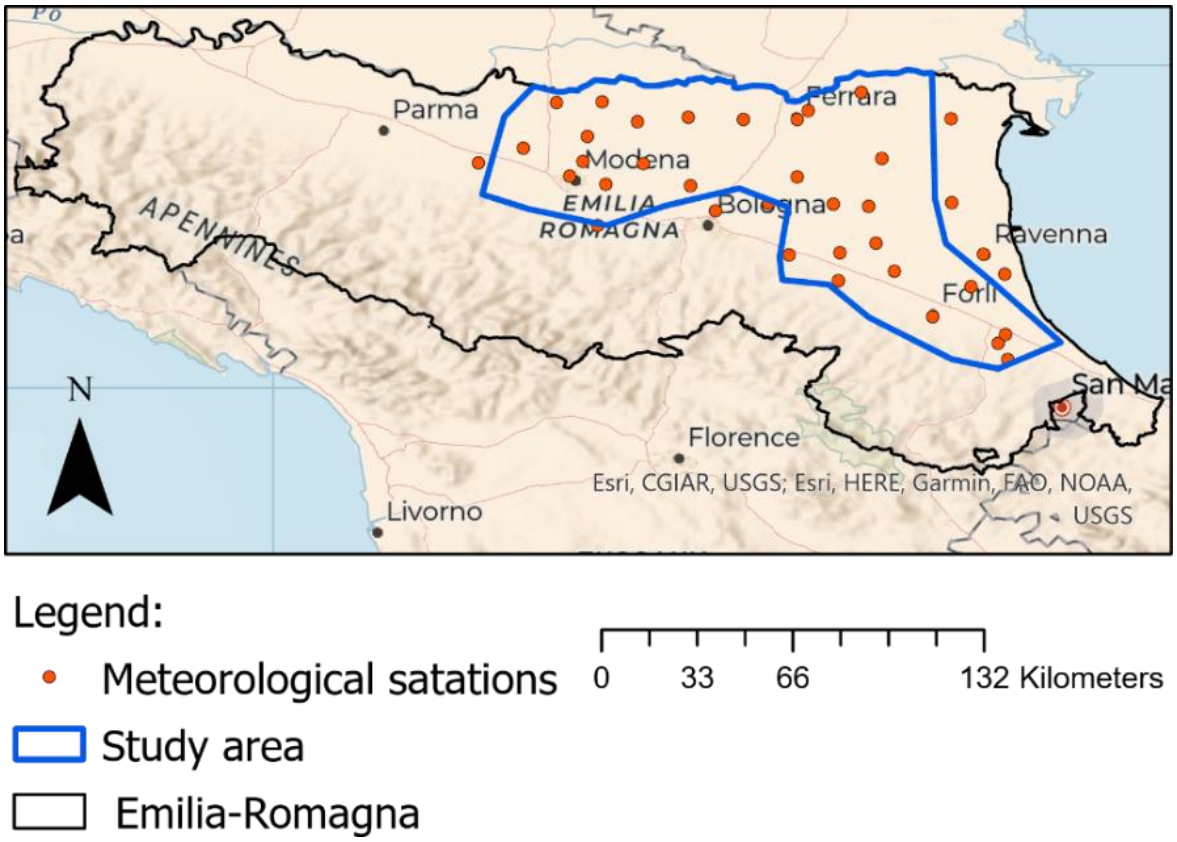

Figure 3. 8- Location of the selected meteorological stations

3.3.3.1. Degree Days

From the parameter temperature, Degree Days (DD) were calculated. The selected DD were $DD_{12,97}$ as the lower threshold is 12.97°C. This value was used by Haye (2014) in Switzerland, and it closely aligns with the average lower thresholds found in the literature for the full development of BMSB. For the higher threshold, the selected value was 36,5ºC, consistent with value used by Haye (2014).

The calculation of degree days (DD) involved considering values above the lower threshold and below the higher threshold for each hour, subsequently transforming them into daily averages. Due to missing temperature data on certain days and stations, daily DD also had missing values. To address this, missing values were replaced with the daily average from all other stations for that specific day. This process was repeated for each day with missing data.

The next step was to accumulate DD values to identify significant time points in the BMSB life cycle. DD accumulation began at the end of diapause, using a photoperiod threshold as a biofix, as mentioned earlier.

The determination of this biofix was based on unpublished data from Costi et al. (2017) and Lara Maistrello (unpublished data) collected between 2015 and 2018 in Reggio-Emilia, under conditions similar to those expected in the field. Oviposition dates were evaluated, and by subtracting the required DD from diapause termination to oviposition, the new date of diapause termination was obtained. Using data from timeanddate.com, the photoperiod for that location at those time points was determined. Finally, literature values regarding the accumulation of DD needed to complete life stages were normalized to fit $DD_{12,97}$.

3.3.3.1. Cumulative DD spatial-temporal model - 2021

A spatial-temporal model for cumulative degree days was constructed for the year 2021. Temperature data from ARPAE were converted into Degree Days (DD), and these DD were further transformed into a cumulative DD function, with one function for each meteorological station and a time interval of one week. The initiation of DD accumulation was set at 14 hours of the photoperiod.

The model was created using the *Leapfrog Geo software*, and the interpolation function employed was a radial basis function (RBF).

3.3.4. Haly.ID sensors data

The temperature and humidity data were retrieved from *InfluxDB*, a platform storing data from Haly.ID sensors, since their deployment on 17-06-2022 at hourly intervals, representing the hourly average values. The data were organized into two tables: one for 2022 (from 17-06-2022 to 31-10-2022) and another for 2023 (from 01-04-2023 to 31-07-2023).

To comprehend the distinctions in climate conditions, considering both macroclimatic conditions in the broader region and microclimatic conditions in the orchard's proximity, meteorological stations nearby were selected (as depicted in Figure 3.9).

Although *Correggio* is the closest station, *Modena Urbana* and *Cortile di Carpi* were also considered due to their similar distances. The sensors were categorized by their height in the tree canopy.

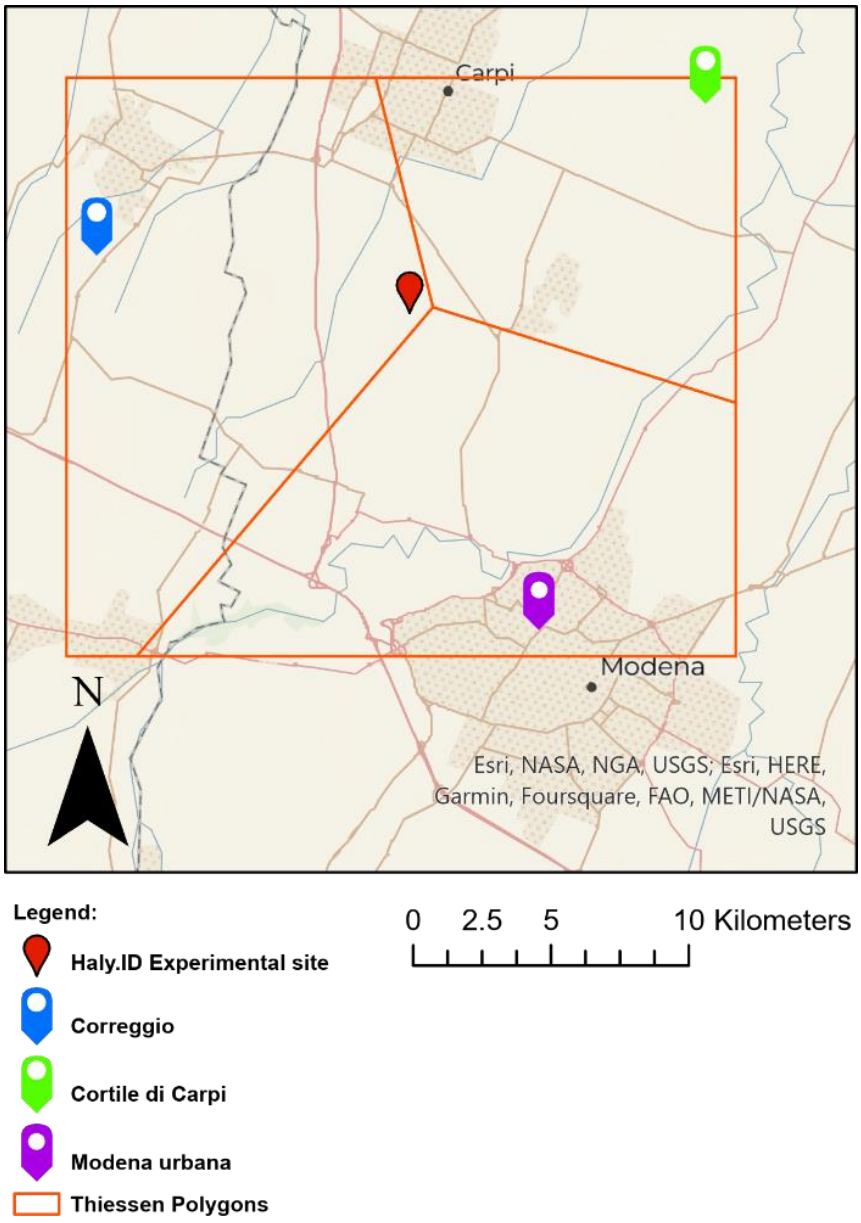

Figure 3. 9 - Selected meteorological stations in the vicinity of the experimental orchard Haly.Id

An assessment of the differences between the sensors and the meteorological stations was conducted. In the Cumulative DD spatial-temporal model of 2021, the temperature from the meteorological stations was used to define DD accumulations.

To understand the divergence between DD accumulations from meteorological stations and microclimatic conditions, accounting for the BMSB's high mobility, the optimal location for DD accumulation was determined for each hour. Subsequently, the variance between this optimal location and the meteorological stations was evaluated.

4. Results

4.1. BMSB Exploratory Data Analysis

4.1.1 BMSB efficiency

The exploratory data analysis initially focused on assessing BMSB data to gauge the effectiveness of traps over the three years under consideration: 2020, 2021, and 2022. As illustrated in Figure 4.1, the charts depict the percentage of active traps, responsible for BMSB counts, for each of the specified years. The number of active traps consistently comprised 86-90% of the total, with the inactive traps constituting 10-14%. This data underscores that the majority of the traps were actively engaged and counting BMSB, indicating a high level of operational efficiency.

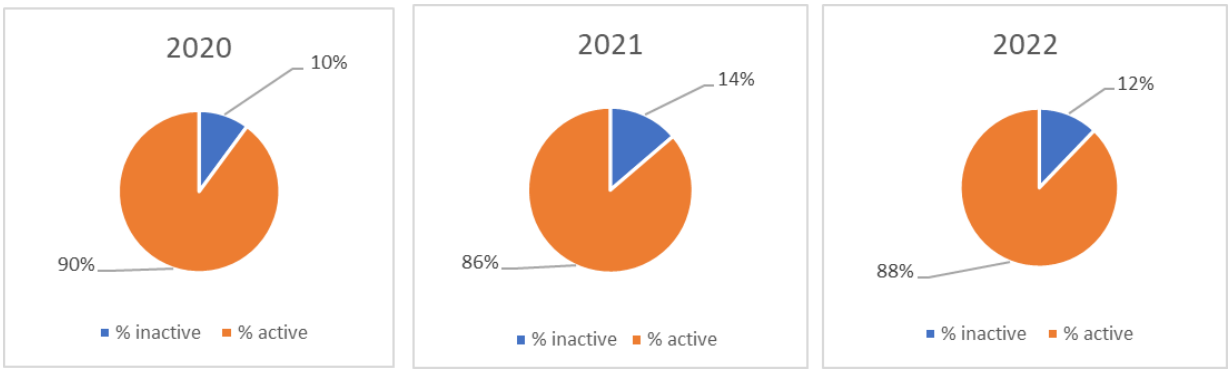

Figure 4.1 - Assessment of Trap Efficiency: Three-year breakdown indicating the percentage of traps that were inactive, assuming they were "off," and the percentage of active traps for the years 2020, 2021, and 2022.

4.1.2. Yearly distribution of BMSB counts

The temporal abundance of BMSB counts over weeks on each trap is illustrated in Figure 4.2, where the overall trend (average counts) is depicted by a bold black line. The graphs pertain to the years 2020, 2021, and 2022 for both Smalls and Adults. Observing the temporal distribution and the overall trend, it is evident that Adults appear first, followed by Smalls, and persist later.

For instance, taking the year 2021 as an example in Figure 4.2-C (Smalls) and Figure 4.2-D (Adults), the initial point of an upward trend in the global tendency curve for Adults-D (1) precedes the corresponding increase in Smalls-C (1). Similarly, D (2) is observed before C (2), and finally, D (3) aligns with the last count increase in Adults. This pattern aligns consistently with what was described in Chapter 2.1.3.1, specifically regarding the

life cycle outlined in the literature review. The two peaks seen in all Smalls graphs, Figure 4.2 A, C and E – peaks (1) and (2), are associated with the appearance of F1 and F2 generations. Additionally, in Adults Figure 4.2 B, D and F, the first peak (1) corresponds to overwinter generation, peak (2) is F1, and peak (3) is F2 generations.

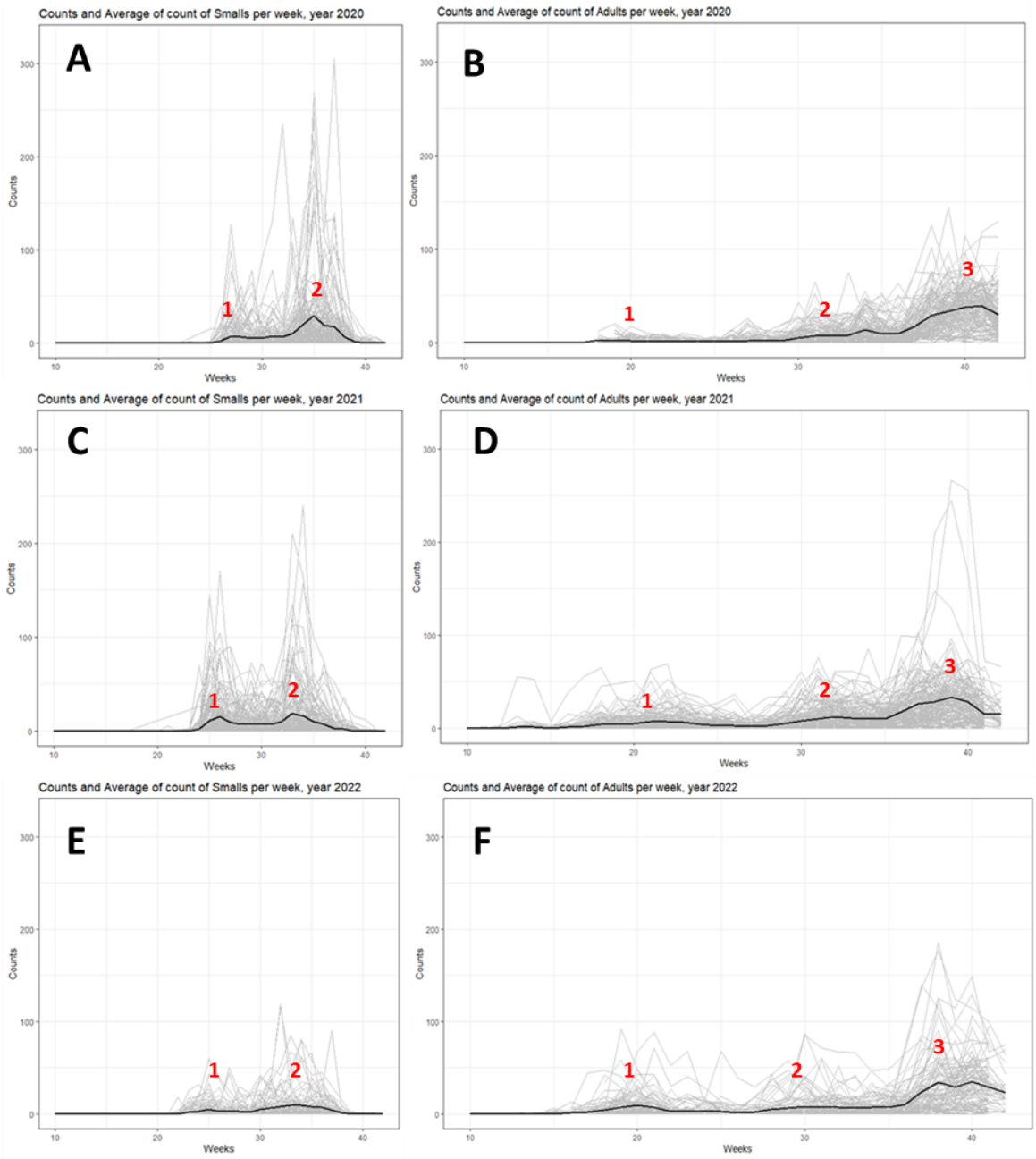

Figure 4.2 - Counts from each trap and the corresponding averages are depicted in the figures. Image A and B represent the weekly counts of Smalls and Adults for the year 2020, respectively. Images C and D correspond to the weekly counts of Smalls and Adults for the year 2021, while Images E and F illustrate the weekly counts for 2022. The x-axis indicates time in weeks, while the y-axis represents the counts.

4.1.3 Univariate analysis

To enhance our comprehension of the collected data in terms of average, dispersion, and skewness, a univariate exploratory data analysis was undertaken. This analysis focused on the years 2020, 2021, and 2022, examining descriptive analysis parameters derived from the BMSB database, as detailed in Table 4.1. The results are categorized by Adults, Small, and Large. Additionally, the findings are presented in two sets: one labelled "All data," displaying results inclusive of all values, including "zero" counts; and a second set, "Non-Zero data," which recomputes these univariate statistics while excluding zero values. Upon assessing the parameters for these distinct datasets ("All data" and "Non-Zero"), it is evident that even when excluding null values, the "All data" dataset exhibits a high degree of variability.

Table 4.1 - Exploratory univariate data analysis from BMSB counts (MV-Missing Values)

Statistics		2020			2021			2022		
		Adults	Small	Large	Adults	Small	Large	Adults	Small	Large
All data	Count	3 475	3 475	3 475	5 445	5 445	5 445	3 030	3 030	3 030
	Minimum	0	0	0	0	0	0	0	0	0
	Maximum	145	305	66	266	240	68	186	119	79
	Median	3	0	0	2	0	0	2	0	0
	Mean	10.76	5.75	2.13	8.47	4.27	1.47	9.18	2.77	1.25
	Count without MV	3 123	3 123	3 123	4 696	4 696	4 696	2 660	2 660	2 660
	Count of MV	352	352	352	749	749	749	370	370	370
	Count of zeros	941	2 045	2 101	1 651	3 307	3 602	990	1 875	2 075
	Standard deviation	17.63	18.76	5.09	15.61	13.18	4.67	17.70	8.23	4.47
	Coefficient of variation	1.64	3.26	2.39	1.84	3.08	3.18	1.93	2.98	3.56
	Skewness	2.46	7.49	4.35	5.13	6.57	6.02	3.56	6.07	7.56
	Kurtosis	7.33	76.66	28.03	53.72	66.56	49.48	17.84	53.17	82.11
	Variance	310.5	351.8	25.9	243.8	173.8	21.8	313.3	67.8	19.9
Non zero data	Count	3 475	3 475	3 475	5 445	5 445	5 445	3 030	3 030	3 030
	Minimum	1	1	1	1	1	1	1	1	1
	Maximum	145	305	66	266	240	68	186	119	79
	Median	7	7	4	7	7	4	6	5	3
	Mean	15.39	16.66	6.50	13.07	14.45	6.31	14.62	9.37	5.70
	Count without MV	2 182	1 078	1 022	3 045	1 389	1 094	1 670	785	585
	Count of MV	1 293	2 397	2 453	2 400	4 056	4 351	1 360	2 245	2 445
	Count of zeros	-	-	-	-	-	-	-	-	-
	Standard deviation	19.32	28.95	7.13	17.78	20.99	7.94	20.49	12.96	8.09
	Coefficient of variation	1.26	1.74	1.10	1.36	1.45	1.26	1.40	1.38	1.42
	Skewness	2.01	4.74	2.83	4.63	3.96	3.22	2.90	3.65	4.00
	Kurtosis	4.92	29.80	12.37	43.88	24.54	13.77	12.00	19.07	22.49
	Variance	373.1	837.4	50.8	315.9	440.3	63.1	419.5	167.7	65.3

4.1.4. Bivariate correlations

To assess the anticipated quality of variograms over time, Pearson's correlations were computed between data of consecutive weeks for BMSB Smalls, Large, and Adults across the three years. These correlations serve as initial indicators of the potential to construct robust variograms. As illustrated in Figures 4.3, the obtained correlations are notably strong, reinforcing the likelihood of establishing effective variograms.

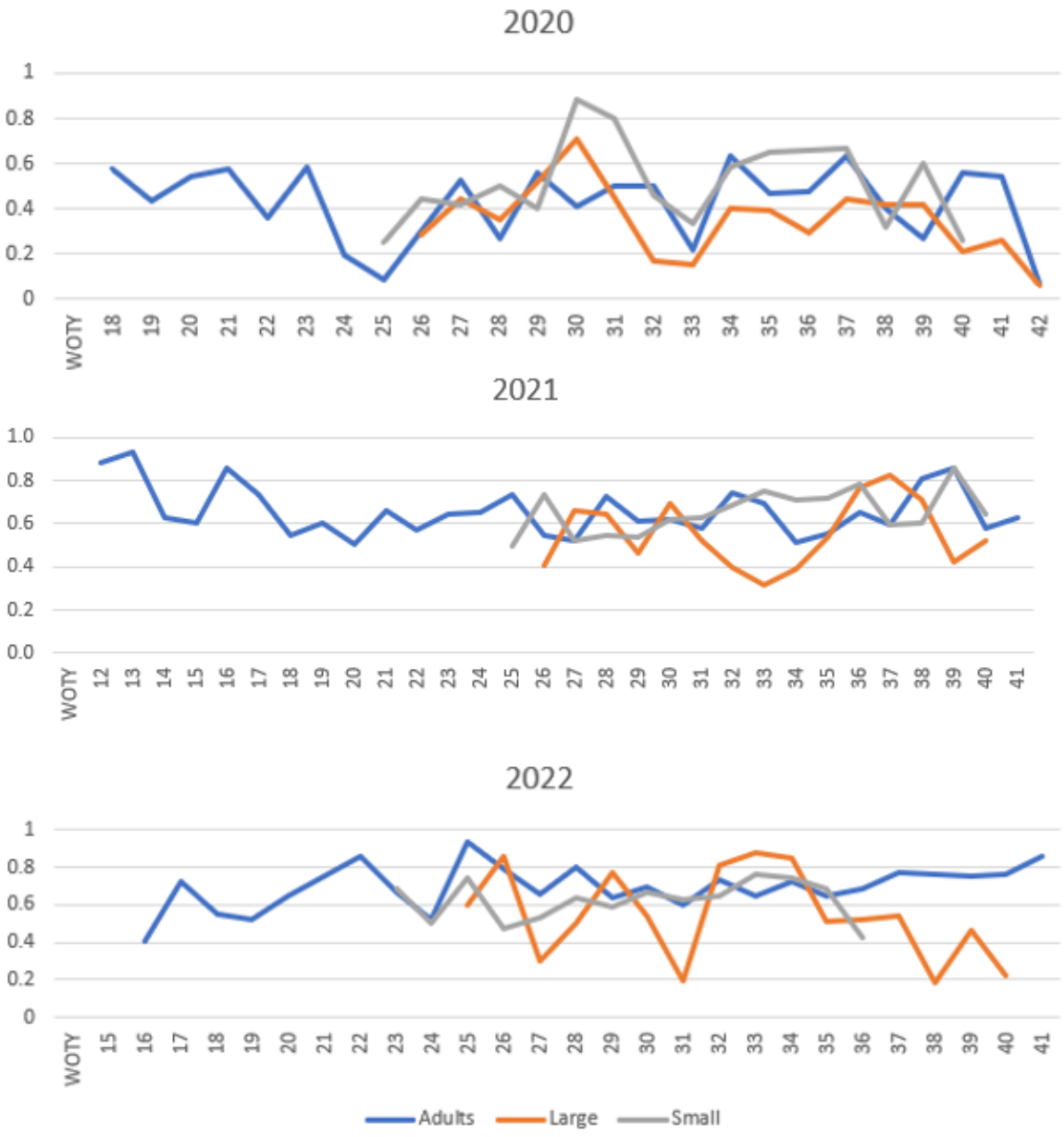

Figure 4.3 - Pearson's correlation between consecutive weeks for the years of 2020,2021 and 2022.

4.2 BMSB space time modelling

4.2.1. Variograms

Variograms were computed for the Small, Large, and Adults groups to evaluate spatial and temporal continuity. Despite exhibiting temporal continuity, as indicated by Pearson correlations, all groups displayed significant spatial dispersion. Notably, the BMSB Small group demonstrated superior results in spatial continuity, leading to its selection for building the spatial-temporal model.

Spatial variograms are illustrated in Figure 4.4-A, C, E, while temporal variograms are represented in Figure 4.4-B, D, F. Image A and B pertain to the Smalls variogram for the year 2020, with A depicting the spatial variogram fitted by a spherical function with two structures—the first featuring a horizontal range of 5km and the second with a horizontal range of 80km. Image B represents the time variogram with a maximum correlation time range of 4 weeks.

Similarly, Image C and D correspond to the Smalls variogram for the year 2021. Image C showcases the spatial variogram fitted by a spherical function with two structures, the first having a horizontal range of 4km and the second with a horizontal range of 80km. Image D portrays the time variogram fitted with a time range of 5 weeks.

Lastly, Image E and F pertain to the Smalls variogram for the year 2022. Image E illustrates the spatial variogram fitted by a spherical function with one structure, featuring a horizontal range of 10km. Image F represents the time variogram with a vertical range of 6 weeks.

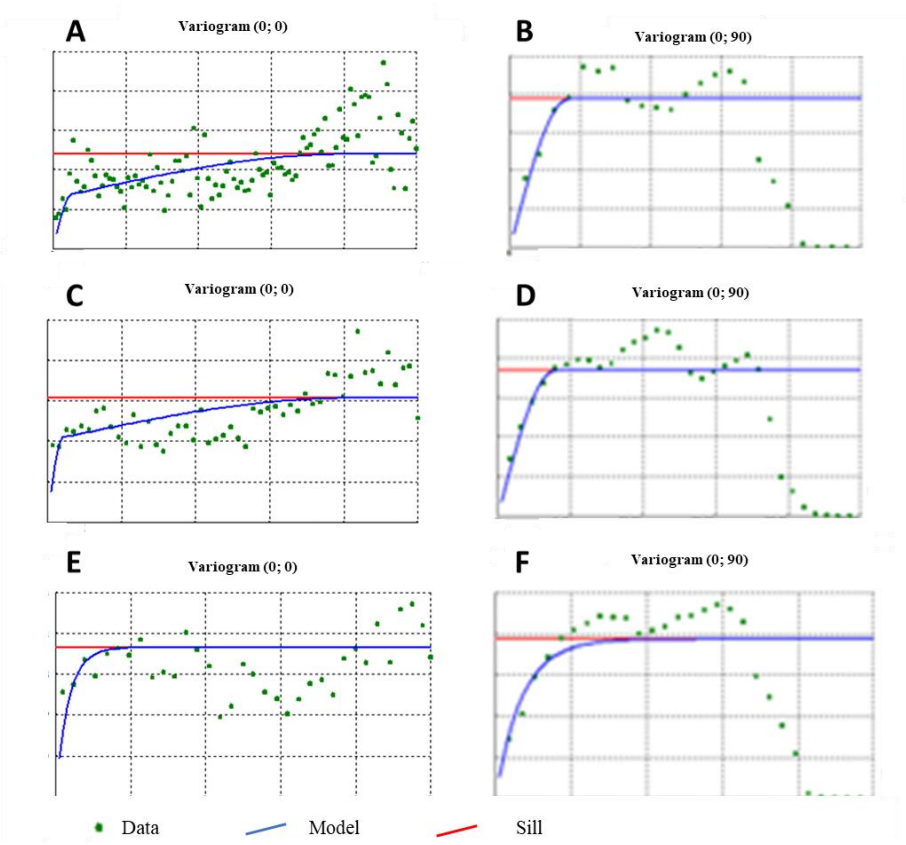

Figure 4.4 - Variograms of the Small in space and time.

4.2.2. Smalls BMSB spatial-temporal model

The Small BMSB spatial model was generated using the geostatistical algorithm Direct Sequential Simulation (DSS), as detailed in section 2.2.2. The spatial resolution is set at 500 meters in both the X and Y directions, while the time resolution is one week. The project coordinate system utilized is Monte Mário TM Emilia Romagna. For each year, 100 images were generated, and their average was computed.

Figure 4.5, 4.6 and 4.7 presents the Small BMSB model for the years 2020, 2021 and 2022, employing Leapfrog Geo software to generate a 3D view, with the third dimension representing time in weeks. In all figures, Image A depicts all counts, Image B represents counts above one, Image C illustrates counts above twenty-five, and Image D shows counts above fifty. The map at the top of Image A and B, and at the bottom of C and D, denotes the polygon defined in Chapter 3.3.2 for BMSB data.

The chronological order along the "zz" axis is from the top (early week) to the bottom (last week). The colour scale ranges from "0" (blue) to ">50" counts (pink).

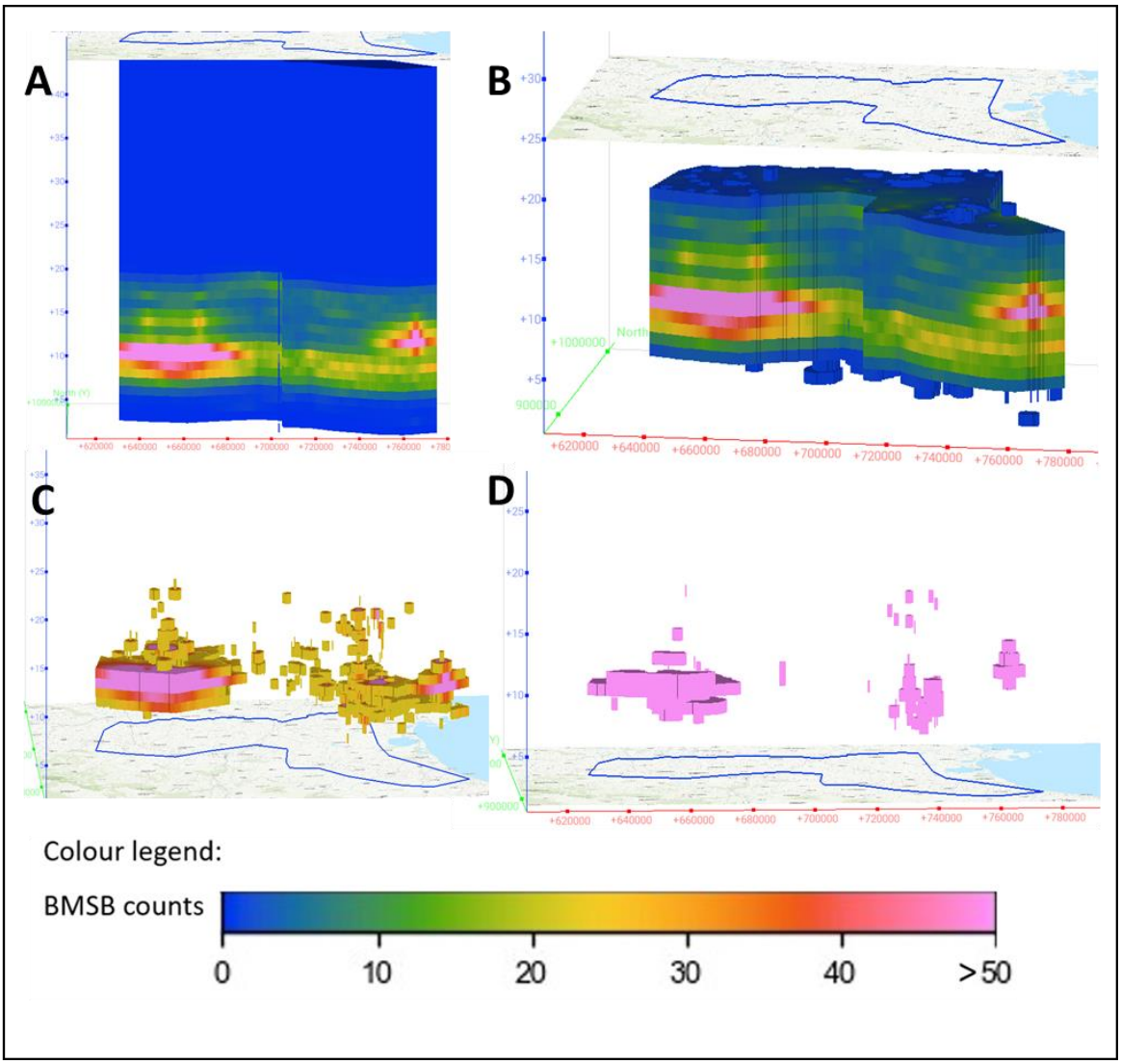

Figure 4.5 - Images of the spatial-temporal model for 2020 are presented in four variations: A – model filtered by all counts; B – only with counts above one; C - only with counts above 25; D - only with counts above 50. The blue polygon positioned above Images A and B, and below Images C and D, delineates the study area. All images are depicted in a perspective view oriented from south to north.

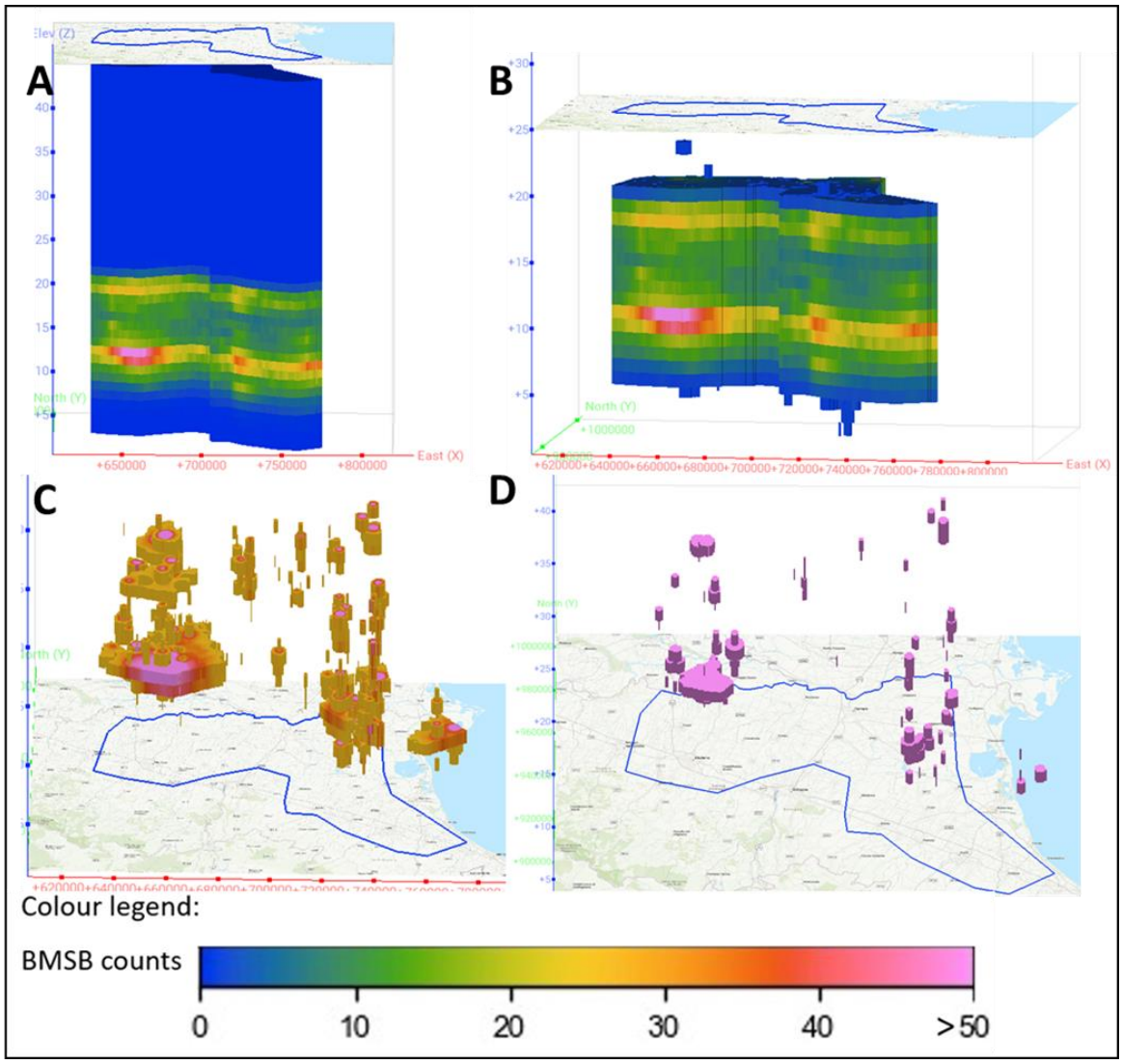

Figure 4.6 - Images of the spatial-temporal model for 2021 are presented in four variations: A – model filtered by all counts; B – only with counts above one; C - only with counts above 25; D - only with counts above 50. The blue polygon positioned above Images A and B, and below Images C and D, delineates the study area. All images are depicted in a perspective view oriented from south to north.

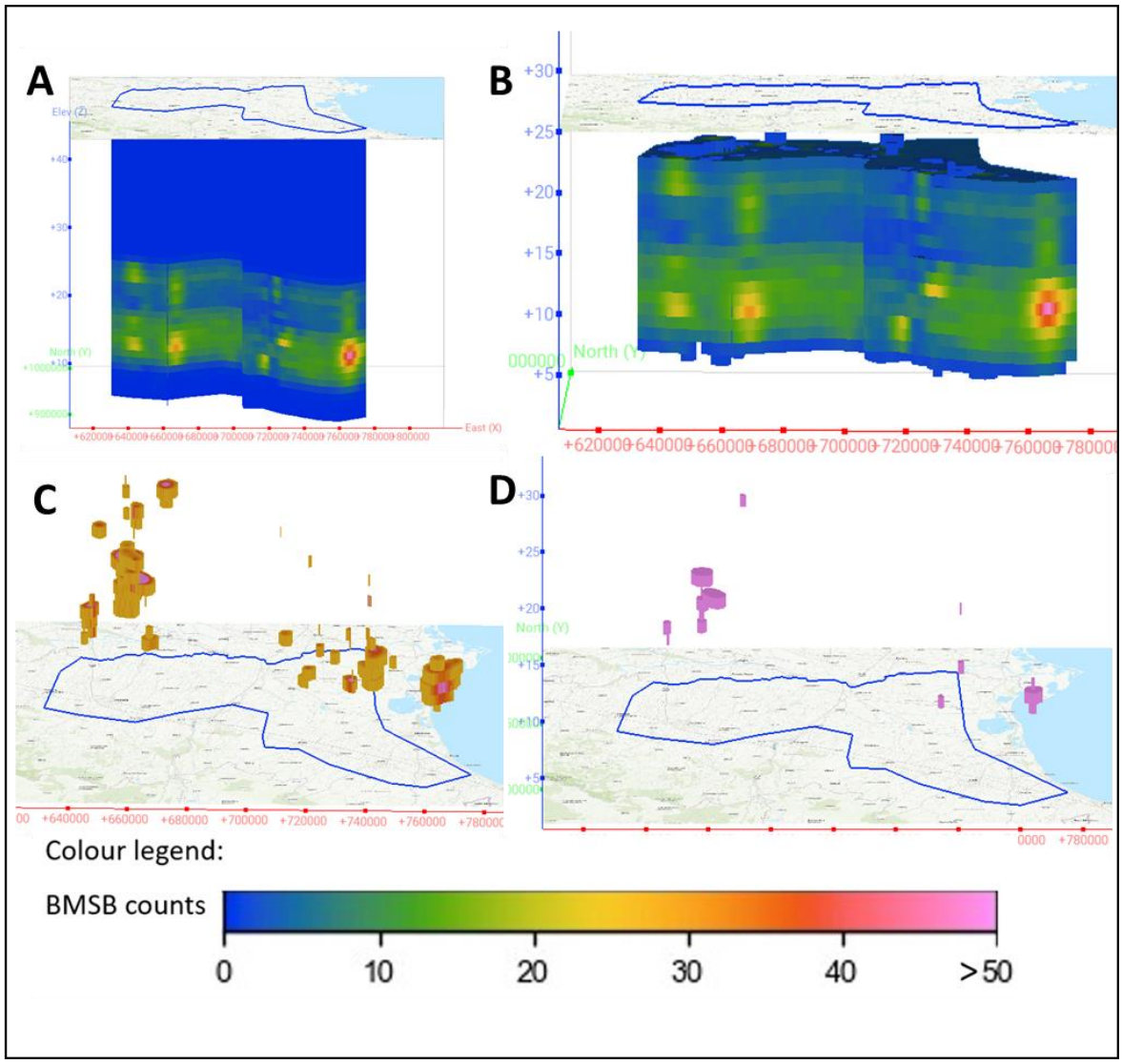

Figure 4.7 - Images of the spatial-temporal model for 2022 are presented in four variations: A – model filtered by all counts; B – only with counts above one; C - only with counts above 25; D - only with counts above 50. The blue polygon positioned above Images A and B, and below Images C and D, delineates the study area. All images are depicted in a perspective view oriented from south to north.

Using this spatial-temporal model and examining it for specific time slices, a temporal comparison between years becomes possible. Table 4.2 presents data for Weeks of the Year (WOTY) 26, 32, and 38 across the years 2020, 2021, and 2022. For instance, in 2021 during Week 26, the count numbers are substantially higher, with the map displaying colours predominantly between green and pink, compared to the years 2020 or 2022. This suggests that the BMSB season in 2021 likely commenced earlier than in the other years. Similarly, in the 38th WOTY of 2020, BMSB counts are significantly higher than in the same WOTY for the years 2021 and 2022, indicating that the 2020 season likely concluded later than the other years. Weeks with blank spaces correspond to zero counts.

Table 4.2 - Comparison between the 2020, 2021 and 2022 years for the same week of the year – time slice perspective.

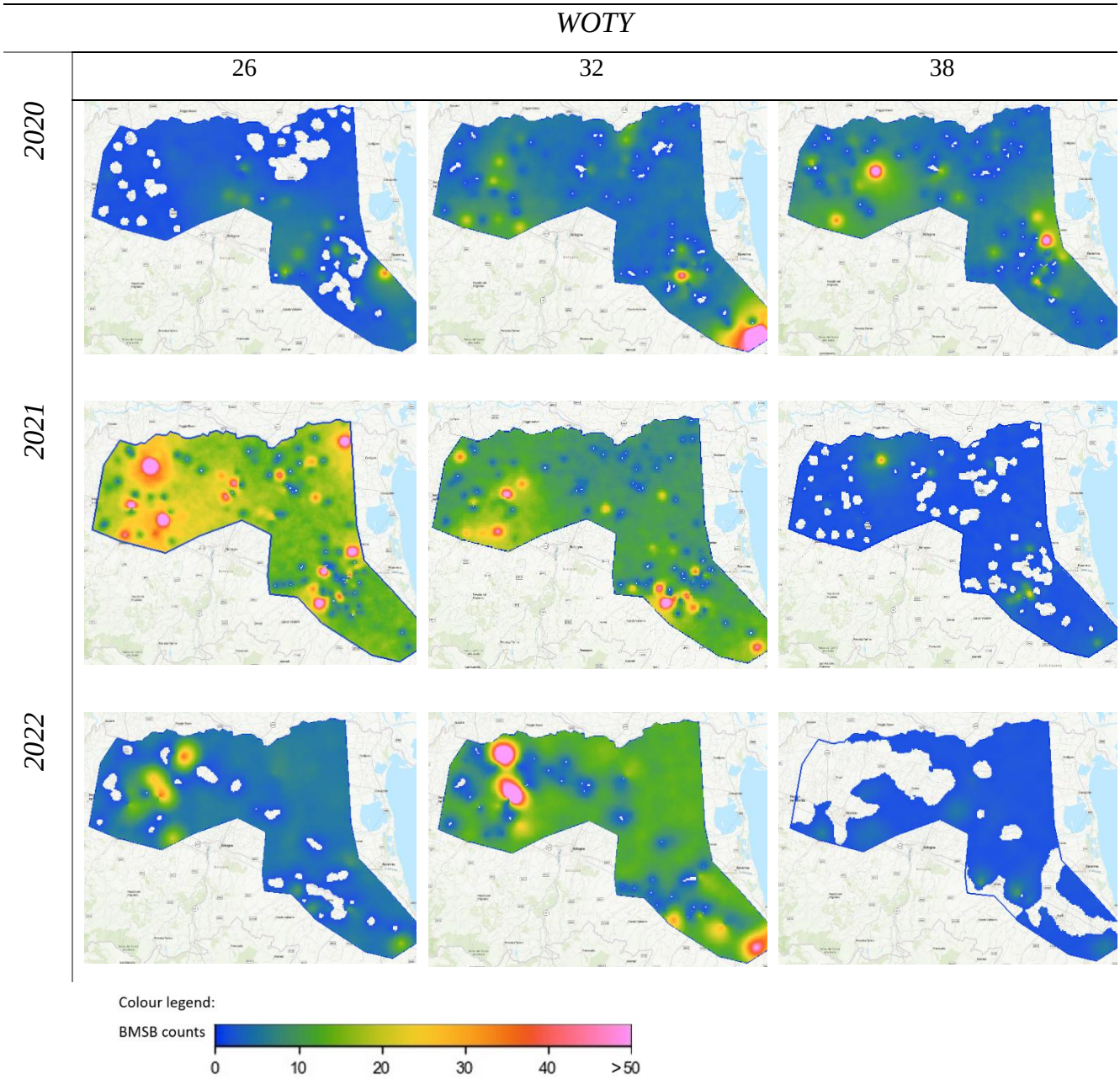

In Figure 4.8, the spatial-temporal model of Small BMSB for 2021 is presented, focusing on counts above 25 and viewed in a south-to-north perspective. Once again, the x and y axes represent space in the coordinate system Monte Mário TM Emilia Romagna, and the z axis represents time in weeks, where top values signify the beginning of the year, and lower values indicate later in the year. The Weeks of the Year (WOTY) are displayed in a horizontal slice, parallel to the x/y coordinate plane. The ellipses indicate different events in time when Smalls were observed in greater numbers.

The image distinctly reveals variations in counts across weeks, with two noticeable groups likely corresponding to two summer generations—the F1, represented by a green ellipse, and the F2, depicted by a red ellipse.

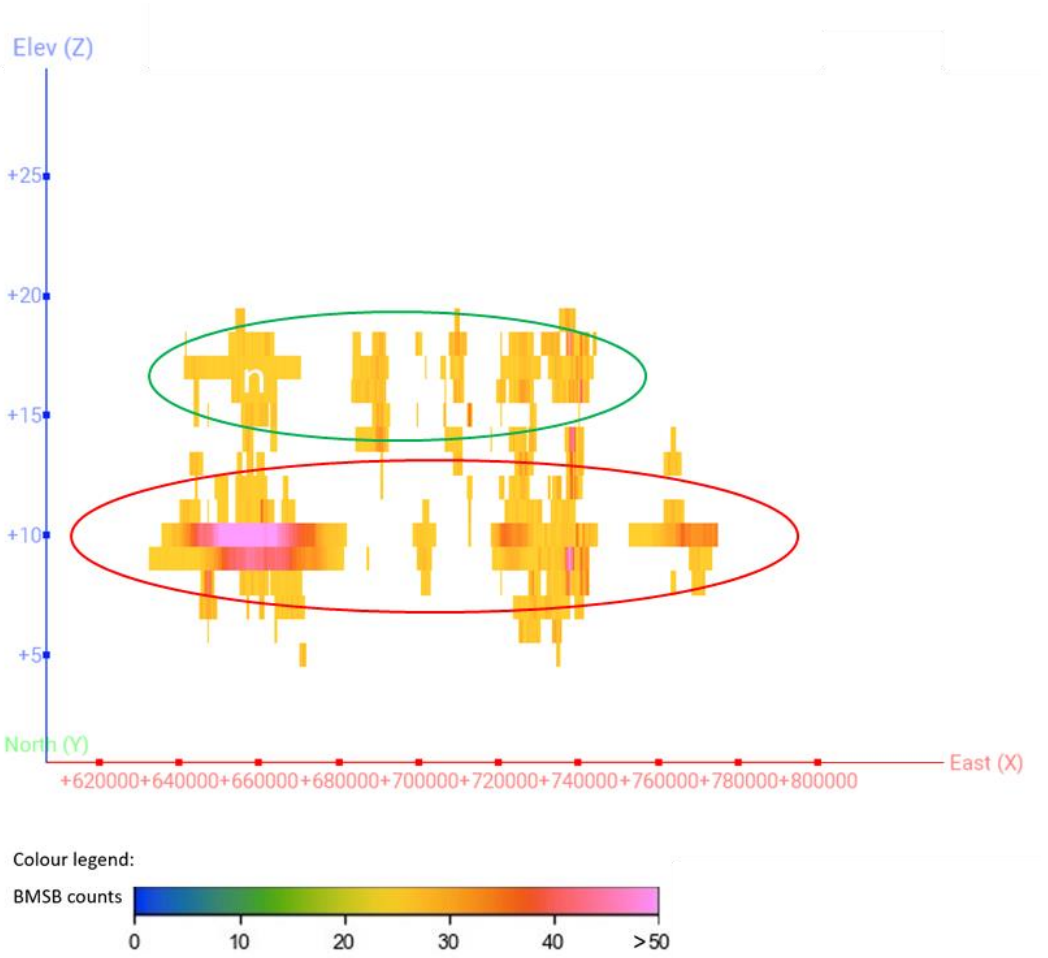

Figure 4.8 - Spatial-temporal model of 2021, specifically highlighting counts above 25, is presented in a south-to-north perspective.

4.3 Analysis and modelling of Degree Days and photoperiod

4.3.1. Data analysis

In Table 4.3, the data obtained from the literature review regarding Degree-Day (DD) accumulations were normalized to align with the previously defined DD12,97. As a result, the values of 541,8 DD12,97, 123,5 DD12,97, and 49,4 DD12,97 were established for complete development, ovarian development, and egg incubation, respectively.

Table 4.3 - Normalisation of DD from the 12,97 thresholds

Complete development			Ovarian development			Egg incubation			*Location*	*Authors*
DD	Lower Threshold	Norm. value	DD	Lower Threshold	Norm. value	DD	Lower Threshold	Norm. value		
-	-	-	119	16.3	0.137	-	-	-	Japan	*(Watanabe, 1980)*
-	-	-	-	-	-	-	-	-	Asia	*(Yanagi and Hagihara, 1980)*
537.63	14.14	0.026	147.65	14.14	0.096	53.3	13.94	0.262	USA	*(Nielsen et al., 2008)*
588.24	12.24	0.021	117.65	12.24	0.104	-	-	-	Switzerland	(Haye et al., 2014b)
546.4	12.8	0.023	-	-	-	-	-	-	Korea	*(Baek et al., 2017)*
560	13.3	0.024	-	-	-	-	-	-	Sochi, Russia	(Musolin et al., 2019a)
537.5	12.2	0.023	118.77	12.2	0.103	-	-	-	Slovenia	(Rot et al., 2022b)
590	13.3	0.023	156	13.3	0.085	-	-	-	Sochi, Russia	*(Reznik et al., 2022)*
520	14.26	0.027	-	-	-	54	14.26	0.264	USA, (NJ)	*(Mermer et al., 2023)*
-	-	0.024	-	-	0.105	-	-	0.263	Average	
541.8	12.97	0.024	123.5	12.97	0.105	49.35	12.97	0.263	Obtained values	

The data presented in the oviposition column in Table 4.4 were obtained from data collected by (E. Costi et al., 2017) and (Lara Maistrello, unpublished data) between 2015 and 2018 in Reggio-Emilia, a region in Emilia-Romagna (ER), under conditions simulating field expectations.

To identify the probable termination of diapause, the date was determined by subtracting the Degree-Days (DD) required for diapause termination from the start of oviposition. The new date was derived through cumulative counting, moving backward until reaching the threshold of 123,5 DD12,97. Data from each year were sourced from ARPAE in ER. Subsequently, utilizing information from timeanddate.com, the photoperiod for that location during those specific time points was defined.

Table 4.4 - Estimation of the photoperiod

	Oviposition		Diapause Termination		Diapause Induction	
Year	Start	End	Date	Photoperiod	Date	Photoperiod
2015	15/may	31/august	27/april	14:02	31/august	13:18
2016	-	-	-	-	-	
2017	26/may	28/august	11/may	14:40	28/august	13:26
2018	22/may	-	29/april	14:08	-	

4.4. Cumulative DD spatial-temporal model for 2021

A chronogram (Figure 4.9) illustrating the Degree-Day (DD) values required for the BMSB or the BMSB population to accumulate and progress through sequential life stages was created using the data listed in Tables 4.3 and 4.4. In the chronogram (Figure 4.9), blue represents the sequential life stages of the BMSB population, starting from the diapause females. In orange are the photoperiods that lead to the end and the start of diapause. In grey are the stages (mentioned in Table 4.3) that refer to the DD needed to reach the next stage, which are added to the previous stage DD (in white), resulting in the values in the green boxes. Consequently, the value in green represents the DD needed to reach the adjacent stage in the blue box.

Starting from females in diapause, the diapause termination is triggered by a photoperiod above 14 hours, initiating the accumulation of degree days. The column in dark blue represents successive stages in the BMSB life cycle. The green column denotes the degree days required to reach the next stage. The grey boxes symbolize the degree days required for a specific process, as defined in Table 4.3. In the white boxes, the value from the previous degree day stage is listed, which is then added to the degree days needed for that specific stage indicated in the grey boxes, resulting in the values in the green boxes. When the photoperiod decreases below 13 hours, diapause starts, and the reproduction ends.

Utilizing the sequence of values obtained in this chronogram, the cumulative Degree-Day (DD) spatial-temporal model for the year 2021 was developed, as illustrated in Figure 4.10.

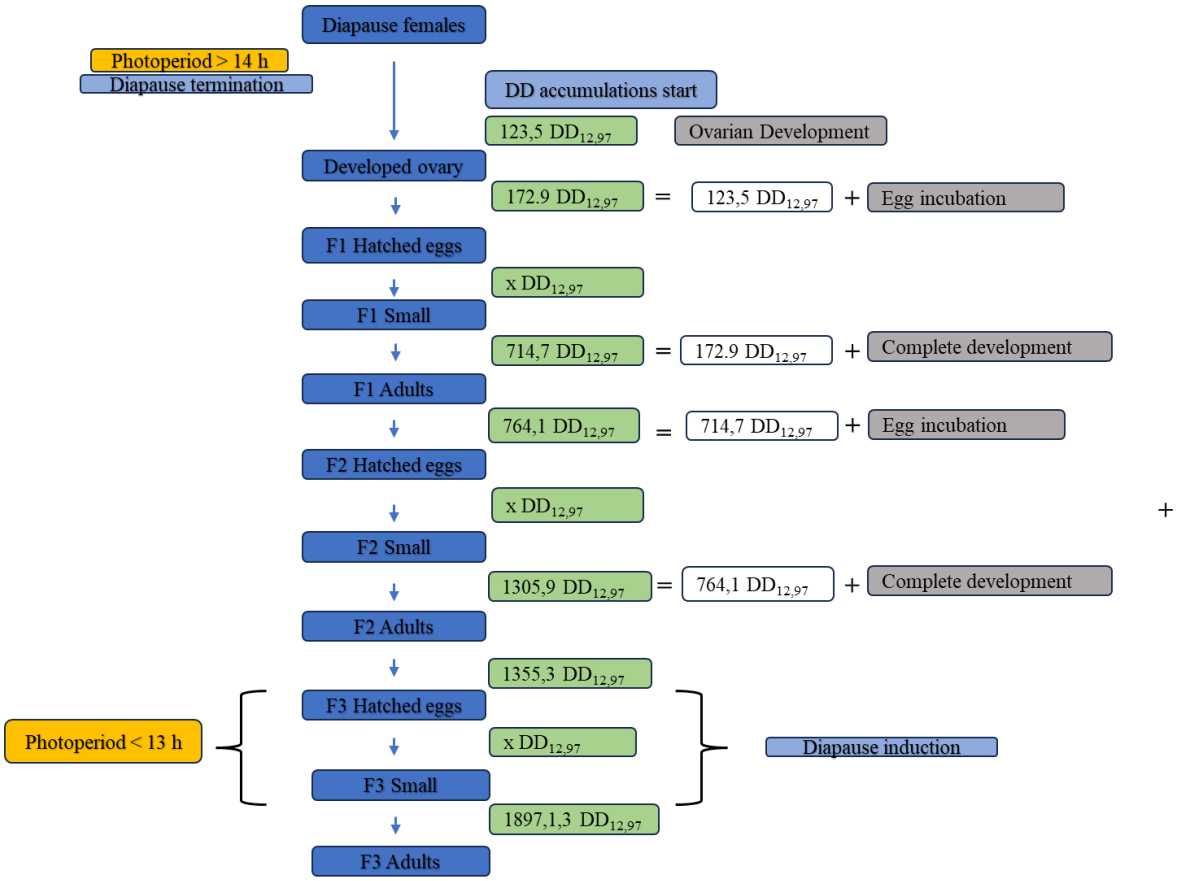

Figure 4.9 - Chronogram illustrating the values essential for the development of the Cumulative Degree-Day (DD) spatial-temporal model.

The cumulative Degree-Day (DD) spatial-temporal model for the year 2021 was estimated using Radial Basin Functions estimator in Leapfrog Geo software and is shown in Figure 4.10. The layers in the model correspond to the DD required for the BMSB to reach crucial stages in its life cycle, indicated by the numbers representing DD12,97.

An alternative visualization is provided through the Weeks of the Year (WOTY) layers where Image A represents the 17th WOTY, corresponding to diapause termination, while image B corresponds to the 37th WOTY, associated with diapause induction.

In all images, again the x and y axes represent spatial dimensions, while the z-axis represents time in weeks. The chronological order along the z-axis progresses from the top (early week) to the bottom (last week), and the blue polygon above the model delineates the study area, like previous images. The perspective view of the model is southwest northeast.

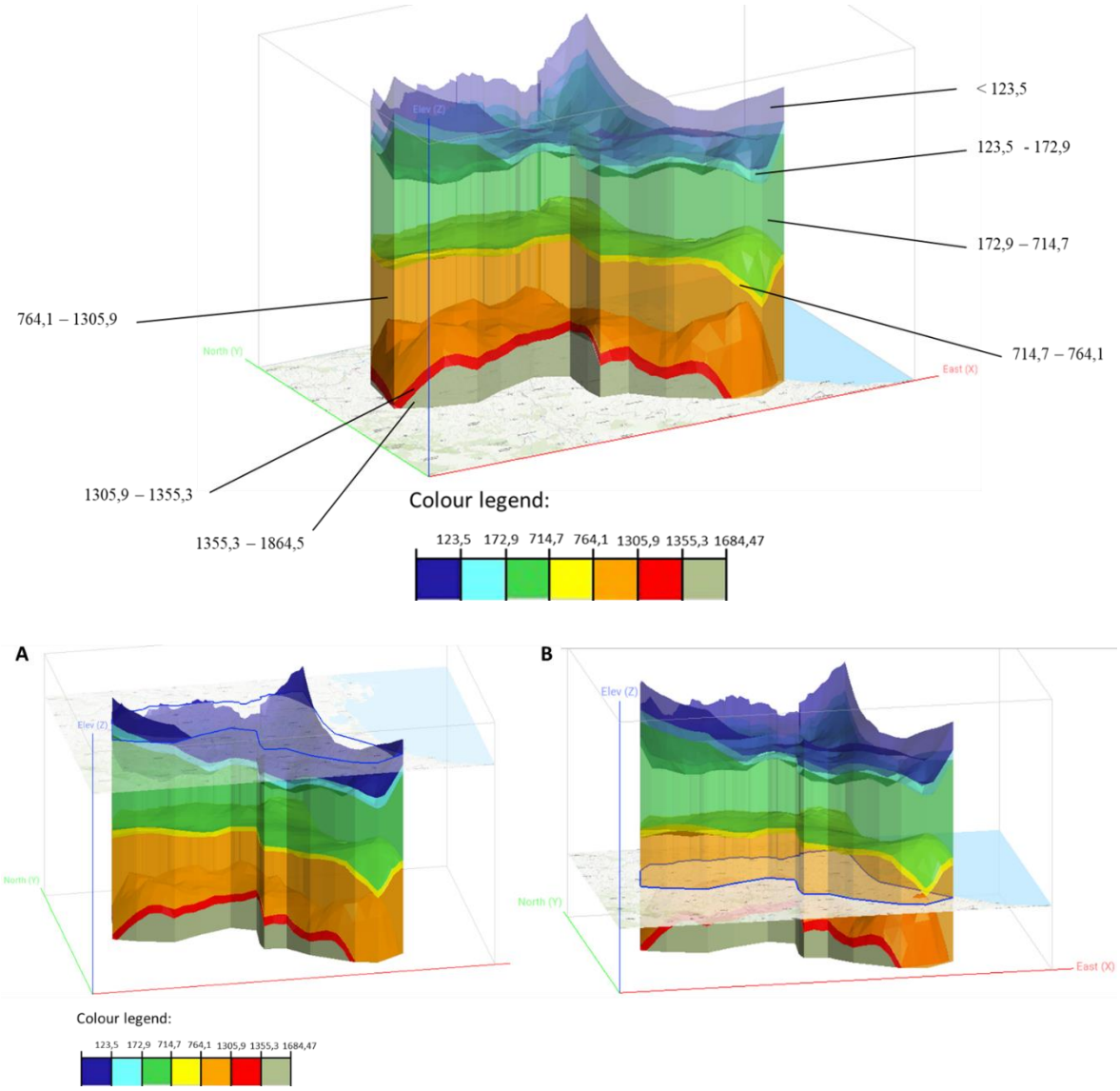

Figure 4.10 - Cumulative degree days spatial-temporal model – 2021. The layers in the model are referent to the DD needed for the BMSB reach important stages in its life cycle, the numbers are the $DD_{12,97}$. A - map position in Diapause termination. B - map position in Diapause induction.

Figure 4.11 consists of six images from the cumulative Degree-Day (DD) spatial-temporal model of 2021, viewed at specific time slices. These images represent a temporal progression of DD layers. The progression of time is evident from Image A to E, with Images A, C, and E corresponding to the 22nd, 23rd, and 24th Weeks of the Year (WOTY), respectively. Similarly, the progression of time from Image B to F is seen, with Images B, D, and F representing the 31st, 32nd, and 33rd WOTY.

Figure 4.11-A, C, and E are associated with the 172,9 DD layer (pale blue), while Figure 4.11-B, D, and F are related to the 764,1 DD layer (yellow). The presence of these

layers in the map signifies that these areas have the conditions for Brown Marmorated Stink Bug (BMSB) hatched eggs. There is a progressive increase in the map area covered by the respective colours (172,9 DD - pale blue and 764,1 DD - yellow) as the number of weeks increases. The appearance of these coloured layers signifies the moment when the probability of encountering Small Brown Marmorated Stink Bugs increases.

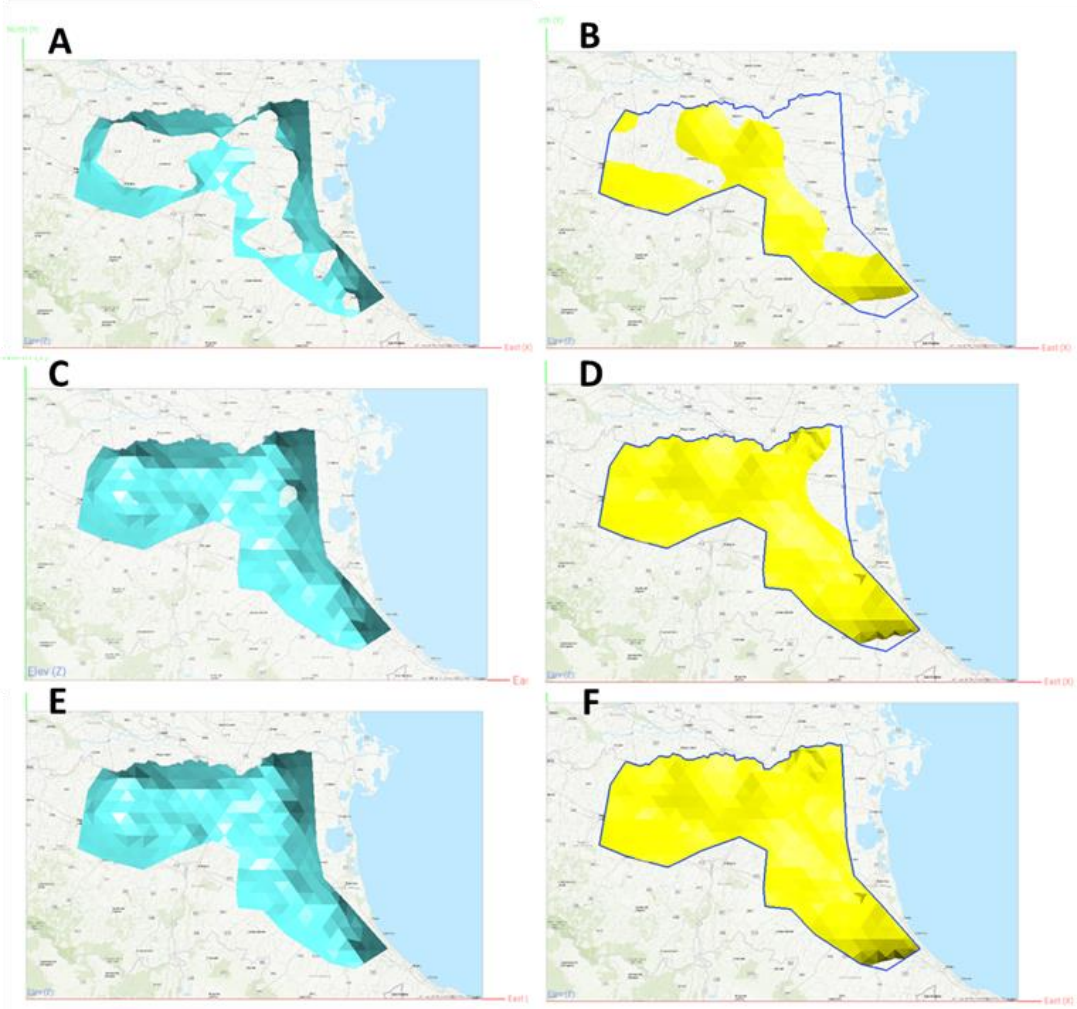

Figure 4. 11 - Temporal progression in the Degree-Day layers. Images A, C, and E correspond to the 23rd, 24th, and 25th Weeks of the Year (WOTY), respectively, and are associated with the 172,9 Degree Days layer (pale blue). Images B, D, and F represent the 31st, 32nd, and 33rd WOTY, respectively, and are related to the 764,1 Degree Days layer (yellow).

Finally, in Figure 4.12, Images A and B depict the BMSB spatial-temporal model of 2021, viewed from above, showcasing counts above 25. Image A represents counts from the 24th to the 29th Weeks of the Year (WOTY), while Image B corresponds to counts from the 32nd to the 34th WOTY. These periods align with the F1 and F2 generations, as previously illustrated in Figure 4.8.

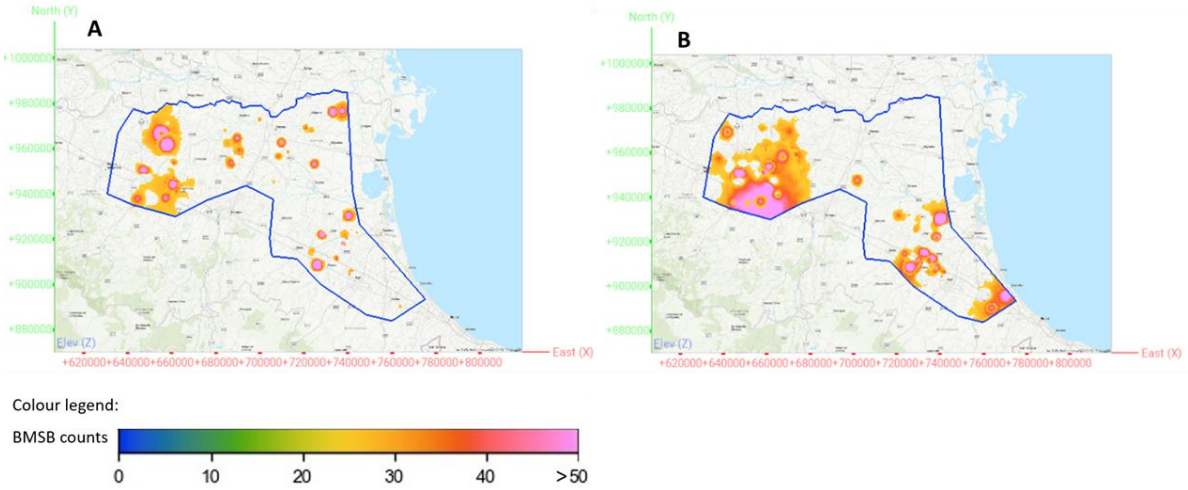

Figure 4.12 - Smalls BMSB spatial-temporal model of 2021, focusing on counts above 25. Image A corresponds to counts from the 24th to the 29th Weeks of the Year (WOTY), while Image B represents counts from the 32nd to the 34th WOTY.

4.5. Haly.id sensor data

The efficacy of the Haly.ID sensors, which collect data for temperature and humidity, was assessed during the period between 17/06/2022 and 31/08/2023, with hourly data presented in Table 4.5. The table demonstrates the overall efficiency of the sensors, where efficiency is defined as the percentage of time during which these sensors were operational. The host is a Raspberry Pi containing specific sensors. Bridge.id serves as the unique identification for each sensor. The results showed that with only one sensor exhibiting efficiency below 60%, and two sensors displaying efficiencies below 80%.

Table 4. 5 – Efficiency of Haly.ID temperature and humidity sensors (%) during the period from 17/06/2022 to 31/08/2023.

Efficiency	88.77	96.81	96.81	96.75	59.54	85.47	96.80	76.50	91.01	90.04	77.61	91.01	96.77
Host	fritz				halyid-pi-01				heinz				igor
Bridge id	52d79	532ee	5372a	53fc4	53af8	53e87	53ea3	547fa	53401	5345a	54019	54281	530e5

To understand the variations in Degree-Day (DD) accumulations influenced by the Brown Marmorated Stink Bug (BMSB) in orchard plants and compare them with DD accumulations at meteorological stations, reductions in DD accumulation at the meteorological stations relative to the optimal DD accumulation location for the 2022 and 2023 seasons were assessed and are presented in Table 4.6. In this table, "Meteo station" refers to the name of the meteorological station, "Host" designates the Raspberry Pi containing specific sensors, "Bridge Id" serves as the identification for each sensor, "Season 1" spans the period between 17/06/2022 and 31/10/2022, and "Season 2" covers the period between 01/04/2023 and 31/07/2023.

Table 4. 6 - Percentage of reduction in Degree-Day (DD) accumulation compared to the optimal location.

Meteo station	Correggio	Modena urbana	Cortile di Carpi	**Host**	fritz				halyid-pi-01				heinz				igor
				Bridge id	52d79	532ee	5372a	53fc4	53af8	53e87	53ea3	547fa	53401	5345a	54019	54281	530e5
Season 1	18.13	4.45	17.85	Season 1	1.88	8.11	10.29	8.99	13.88	11.99	7.31	14.68	33.72	33.85	30.18	37.29	9.66
Season 2	18.74	12.87	20.76	Season 2	5.72	9.53	13.32	10.33	-	14.59	6.28	13.91	14.82	19.18	3.08	21.97	4.32

This table illustrates a significant discrepancy in the comparison between the optimal orchard location for Degree-Day (DD) accumulations and the positions of both the sensors and meteorological stations. The reduction in percentage ranged from 4.45% to 20.76% for the meteorological stations, whereas for the sensor locations within the orchard, this reduction varied from 1.88% to 37.29%.

5. Discussion

Conventional spatial-temporal models rely on the use of graphics, similar to those presented by (Goane et al., 2013; Ntiri et al., 2019), to represent counts of the pest in specific locations or the density of the pest in different timepoints and locations. Alternatively, interpolation maps like the ones performed by (Espinosa et al., 2016; Grabarczyk et al., 2022; Milonas et al., 2016) are employed to characterize the distribution of a pest within a specified area across different timepoints.

On this dissertation, a spatial-temporal simulation geostatistical model was developed, utilizing data acquired over three years, 2020-22. The data is sourced from an average of 135 traps and were collected on weekly basis around 30 timepoints per year. To ensure alignment with the space-time continuity prerequisites intrinsic to geostatistical models, testing has been confined to the Small group of BMSB.

To develop this space-time model of BMSB counts, the Direct Sequential Simulation (DSS) algorithm was employed to generate several equiprobable simulated images of the counts, and subsequently, the average image was computed. This algorithm is commonly utilized in geosciences (Barrela et al., 2017; Caeiro et al., 2015; Linsel et al., 2020) and for climatic variables (Costa & Soares, 2009; S. Ribeiro et al., 2016). Nevertheless, the use of the DSS algorithm for this specific application yielded satisfactory results, as demonstrated in chapter 4. The value of the spatial-temporal model naturally lies in its simplistic visualization of BMSB locations in the ER region. Additionally, this model proves useful for validating the forecast model the (Cumulative DD spatial-temporal model for 2021).

The Cumulative Degree-Day spatial-temporal model of 2021 was developed using temperatures gathered from meteorological stations situated within or near the polygon delimiting the study area in the ER region. This model accounts for the photoperiod affecting the BMSB and calculates the cumulative DD required by this pest (see figure 4.10). This model delineates the timepoint (Week of the Year - WOTY) and location of BMSB summer generations in relation to abiotic conditions, specifically temperature, presented in the form of Degree-Days.

The temperature data obtained from meteorological stations differs from that collected by sensors positioned within the orchard, near the plants. Discrepancies in height and geographical positioning between the stations and sensors naturally result in variations in the measured temperature values. Additionally, as highlighted by Lembrechts et al (2019), microclimatic data recorded by sensors is influenced by biological and ecological processes.

Consequently, the temperature experienced by the BMSB on the plant may differ from the one measured by the meteorological stations.

In accordance with Havko et al (2020), insects have the ability to manipulate their position in the tree canopy to either decrease or enhance heat accumulations based on their requirements. The comparison was made between the reduction of accumulated DD at various locations (meteorological stations and sensor positions) and the optimal tree location for DD accumulations.

The DD data obtained from temperatures recorded at meteorological stations were juxtaposed with the optimal location that the BMSB can go in the canopy, in order to accumulate the DD required for their development. The DD accumulation at the identified optimal location surpassed that at any of the nearby meteorological stations. Reductions in DD accumulations at the meteorological stations varied between 4,45% and 20,76%. Based on these findings, it is concluded that the forecast model relying on DD recorded by meteorological stations is one of the errors associated to the forecast model. Interestingly, the best location to accumulate DD does not seem to be the strategy used by the BMSB since this strategy would also diminish their lifespan.

The analysis of photoperiod holds significant importance in determining the daylength thresholds for diapause termination and induction. The photoperiod duration of diapause induction was defined when the daylength decrease below the 13-hour threshold, indicating a phase where BMSB are not mature for reproduction. To reach this value, the Small count data of 2021 was analysed and concluded diapause induction to be between 13-hours to 12,5-hours. The results provided by this dissertation match those from literature, such as studies by (Costi et al., 2017) and (Lara Maistrello, unpublished data), who report diapause induction values below 13,5 hours. Similarly, Rot (2022) in Slovenia, also associates the 13-hour threshold with diapause induction.

Furthermore, diapause termination was established when the daylength increased above 14 hours corroborated by data from (Costi et al., 2017) and (Lara Maistrello, unpublished data). In the forecast model, 17 WOTY corresponds to diapause termination, while 37 WOTY signifies diapause induction. Consequently, during the period from 17 WOTY to 37 WOTY, BMSB can be reproductively active.

According to the generated forecast model of 2021 (Figure 4.11) at 123,5 DD12,97 (dark blue layer on DD spatial-temporal model), females are likely to have a developed reproductive system. With an additional 49,4 DD12,97, accounting for the necessary time

for egg incubation, the total reaches 172,9 DD (pale blue on DD spatial-temporal model), making it possible at this stage to have F1 hatched eggs. Continuing with an accumulation of another 541,8 DD12,97, representing the required time for complete development, the total reaches 714,7 DD12,97 (green on DD spatial-temporal model), and at this stage encountering F1 adults became plausible.

Adding another 49.4 DD12.97, the necessary time for egg incubation, results in a cumulative total of 764.1 DD12.97 (yellow on DD spatial-temporal model), marking the stage where F2 hatched eggs may be encountered. Summing another 541.8 DD12.97, representing the necessary time for complete development, brings the total to 1305.9 DD12.97 (orange on DD spatial-temporal model), suggesting the likelihood of encountering F2 adults at this stage.

Continuing the cycle, it was expected to find the presence of F3 hatched eggs at 1355.3 DD and F3 adults at 1864.5 DD. However, this expected pattern is not observed. Just before reaching the 1355.3 DD mark, the threshold of 13 hours in daylength is crossed, triggering diapause induction. As a result, reproduction comes to a halt, and shortly after this event, small BMSB cease to appear on the spatial-temporal model of 2021. This observation validates the determination of the 13-hour threshold for diapause induction, as it corresponds to a significant shift in the reproductive cycle of the BMSB.

From an intervention perspective aimed at controlling BMSB, the Cumulative DD spatial-temporal model of 2021 becomes a valuable tool. It enables the definition of recommended time points for implementing control methods, providing strategic guidance in managing BMSB populations effectively.

The use of egg parasitoids to target and destroy BMSB eggs is recommended to commence at two crucial time points: when reaching 123,5 DD and 714,7 DD. The importance of 123,5 DD lies in the fact that, from this point onward, the reproductive system of BMSB females is mature, and the appearance of eggs is imminent. Therefore, it is essential to have egg parasitoids present at this stage. The importance of 714,7 DD is that, starting from this moment, the F1 generation undergoes moulting into mature adults, leading to the imminent appearance of eggs once again. Hence, it is crucial to deploy egg parasitoids promptly to manage BMSB populations effectively.

The utilization of chemicals to control BMSB represents another available method, with some authors suggesting that nymphs are more susceptible to insecticides than adults, making them easier to eliminate. With this strategy, the optimal time to act would be at 172,9

DD and 764,1 DD. From these points forward, both the F1 and F2 generations have accumulated the necessary DD to reach the stage of egg hatching, and nymphs are expected to emerge. Acting at these specific time points ensures that the chemical intervention is timed to coincide with the vulnerable nymph stage, maximizing the effectiveness of the control method.

By systematically exploring the Cumulative DD spatial-temporal model of 2021 on a weekly basis and navigating through its layers (z axis - weeks) across the geographical map of ER, it becomes evident whether the entire region fulfils the requirements for the BMSB to reach a certain lifecycle stage. The primary purpose of spatial representations, such as the one depicted in Figure 4.11, is to pinpoint the areas within the ER region and the corresponding timepoints where BMSB have accumulated the necessary DD to reach certain developmental stages. In this representation, the pale blue areas correspond to the F1 generation hatched eggs, while the yellow areas correspond to the F2 generation hatched eggs.

To conclude this discussion, it is crucial to emphasize that the value of the Cumulative DD spatial-temporal model for 2021 lies in its predictive utility. The Smalls BMSB spatial-temporal model of 2021, illustrated in Figure 4.12, indicates that the emergence of small BMSB occurs only when the DD requirements predicted in Figure 4.11 are fulfilled. This underscores the predictive power of the cumulative DD model in anticipating the appearance of small BMSB and underscores its significance in informing proactive measures for monitoring and control.

Certainly, it's important to mention several potential limitations in the Cumulative DD spatial-temporal model. These include:

Abiotic Focus: The model is primarily based on abiotic factors, specifically temperature. While temperature is a crucial factor, there are other variables such as humidity that could play a role in the BMSB lifecycle.

Biotic Considerations: The model currently doesn't account for biotic factors, such as interactions with other organisms and food availability, which are known to influence the BMSB lifecycle.

Seasonal Variation: Literature suggests that high temperatures and food availability in the winter can potentially override diapause in the BMSB. Applying this model in different locations may require considering such seasonal variations and specific local factors to improve its applicability.

Spatial Continuity Requirement: The construction of the model relies on the existence of spatial continuity in the available data, thus ensuring a correct trap locations set is critical for accurate predictions.

Addressing these limitations can contribute to the refinement and enhancement of the Cumulative DD spatial-temporal model, making it a more comprehensive and reliable tool for forecasting BMSB behaviour across diverse environmental conditions.

6. Conclusions

The Brown Marmorated Stink Bug (BMSB) has emerged as a worldwide pest with substantial economic impacts in agriculture. While effective methods for its control exist, determining the optimal timing for their application poses a current challenge.

In the present thesis, a spatial temporal model for BMSB was created for the region of Emilia-Romagna in Italy, a location drastically affected by the presence of the BMSB. This model maps the location and density of Small BMSB abundance over time (weeks) and brings relevant information on past behaviour of the pest.

However, the goal of this research is interpreting this data on the context of BMSB lifecycle and build a cumulative DD forecast model. This forecast model importance resides in the ability in providing results that can predict the appearance of the pest. The interpretation of this model allows for a more informed decision on the areas and the ideal timepoints for the application of control measures. In a near future, artificial intelligence (AI) systems would be able to use this model for an almost real-time prediction of the pest spatial-temporal distribution.

Further developments should focus on replicating similar models for different regions and pests. From a technical standpoint, the use of the geostatistical simulation algorithms such as DSS and the generation of 3D representation models prove to be suitable, enhancing the interpretation of data in comparison with conventional maps and graphs.

7. Bibliographic references

Abram, P. K., Hoelmer, K. A., Acebes-Doria, A., Andrews, H., Beers, E. H., Bergh, J. C., Bessin, R., Biddinger, D., Botch, P., Buffington, M. L., Cornelius, M. L., Costi, E., Delfosse, E. S., Dieckhoff, C., Dobson, R., Donais, Z., Grieshop, M., Hamilton, G., Haye, T., … Wiman, N. G. (2017). Indigenous arthropod natural enemies of the invasive brown marmorated stink bug in North America and Europe. *Journal of Pest Science*, *90*(4), 1009–1020. https://doi.org/10.1007/s10340-017-0891-7

Acebes-Doria, A. L., Leskey, T. C., & Bergh, J. C. (2017). Temporal and Directional Patterns of Nymphal Halyomorpha halys (Hemiptera: Pentatomidae) Movement on the Trunk of Selected Wild and Fruit Tree Hosts in the Mid-Atlantic Region. *Environmental Entomology*, *46*(2), 258–267. https://doi.org/10.1093/EE/NVW164

Aigner, J. D., & Kuhar, T. P. (2016). Lethal High Temperature Extremes of the Brown Marmorated Stink Bug (Hemiptera: Pentatomidae) and Efficacy of Commercial Heat Treatments for Control in Export Shipping Cargo1. *Https://Doi.Org/10.3954/1523-5475-32.1.1*, *32*(1), 1–6. https://doi.org/10.3954/1523-5475-32.1.1

Baek, S., Hwang, A., Kim, H., Lee, H., & Lee, J. H. (2017). Temperature-dependent development and oviposition models of Halyomorpha halys (Hemiptera: Pentatomidae). *Journal of Asia-Pacific Entomology*, *20*(2), 367–375. https://doi.org/10.1016/j.aspen.2017.02.009

Bale, J. S. (1991). Insects at Low Temperature: A Predictable Relationship? *Functional Ecology*, *5*(2), 291. https://doi.org/10.2307/2389267

Bariselli, M., Bugiani, R., & Maistrello, L. (2016). Distribution and damage caused by Halyomorpha halys in Italy. *EPPO Bulletin*, *46*(2), 332–334. https://doi.org/10.1111/EPP.12289

Barrela, E., Azevedo, L., & Demyanov, V. (2017). Geostatistical history matching - A zonation-based approach using direct sequential simulation. *79th EAGE Conference and Exhibition 2017*, *2017*(1), 1–5. https://doi.org/10.3997/2214-4609.201700970/CITE/REFWORKS

Bergh, J. C., Morrison, W. R., Joseph, S. V., & Leskey, T. C. (2017). Characterizing spring emergence of adult Halyomorpha halys using experimental overwintering shelters and commercial pheromone traps. *Entomologia Experimentalis et Applicata*, *162*(3), 336–345. https://doi.org/10.1111/eea.12539

Bosco, L., Moraglio, S. T., & Tavella, L. (2018). Halyomorpha halys, a serious threat for hazelnut in newly invaded areas. *Journal of Pest Science*, *91*(2), 661–670.

https://doi.org/10.1007/S10340-017-0937-X/TABLES/5

Bramer, I., Anderson, B. J., Bennie, J., Bladon, A. J., De Frenne, P., Hemming, D., Hill, R. A., Kearney, M. R., Körner, C., Korstjens, A. H., Lenoir, J., Maclean, I. M. D., Marsh, C. D., Morecroft, M. D., Ohlemüller, R., Slater, H. D., Suggitt, A. J., Zellweger, F., & Gillingham, P. K. (2018). Advances in Monitoring and Modelling Climate at Ecologically Relevant Scales. *Advances in Ecological Research*, *58*, 101–161. https://doi.org/10.1016/BS.AECR.2017.12.005

Caeiro, M. H., Demyanov, V., & Soares, A. (2015). Optimized History Matching with Direct Sequential Image Transforming for Non-Stationary Reservoirs. *Mathematical Geosciences*, *47*(8), 975–994. https://doi.org/10.1007/S11004-015-9591-0/FIGURES/7

Callot, H., L'Entomologiste, C. B.-, & 2013, undefined. (n.d.). Halyomorpha halys (Stål, 1855), la Punaise diabolique, nouvelle espèce pour la faune de France (Heteroptera Pentatomidae). *Soc.Als.Entomo.Free.Fr*. Retrieved May 6, 2023, from http://soc.als.entomo.free.fr/Documents PDF/CALLOT&BRUA_2013_Halyomorpha_halys_L_ENTOMOLOGISTE_69.pdf

Calvini, R., Ferrari, V., Maistrello, L., & Ulrici, A. (n.d.). *Monitoring of insect pests in crop fields using spectral imaging*.

Cianferoni, F., Graziani, F., Dioli, P., & Ceccolini, F. (2018). Review of the occurrence of Halyomorpha halys (Hemiptera: Heteroptera: Pentatomidae) in Italy, with an update of its European and World distribution. *Biologia (Poland)*, *73*(6), 599–607. https://doi.org/10.2478/S11756-018-0067-9/FIGURES/4

Cira, T. M., Venette, R. C., Aigner, J., Kuhar, T., Mullins, D. E., Gabbert, S. E., & Hutchison, W. D. (2016). Cold Tolerance of Halyomorpha halys (Hemiptera: Pentatomidae) Across Geographic and Temporal Scales. *Environmental Entomology*, *45*(2), 484–491. https://doi.org/10.1093/EE/NVV220

Costa, A. C., & Soares, A. (2009). Homogenization of climate data: Review and new perspectives using geostatistics. *Mathematical Geosciences*, *41*(3), 291–305. https://doi.org/10.1007/S11004-008-9203-3/METRICS

Costi, E., Haye, T., & Maistrello, L. (2017). Biological parameters of the invasive brown marmorated stink bug, Halyomorpha halys, in southern Europe. *Journal of Pest Science*, *90*(4), 1059–1067. https://doi.org/10.1007/S10340-017-0899-Z

Costi, Elena, Di Bella, E., Iotti, D., & Maistrello, L. (2022). Biocontrol implications of

multiparasitism by Trissolcus mitsukurii and Trissolcus japonicus on the invasive brown marmorated stink bug. *Entomologia Experimentalis et Applicata*, *170*(9), 772–781. https://doi.org/10.1111/eea.13185

Couto, S., Frescata, C., & Mayor, T. S. (2012). Assessment of Delta traps performance by FEM-based approach. *IOBC/WPRS Working Group "Pheromones and Other Semio-Chemicals in Integrated Production," January 2015*, 37–38.

Damos, P., & Savopoulou-Soultani, M. (2012). Temperature-driven models for insect development and vital thermal requirements. *Psyche (London)*. https://doi.org/10.1155/2012/123405

Damos, P., Soulopoulou, P., & Thomidis, T. (2020). First record and current status of the brown marmorated sting bug Halyomorpha halys damaging peaches and olives in northern Greece. *Journal of Plant Protection Research*, *60*(3), 323–326. https://doi.org/10.24425/JPPR.2020.133317

De Frenne, P., Lenoir, J., Luoto, M., Scheffers, B. R., Zellweger, F., Aalto, J., Ashcroft, M. B., Christiansen, D. M., Decocq, G., De Pauw, K., Govaert, S., Greiser, C., Gril, E., Hampe, A., Jucker, T., Klinges, D. H., Koelemeijer, I. A., Lembrechts, J. J., Marrec, R., … Hylander, K. (2021). Forest microclimates and climate change: Importance, drivers and future research agenda. *Global Change Biology*, *27*(11), 2279–2297. https://doi.org/10.1111/GCB.15569

Dioli, P., Leo, P., & Maistrello, L. (2016). Prime segnalazioni in Spagna e in Sardegna della specie aliena Halyomorpha halys (Stål, 1855) e note sulla sua distribuzione in Europa (Hemiptera, Pentatomidae). *Revista Gaditana de Entomología*, *ISSN-e 2172-2595, Vol. 7, Nº. 1, 2016, Págs. 539-548*, *7*(1), 539–548. https://dialnet.unirioja.es/servlet/articulo?codigo=5974946&info=resumen&idioma=ENG

Donatelli, M., Magarey, R. D., Bregaglio, S., Willocquet, L., Whish, J. P. M., & Savary, S. (2017). Modelling the impacts of pests and diseases on agricultural systems. *Agricultural Systems*, *155*, 213–224. https://doi.org/10.1016/J.AGSY.2017.01.019

Espinosa, M., Weinberg, D., Rotela, C. H., Polop, F., Abril, M., & Scavuzzo, C. M. (2016). Temporal Dynamics and Spatial Patterns of Aedes aegypti Breeding Sites, in the Context of a Dengue Control Program in Tartagal (Salta Province, Argentina). *PLoS Neglected Tropical Diseases*, *10*(5), 1–21. https://doi.org/10.1371/journal.pntd.0004621

Fisher, J. J., Rijal, J. P., & Zalom, F. G. (2021). Temperature and Humidity Interact to Influence Brown Marmorated Stink Bug (Hemiptera: Pentatomidae), Survival. *Environmental Entomology*, *50*(2), 390–398. https://doi.org/10.1093/ee/nvaa146

Funayama, K. (2012). Control effect on the brown-marmorated stink bug, Halyomorpha halys (Hemiptera: Pentatomidae), by combined spraying of pyrethroid and neonicotinoid insecticides in apple orchards in northern Japan. *Applied Entomology and Zoology*, *47*(1), 75–78. https://doi.org/10.1007/S13355-011-0083-5/FIGURES/2

Gapon, D. A. (2016). First records of the brown marmorated stink bug Halyomorpha halys (Stål, 1855) (Heteroptera, Pentatomidae) in Russia, Abkhazia, and Georgia. *Entomological Review*, *96*(8), 1086–1088. https://doi.org/10.1134/S001387381608011X/METRICS

Gireesh, M., Rijal, J. P., & Joseph, S. V. (2021). Spatial distribution of hunting billbugs (Coleoptera: Curculionidae) in sod farms. *Insects*, *12*(5), 1–14. https://doi.org/10.3390/insects12050402

Goane, L., Casmuz, A., Salas, H., Lizondo, M., Gastaminza, G., & Vera, M. T. (2013). Spatial and Temporal Variation in Chaetanaphothrips orchidii Moulton (Thysanoptera: Thripidae) Population and Its Damage on Lemon. *Neotropical Entomology*, *42*(1), 72–81. https://doi.org/10.1007/s13744-012-0081-5

Govindan, B. N., & Hutchison, W. D. (2020). Influence of Temperature on Age-Stage, Two-Sex Life Tables for a Minnesota-Acclimated Population of the Brown Marmorated Stink Bug (Halyomorpha halys). *Insects*, *11*(2). https://doi.org/10.3390/INSECTS11020108

Grabarczyk, E. E., Mizell, R. F., Greene, J. K., Herzog, G. A., Tillman, P. G., & Cottrell, T. E. (2022). Spatiotemporal Distribution of Two Euschistus spp. Stink Bugs (Hemiptera: Pentatomidae) in Southeastern Farmscapes. *Journal of Insect Science*, *22*(1). https://doi.org/10.1093/jisesa/ieab111

Grosso-Silva, J. M., Stro, S., Gaspar, H., & Heyden, T. van der. (2020). Confirmation of the presence of Halyomorpha halys (Stål, 1855) (Hemiptera: Pentatomidae) in mainland Portugal. *Arquivos Entomolóxicos*. https://www.academia.edu/44375201/Confirmation_of_the_presence_of_Halyomorpha_halys_Stål_1855_Hemiptera_Pentatomidae_in_mainland_Portugal

Güncan, A., & Gümüş, E. (2019). Brown Marmorated Stink Bug, Halyomorpha halys (StåL, 1855) (Hemiptera: Heteroptera, Pentatomidae), a New and Important Pest in

Turkey. *Entomological News*, *128*(2), 204–210. https://doi.org/10.3157/021.128.0208

Hahn, D. A., & Denlinger, D. L. (2007). Meeting the energetic demands of insect diapause: nutrient storage and utilization. *Journal of Insect Physiology*, *53*(8), 760–773. https://doi.org/10.1016/J.JINSPHYS.2007.03.018

Hajek, A. E., Solter, L. F., Maddox, J. V., Huang, W. F., Estep, A. S., Krawczyk, G., Weber, D. C., Hoelmer, K. A., Sanscrainte, N. D., & Becnel, J. J. (2018). Nosema maddoxi sp. nov. (Microsporidia, Nosematidae), a Widespread Pathogen of the Green Stink Bug Chinavia hilaris (Say) and the Brown Marmorated Stink Bug Halyomorpha halys (Stål). *The Journal of Eukaryotic Microbiology*, *65*(3), 315–330. https://doi.org/10.1111/JEU.12475

Havko, N. E., Das, M. R., McClain, A. M., Kapali, G., Sharkey, T. D., & Howe, G. A. (2020). Insect herbivory antagonizes leaf cooling responses to elevated temperature in tomato. *Proceedings of the National Academy of Sciences of the United States of America*, *117*(4), 2211–2217. https://doi.org/10.1073/PNAS.1913885117/SUPPL_FILE/PNAS.1913885117.SAPP.PDF

Haye, T., Abdallah, S., Gariepy, T., & Wyniger, D. (2014). Phenology, life table analysis and temperature requirements of the invasive brown marmorated stink bug, Halyomorpha halys, in Europe. *Journal of Pest Science*, *87*(3), 407–418. https://doi.org/10.1007/s10340-014-0560-z

Haye, Tim, Gariepy, T., Hoelmer, K., Rossi, J. P., Streito, J. C., Tassus, X., & Desneux, N. (2015). Range expansion of the invasive brown marmorated stinkbug, Halyomorpha halys: an increasing threat to field, fruit and vegetable crops worldwide. *Journal of Pest Science*, *88*(4), 665–673. https://doi.org/10.1007/s10340-015-0670-2

Headrick, D. (2021). The future of organic insect pest management: Be a better entomologist or pay for someone who is. *Insects*, *12*(2), 1–19. https://doi.org/10.3390/insects12020140

Heckmann, R. (2012). First Evidence of Halyomorpha halys (Stål,1855) (Heteroptera: Pentatomidae) in Germany. *Heteropteron*, *36*, 17–18.

Hemala, V., & Kment, P. (2017). First record of Halyomorpha halys and mass occurrence of Nezara viridula in Slovakia. *Plant Protection Science*, *53*(4), 247–253. https://doi.org/10.17221/166/2016-PPS

Hoebeke, E., & Carter, M. (2003). *Halyomorpha halys (Stål) (Heteroptera:*

Pentatomidae): a polyphagous plant pest from Asia newly detected in North America.

Hoebeke, E. R. (2003). *Halyomorpha halys (Stål) (Heteroptera: Pentatomidae): A polyphagous plant pest from Asia newly detected in North America Detection of and Survey for Non-native (adventive) Species in North America View project ALEOCHARINE ROVE BEETLES OF BRITISH COLUMBIA, A HOTSPOT OF CANADIAN BIODIVERSITY (COLEOPTERA, STAPHYLINIDAE) View project*. https://www.researchgate.net/publication/279897494

Ingels, C. A., & Daane, K. M. (2018). Phenology of Brown Marmorated Stink Bug in a California Urban Landscape. *Journal of Economic Entomology*, *111*(2), 780–786. https://doi.org/10.1093/JEE/TOX361

Inkley, D. B. (2012). Characteristics of Home Invasion by the Brown Marmorated Stink Bug (Hemiptera: Pentatomidae). *Journal of Entomological Science*, *47*(2), 125–130. https://doi.org/10.18474/0749-8004-47.2.125

Kamiyama, M. T., Matsuura, K., Yoshimura, T., & Yang, C. C. S. (2021). Improving invasive species management using predictive phenology models: an example from brown marmorated stink bug (Halyomorpha halys) in Japan. *Pest Management Science*, *77*(12), 5489–5497. https://doi.org/10.1002/PS.6589

Kawada, H., Kitamura, C., Kawada, H., & Kitamura, C. (1983). The Reproductive Behavior of the Brown Marmorated Stink Bug, Halyomorpha mista Uhler (Heteroptera: Pentatomidae) I. Observation of Mating Behavior and Multiple Copulation. *Applied Entomology and Zoology*, *18*(2), 234–242. https://doi.org/10.1303/aez.18.234

Khadka, A., Hodges, A. C., Leppla, N. C., & Tillman, P. G. (2020). The Effects of Relative Humidity on Halyomorpha halys (Stål) (Hemiptera: Pentatomidae) Egg Hatch, Nymph Survival, and Adult Reproduction. *Https://Doi.Org/10.1653/024.103.0424*, *103*(1), 136–138. https://doi.org/10.1653/024.103.0424

Kim, K. N., Huang, Q. Y., & Lei, C. L. (2019). Advances in insect phototaxis and application to pest management: a review. *Pest Management Science*, *75*(12), 3135–3143. https://doi.org/10.1002/ps.5536

Kistner, E. J. (2017). Climate Change Impacts on the Potential Distribution and Abundance of the Brown Marmorated Stink Bug (Hemiptera: Pentatomidae) with Special Reference to North America and Europe. *Environmental Entomology*, *46*(6), 1212–

1224. https://doi.org/10.1093/ee/nvx157

Kozlov, M. V., Sokolova, I. V., Zverev, V., Egorov, A. A., Goncharov, M. Y., & Zvereva, E. L. (2020). Biases in estimation of insect herbivory from herbarium specimens. *Scientific Reports 2020 10:1*, *10*(1), 1–9. https://doi.org/10.1038/s41598-020-69195-5

Kriticos, D. J., Kean, J. M., Phillips, C. B., Senay, S. D., Acosta, H., & Haye, T. (2017). The potential global distribution of the brown marmorated stink bug, Halyomorpha halys, a critical threat to plant biosecurity. *Journal of Pest Science*, *90*(4), 1033–1043. https://doi.org/10.1007/S10340-017-0869-5

L.I. Macavei, R. I. B. T. F. M. V. E. C. L. M. (2015). First Detection of Halyomorpha halys Stål, a New Invasive Species with a High Potential of Damage on Agricultural Crops in Romania. *Lucrari Stiintifice, Universitatea de Stiinte Agricole Si Medicin a Veterinar a Iasi "Ion Ionescu de La Brad" Iasi, Seria Agronomie*, *58*(1), 105–108.

Lee, D. H., Nielsen, A. L., & Leskey, T. C. (2014). Dispersal Capacity and Behavior of Nymphal Stages of Halyomorpha halys (Hemiptera: Pentatomidae) Evaluated Under Laboratory and Field Conditions. *Journal of Insect Behavior*, *27*(5), 639–651. https://doi.org/10.1007/s10905-014-9456-2

Lee, D. H., Short, B. D., Joseph, S. V., Bergh, J. C., & Leskey, T. C. (2013). Review of the biology, ecology, and management of Halyomorpha halys (Hemiptera: Pentatomidae) in China, Japan, and the Republic of Korea. *Environmental Entomology*, *42*(4), 627–641. https://doi.org/10.1603/EN13006

Lembrechts, J. J., Nijs, I., & Lenoir, J. (2019). Incorporating microclimate into species distribution models. *Ecography*, *42*(7), 1267–1279. https://doi.org/10.1111/ECOG.03947

Leskey, T. C., Hamilton, G. C., Nielsen, A. L., Polk, D. F., Rodriguez-Saona, C., Christopher Bergh, J., Ames Herbert, D., Kuhar, T. P., Pfeiffer, D., Dively, G. P., Hooks, C. R. R., Raupp, M. J., Shrewsbury, P. M., Krawczyk, G., Shearer, P. W., Whalen, J., Koplinka-Loehr, C., Myers, E., Inkley, D., … Wright, S. E. (2012). Pest status of the brown marmorated stink bug, Halyomorpha halys in the USA. *Outlooks on Pest Management*, *23*(5), 218–226. https://doi.org/10.1564/23OCT07

Leskey, T. C., & Nielsen, A. L. (2018). Impact of the Invasive Brown Marmorated Stink Bug in North America and Europe: History, Biology, Ecology, and Management. *Annual Review of Entomology*, *63*, 599–618. https://doi.org/10.1146/ANNUREV-ENTO-020117-043226

Linsel, A., Sebastianwiesler, Haas, J., Bär, K., & Hinderer, M. (2020). Accounting for Local Geological Variability in Sequential Simulations—Concept and Application. *ISPRS International Journal of Geo-Information 2020, Vol. 9, Page 409*, *9*(6), 409. https://doi.org/10.3390/IJGI9060409

López, O., Rach, M. M., Migallon, H., Malumbres, M. P., Bonastre, A., & Serrano, J. J. (2012). Monitoring pest insect traps by means of low-power image sensor technologies. *Sensors (Switzerland)*, *12*(11), 15801–15819. https://doi.org/10.3390/s121115801

Lowenstein, D. M., & Walton, V. M. (2018). Halyomorpha halys (Hemiptera: Pentatomidae) Winter Survival, Feeding Activity, and Reproduction Rates Based on Episodic Cold Shock and Winter Temperature Regimes. *Journal of Economic Entomology*, *111*(3), 1210–1218. https://doi.org/10.1093/JEE/TOY093

M J Tauber, and, & Tauber, C. A. (2003). Insect Seasonality: Diapause Maintenance, Termination, and Postdiapause Development. *Https://Doi.Org/10.1146/Annurev.En.21.010176.000501*, *21*(1), 81–107. https://doi.org/10.1146/ANNUREV.EN.21.010176.000501

Maistrello, L., Dioli, P., Vaccari, G., Nannini, R., Bortolotti, P., Caruso, S., Costi, E., Montermini, A., Casoli, L., & Bariselli, M. (2014). *First Records in Italy of the Asian Stinkbug , a New Threat for Fruit Crops* (pp. 283–288). Alma Mater Studiorum, Universitá di Bologna.

Maistrello, Lara, Dioli, P., Dutto, M., Volani, S., Pasquali, S., & Gilioli, G. (2018). Tracking the spread of sneaking aliens by integrating crowdsourcing and spatial modeling: The Italian invasion of halyomorpha halys. *BioScience*, *68*(12), 979–989. https://doi.org/10.1093/BIOSCI/BIY112

Maistrello, Lara, Vaccari, G., Caruso, S., Costi, E., Bortolini, S., Macavei, L., Foca, G., Ulrici, A., Bortolotti, P. P., Nannini, R., Casoli, L., Fornaciari, M., Mazzoli, G. L., & Dioli, P. (2017). Monitoring of the invasive Halyomorpha halys, a new key pest of fruit orchards in northern Italy. *Journal of Pest Science*, *90*(4), 1231–1244. https://doi.org/10.1007/S10340-017-0896-2

Maslen, E. A. (2016). *The Impact of Temperature on Halyomorpha halys (Hemiptera: Pentatomidae) Life Table Parameters and Feeding Pressure*. https://ir.library.oregonstate.edu/concern/graduate_thesis_or_dissertations/pr76f567d?locale=en

McCravity, K. W., & Berisford, C. W. (2001). Effects of vegetation control on parasitoids of the nantucket pine tip moth, Rhyacionia frustrana (Lepidoptera: Tortricidae). *Florida Entomologist*, *84*(2), 282–287. https://doi.org/10.2307/3496180

McCravy, K. W. (2018). A Review of Sampling and Monitoring Methods for Beneficial Arthropods in Agroecosystems. *Insects 2018, Vol. 9, Page 170*, *9*(4), 170. https://doi.org/10.3390/INSECTS9040170

McDougall, R. N., Ogburn, E. C., Walgenbach, J. F., & Nielsen, A. L. (2021). Diapause Termination in Invasive Populations of the Brown Marmorated Stink Bug (Hemiptera: Pentatomidae) in Response to Photoperiod. *Environmental Entomology*, *50*(6), 1400–1406. https://doi.org/10.1093/EE/NVAB089

Medal, J., Smith, T., & Cruz, A. S. (2013). Biology of the brown marmorated stink bug halyomorpha halys (Heteroptera: Pentatomidae) in the laboratory. *Florida Entomologist*, *96*(3), 1209–1212. https://doi.org/10.1653/024.096.0370

Mermer, S., Maslen, E. A., Dalton, D. T., Nielsen, A. L., Rucker, A., Lowenstein, D., Wiman, N., Bhattarai, M., Soohoo-Hui, A., Harris, E. T., Pfab, F., & Walton, V. M. (2023). Temperature-Dependent Life Table Parameters of Brown Marmorated Stink Bug, Halyomorpha halys (Stål) (Hemiptera: Pentatomidae) in the United States. *Insects*, *14*(3), 248. https://doi.org/10.3390/INSECTS14030248

Milonas, P., Gogou, C., Papadopoulou, A., Fountas, S., Liakos, V., & Papadopoulos, N. T. (2016). Spatio-Temporal Distribution of Helicoverpa armigera (Hübner) (Lepidoptera: Noctuidae) and Pectinophora gossypiella (Saunders) (Lepidoptera: Gelechiidae) in a Cotton Production Area. *Neotropical Entomology*, *45*(3), 240–251. https://doi.org/10.1007/s13744-015-0358-6

Mohekar, P., Osborne, J., Wiman, N. G., Walton, V., & Tomasino, E. (2017). Influence of winemaking processing steps on the amounts of (E)-2-decenal and tridecane as off-odorants caused by brown marmorated stink bug (Halyomorpha halys). *Journal of Agricultural and Food Chemistry*, *65*(4), 872–878. https://doi.org/10.1021/acs.jafc.6b04268

Morrison, W. R., Mathews, C. R., & Leskey, T. C. (2016). Frequency, efficiency, and physical characteristics of predation by generalist predators of brown marmorated stink bug (Hemiptera: Pentatomidae) eggs. *Biological Control*, *97*, 120–130. https://www.academia.edu/28222890/Frequency_efficiency_and_physical_characteristics_of_predation_by_generalist_predators_of_brown_marmorated_stink_bug_Hemip

tera_Pentatomidae_eggs

Murray, M. (2008). *Using Degree Days to Time Treatments for Insect Pests*.

Murvanidze, M., Krawczyk, G., Inasaridze, N., Dekanoidze, L., Samsonadze, N., Macharashvili, M., Khutsishvili, S., & Shengelaia, S. (2018). Preliminary data on the biology of brown marmorated stink bug halyomorpha halys (Hemiptera, pentatomidae) in georgia. *Turkish Journal of Zoology*, *42*(6), 617–624. https://doi.org/10.3906/ZOO-1802-34

Musolin, D. L., Dolgovskaya, M. Y., Protsenko, V. Y., Karpun, N. N., Reznik, S. Y., & Saulich, A. K. (2019). Photoperiodic and temperature control of nymphal growth and adult diapause induction in the invasive Caucasian population of the brown marmorated stink bug, Halyomorpha halys. *Journal of Pest Science*, *92*(2), 621–631. https://doi.org/10.1007/s10340-019-01080-1

Musolin, Dmitry L., Dolgovskaya, M. Y., Zakharchenko, V. Y., Karpun, N. N., Haye, T., Saulich, A. K., & Reznik, S. Y. (2022). Flying over Eurasia: Geographic Variation of Photoperiodic Control of Nymphal Development and Adult Diapause Induction in Native and Invasive Populations of the Brown Marmorated Stink Bug, Halyomorpha halys (Hemiptera: Heteroptera: Pentatomidae). *Insects*, *13*(6). https://doi.org/10.3390/INSECTS13060522

Nielsen, A. L., Chen, S., & Fleischer, S. J. (2016). Coupling developmental physiology, photoperiod, and temperature to model phenology and dynamics of an invasive heteropteran, Halyomorpha halys. *Frontiers in Physiology*, *7*(MAY). https://doi.org/10.3389/fphys.2016.00165

Nielsen, A. L., Fleischer, S., Hamilton, G. C., Hancock, T., Krawczyk, G., Lee, J. C., Ogburn, E., Pote, J. M., Raudenbush, A., Rucker, A., Saunders, M., Skillman, V. P., Sullivan, J., Timer, J., Walgenbach, J., Wiman, N. G., & Leskey, T. C. (2017). Phenology of brown marmorated stink bug described using female reproductive development. *Ecology and Evolution*, *7*(17), 6680–6690. https://doi.org/10.1002/ECE3.3125

Nielsen, A. L., & Hamilton, G. C. (2009). Life history of the invasive species Halyomorpha halys (Hemiptera: Pentatomidae) in northeastern United States. *Annals of the Entomological Society of America*, *102*(4), 608–616. https://doi.org/10.1603/008.102.0405

Nielsen, A. L., Hamilton, G. C., & Matadha, D. (2008). Developmental rate estimation and

life table analysis for Halyomorpha halys (Hemiptera: Pentatomidae). *Environmental Entomology*, *37*(2), 348–355. https://doi.org/10.1603/0046-225X(2008)37[348:DREALT]2.0.CO;2

Niva, C. C., & Takeda, M. (2003). Effects of photoperiod, temperature and melatonin on nymphal development, polyphenism and reproduction in Halyomorpha halys (Heteroptera: Pentatomidae). *Zoological Science*, *20*(8), 963–970. https://doi.org/10.2108/ZSJ.20.963

Noce, M. E., Belfiore, T., Scalercio, S., Vizzarri, V., & Iannotta, N. (2009). Efficacy of new mass-trapping devices against Bactrocera oleae (Diptera tephritidae) for minimizing pesticide input in agroecosystems. *Journal of Environmental Science and Health - Part B Pesticides, Food Contaminants, and Agricultural Wastes*, *44*(5), 442–448. https://doi.org/10.1080/03601230902935105

Ntiri, E. S., Calatayud, P. A., Van Den Berg, J., & Le Ru, B. P. (2019). Spatio-temporal interactions between maize lepidopteran stemborer communities and possible implications from the recent invasion of spodoptera frugiperda (Lepidoptera: Noctuidae) in Sub-Saharan Africa. *Environmental Entomology*, *48*(3), 573–582. https://doi.org/10.1093/ee/nvz024

Ogburn, E. C., Ohmen, T. M., Huseth, A. S., Reisig, D. D., Kennedy, G. G., & Walgenbach, J. F. (2023). Temperature-driven differences in phenology and habitat suitability for brown marmorated stink bug, Halyomorpha halys, in two ecoregions of North Carolina. *Journal of Pest Science*, *96*(1), 373–387. https://doi.org/10.1007/S10340-022-01497-1/FIGURES/8

Panthi, B. R., Renkema, J. M., Lahiri, S., & Liburd, O. E. (2021). Spatio-temporal distribution and fixed-precision sampling plan of scirtothrips dorsalis (Thysanoptera: Thripidae) in florida blueberry. *Insects*, *12*(3). https://doi.org/10.3390/insects12030256

Penca, C., & Hodges, A. (2018). First Report of Brown Marmorated Stink Bug (Hemiptera: Pentatomidae) Reproduction and Localized Establishment in Florida. *Https://Doi.Org/10.1653/024.101.0413*, *101*(4), 708–711. https://doi.org/10.1653/024.101.0413

Pereira, P. S., Sarmento, R. A., Lima, C. H. O., Pinto, C. B., Silva, G. A., Dos Santos, G. R., & Picanço, M. C. (2020). Geostatistical assessment of frankliniella schultzei (Thysanoptera: Thripidae) spatial distribution in commercial watermelon crops.

Journal of Economic Entomology, *113*(1), 489–495. https://doi.org/10.1093/jee/toz253

Poley, K., Bahlai, C., & Grieshop, M. (2018). Functional Response of Generalist Predators to Halyomorpha halys (Hemiptera: Pentatomidae) Eggs. *Environmental Entomology*, *47*(5), 1117–1127. https://doi.org/10.1093/EE/NVY110

Rebaudo, F., Struelens, Q., & Dangles, O. (2018). Modelling temperature-dependent development rate and phenology in arthropods: The devRate package for r. *Methods in Ecology and Evolution*, *9*(4), 1144–1150. https://doi.org/10.1111/2041-210X.12935

Reznik, S. Y., Karpun, N. N., Zakharchenko, V. Y., Shoshina, Y. I., Dolgovskaya, M. Y., Saulich, A. K., & Musolin, D. L. (2022). To Every Thing There Is a Season: Phenology and Photoperiodic Control of Seasonal Development in the Invasive Caucasian Population of the Brown Marmorated Stink Bug, Halyomorpha halys (Hemiptera: Heteroptera: Pentatomidae). *Insects*, *13*(7). https://doi.org/10.3390/INSECTS13070580

Ribeiro, S., Caineta, J., Costa, A. C., Henriques, R., & Soares, A. (2016). Detection of inhomogeneities in precipitation time series in Portugal using direct sequential simulation. *Atmospheric Research*, *171*, 147–158. https://doi.org/10.1016/J.ATMOSRES.2015.11.014

Ribeiro, A. V., Ramos, R. S., de Araújo, T. A., Soares, J. R. S., Paes, J. da S., de Araújo, V. C. R., Bastos, C. S., Koch, R. L., & Picanço, M. C. (2021). Spatial distribution and colonization pattern of Bemisia tabaci in tropical tomato crops. In *Pest Management Science* (Vol. 77, Issue 4). https://doi.org/10.1002/ps.6237

Rice, K. B., Bergh, C. J., Bergmann, E. J., Biddinger, D. J., Dieckhoff, C., Dively, G., Fraser, H., Gariepy, T., Hamilton, G., Haye, T., Herbert, A., Hoelmer, K., Hooks, C. R., Jones, A., Krawczyk, G., Kuhar, T., Martinson, H., Mitchell, W., Nielsen, A. L., … Tooker, J. F. (2014). Biology, ecology, and management of brown marmorated stink bug (Hemiptera: Pentatomidae). *Journal of Integrated Pest Management*, *5*(3), 1–13. https://doi.org/10.1603/ipm14002

Rijal, J. P., Brewster, C. C., & Bergh, J. C. (2014). Spatial distribution of grape root borer (Lepidoptera: Sesiidae) infestations in virginia vineyards and implications for sampling. *Environmental Entomology*, *43*(3), 716–728. https://doi.org/10.1603/EN13285

Rot, M., Devetak, M., Carlevaris, B., Žežlina, J., & Žežlina, I. (2018). First record of

brown marmorated stink bug (Halyomorpha halys (Stål, 1855)) (Hemiptera: Pentatomidae) in Slovenia. *Acta Entomologica Slovenica*, *26*(1), 5–12.

Rot, Mojca, Maistrello, L., Costi, E., & Trdan, S. (2022). Biological Parameters, Phenology and Temperature Requirements of Halyomorpha halys (Hemiptera: Pentatomidae) in the Sub-Mediterranean Climate of Western Slovenia. *Insects*, *13*(10). https://doi.org/10.3390/INSECTS13100956

Sakai, A. K., Allendorf, F. W., Holt, J. S., Lodge, D. M., Molofsky, J., With, K. A., Baughman, S., Cabin, R. J., Cohen, J. E., Ellstrand, N. C., McCauley, D. E., O'Neil, P., Parker, I. M., Thompson, J. N., & Weller, S. G. (2003). The Population Biology of Invasive Species. *Https://Doi.Org/10.1146/Annurev.Ecolsys.32.081501.114037*, *32*, 305–332. https://doi.org/10.1146/ANNUREV.ECOLSYS.32.081501.114037

Šapina, I., & Jelaska, L. Š. (2018). First report of invasive brown marmorated stink bug Halyomorpha halys (Stål, 1855) in Croatia. *EPPO Bulletin*, *48*(1), 138–143. https://doi.org/10.1111/EPP.12449

Saulich, A. K., & Musolin, D. L. (2012). Diapause in the seasonal cycle of stink bugs (Heteroptera, Pentatomidae) from the Temperate Zone. *Entomological Review*, *92*(1), 1–26. https://doi.org/10.1134/S0013873812010010

Scaccini, D., Duso, C., & Pozzebon, A. (2019). Lethal Effects of High Temperatures on Brown Marmorated Stink Bug Adults before and after Overwintering. *Insects*, *10*(10). https://doi.org/10.3390/INSECTS10100355

Scaccini, D., Vanishvili, L., Tirello, P., Walton, V. M., Duso, C., & Pozzebon, A. (2020). Lethal and sub-lethal effects of low-temperature exposures on Halyomorpha halys (Hemiptera: Pentatomidae) adults before and after overwintering. *Scientific Reports*, *10*(1). https://doi.org/10.1038/S41598-020-72120-5

Sciarretta, A., Tabilio, M. R., Lampazzi, E., Ceccaroli, C., Colacci, M., & Trematerra, P. (2018). Analysis of the Mediterranean fruit fly [Ceratitis capitata (Wiedemann)] spatiotemporal distribution in relation to sex and female mating status for precision IPM. *PLoS ONE*, *13*(4), 1–23. https://doi.org/10.1371/journal.pone.0195097

Seethalam, M., Bapatla, K. G., Kumar, M., Nisa, S., Chandra, P., Mathyam, P., & Sengottaiyan, V. (2021). Characterization of Helicoverpa armigera spatial distribution in pigeonpea crop using geostatistical methods. *Pest Management Science*, *77*(11), 4942–4950. https://doi.org/10.1002/ps.6536

Shrestha, G., Rijal, J. P., & Reddy, G. V. P. (2021). Characterization of the spatial

distribution of alfalfa weevil, Hypera postica, and its natural enemies, using geospatial models. *Pest Management Science*, *77*(2), 906–918. https://doi.org/10.1002/ps.6100

Silva, G. A., Santos, I. B., Campos, S. O., Silva Galdino, T. V., Fidelis Morais, E. G., Martins, J. C., Roberto Ferreira, L., Carvalho Guedes, R. N., & Picanço, M. C. (2018). Spatial distribution and losses by grain destroying insects in transgenic corn expressing the toxin Cry1Ab. *PLoS ONE*, *13*(8), 1–14. https://doi.org/10.1371/journal.pone.0201201

Sorbelli, F. B., Coro, F., Das, S. K., Di Bella, E., Maistrello, L., Palazzetti, L., & Pinotti, C. M. (2022). A Drone-based Application for Scouting Halyomorpha halys Bugs in Orchards with Multifunctional Nets. *2022 IEEE International Conference on Pervasive Computing and Communications Workshops and Other Affiliated Events, PerCom Workshops 2022, February*, 127–129. https://doi.org/10.1109/PerComWorkshops53856.2022.9767309

Sridhar, V., & Reddy, P. V. R. (2013). Use of Degree Days and Plant Phenology: A Reliable Tool for Predicting Insect Pest Activity Under Climate Change Conditions. *Climate-Resilient Horticulture: Adaptation and Mitigation Strategies*, 287–294. https://doi.org/10.1007/978-81-322-0974-4_25

Stoeckli, S., Felber, R., & Haye, T. (2020). Current distribution and voltinism of the brown marmorated stink bug, Halyomorpha halys, in Switzerland and its response to climate change using a high-resolution CLIMEX model. *International Journal of Biometeorology*, *64*(12), 2019–2032. https://doi.org/10.1007/S00484-020-01992-Z

Tassini, C., & Mifsud, D. (2019). The brown marmorated stink bug, Halyomorpha halys (Hemiptera: Heteroptera: Pentatomidae) in Malta. *EPPO Bulletin*, *49*(1), 132–136. https://doi.org/10.1111/EPP.12557

Trufelea, R., Dimoiu, M., Ichim, L., & Popescu, D. (2021). Detection of harmful insects for orchard using convolutional neural networks. *UPB Scientific Bulletin, Series C: Electrical Engineering and Computer Science*, *83*(4), 85–96.

Tsutsumi T. (2003). *Fruit Tree Stink Bug-Interesting Ecology and Clever Prevention.*

Vanegas, F., Bratanov, D., Powell, K., Weiss, J., & Gonzalez, F. (2018). A Novel Methodology for Improving Plant Pest Surveillance in Vineyards and Crops Using UAV-Based Hyperspectral and Spatial Data. *Sensors 2018, Vol. 18, Page 260*, *18*(1), 260. https://doi.org/10.3390/S18010260

Vanoye-Eligio, V., Barrientos-Lozano, L., Pérez-Castañeda, R., Gaona-Garciá, G., & Lara-

Villalon, M. (2015). Regional-Scale Spatio-Temporal Analysis of Anastrepha ludens (Diptera: Tephritidae) Populations in the Citrus Region of Santa Engracia, Tamaulipas, Mexico. *Journal of Economic Entomology*, *108*(4), 1655–1664. https://doi.org/10.1093/jee/tov134

Vétek, G., & Korányi, D. (2017). Severe damage to vegetables by the invasive brown marmorated stink bug, Halyomorpha halys (Hemiptera: Pentatomidae), in Hungary. *Periodicum Biologorum*, *119*(2), 131–135. https://doi.org/10.18054/PB.V119I2.4935

Weyman, G. S., Jepson, P. C., & Sunderland, K. D. (1995). Do seasonal changes in numbers of aerially dispersing spiders reflect population density on the ground or variation in ballooning motivation? *Oecologia*, *101*(4), 487–493. https://doi.org/10.1007/BF00329428

Wiman, N. G., Walton, V. M., Shearer, P. W., Rondon, S. I., & Lee, J. C. (2015). Factors affecting flight capacity of brown marmorated stink bug, Halyomorpha halys (Hemiptera: Pentatomidae). *Journal of Pest Science*, *88*(1), 37–47. https://doi.org/10.1007/S10340-014-0582-6/FIGURES/7

Zalom, F.G.; Goodell, P.B.; Wilson, L.T.; Barnett, W.W.; Bentley, W. J. (1983). *Degree-Days: The Calculation and Use of Heat Units in Pest Management*.

Zhu, G., Bu, W., Gao, Y., & Liu, G. (2012). Potential geographic distribution of brown marmorated stink bug invasion (Halyomorpha halys). *PLoS ONE*, *7*(2). https://doi.org/10.1371/journal.pone.0031246